

The Pennsylvania State University
The Graduate School
Department of Civil and Environmental Engineering

**THE VIABILITY OF PARTIALLY POST-TENSIONED CONCRETE MEMBERS
IN AN AGGRESSIVE ENVIRONMENT, INCLUDING CYCLIC LOADING**

A Dissertation in
Civil Engineering
by
Jeffery Scott Volz

© 2008 Jeffery Scott Volz

Submitted in Partial Fulfillment
of the Requirements
for the Degree of

Doctor of Philosophy

December 2008

The dissertation of Jeffery Scott Volz was reviewed and approved* by the following:

Andrea J. Schokker
Associate Professor of Civil and Environmental Engineering
Dissertation Advisor
Chair of Committee

Jeffrey A. Laman
Associate Professor of Civil and Environmental Engineering

Daniel G. Linzell
Associate Professor of Civil and Environmental Engineering

Howard W. Pickering
Distinguished Professor Emeritus of Metallurgy

Peggy A. Johnson
Professor of Civil and Environmental Engineering
Head of the Department of Civil and Environmental Engineering

*Signatures are on file in the Graduate School

ABSTRACT

Partially prestressed concrete offers several advantages over fully prestressed designs including increased ductility, increased energy absorption, decreased cost, decreased camber, and decreased anchor zone congestion. However, design codes have been slow to adopt provisions for the design of partially prestressed concrete because of concerns over fatigue and corrosion. The overall objective of this study was to determine the viability of partially post-tensioned concrete members in an aggressive environment, including the impact of cyclic loading.

This objective was investigated through an experimental program, which included both individual strand testing and full-scale, post-tensioned beam specimens. The strand testing phase consisted of corroding samples to different amounts of section loss, and then testing them under cyclic loading until failure. The beam testing phase included 12 full-scale, post-tensioned beam specimens combining long-term static exposure testing with fatigue testing. One of the most important limitations of the study was that the experimental program followed the specific sequence of exposure (corrosion) followed by fatigue to failure.

With regard to the individual strand testing, there was a significant drop-off in fatigue capacity at relatively small pit depths. On average, the fatigue capacity was reduced 50 percent for pitting that measured 0.010 to 0.015 inches in depth. Furthermore, an empirical relationship based on an exponential decay function was found to be the most reliable method of predicting the response of corroded prestressing strand for the specific sequence of corrosion followed by fatigue to failure. In particular, average pit

depth offered the best correlation between fatigue capacity and the amount of localized corrosion.

With regard to the full-scale beam testing, there were several conclusions reached as to the behavior of the tendon – duct, grout, and strand – under exposure and fatigue testing. First, a robust plastic duct is required as it serves as the primary protection method for the tendon and also performs very well under cyclic loading. Furthermore, the plastic duct requires steel or plastic saddles at tendon deviation points to eliminate the potential for puncturing the duct during the strand stressing operation. Next, without full encapsulation of the strand by the grout, the tendon will act as a conduit for chloride transport, thus spreading the potential for corrosion from a single breach in the duct. Furthermore, even within a well grouted tendon, the grout will contain both longitudinal and circumferential cracking, reducing the ability of the grout to protect the strand. Finally, grouting defects, such as voids and fine cracks, do not adversely affect fatigue performance of the strand, but these defects do adversely affect corrosion protection of the strand, allowing chlorides access to the strand.

A set of best practices are also included in the recommendation section for the durability of partially post-tensioned concrete members in an aggressive environment, including cyclic loading. These best practices focus on tension and compression stress limits for the concrete, detailing issues for the tendon, and areas of concern with regard to the anchorage zones and long-term durability. With regard to the study's overall objective, partially post-tensioned concrete is a viable construction method in an aggressive environment, even with cyclic loading, but it relies on a robust plastic duct system as the primary protection method for the tendon.

TABLE OF CONTENTS

LIST OF FIGURES	viii
LIST OF TABLES	xiii
ACKNOWLEDGEMENTS	xv
Chapter 1 Introduction	1
1.1 Background and Motivation	1
1.2 Problem Statement	3
1.3 Scope of Study	5
1.4 Objectives and Scope of Work	7
1.5 Research Plan	8
1.6 Thesis Organization	9
1.7 Prestressing Terminology	9
Chapter 2 Literature Review	12
2.1 Fabrication of Prestressing Strand	12
2.2 Corrosion of Prestressing Strand	15
2.3 Corrosion-Induced Failure of Prestressing Strand	19
2.4 Individual Strand Fatigue Testing	22
2.5 Corrosion Fatigue	25
2.6 Fatigue in Post-Tensioned Members	27
2.7 Chloride-Induced Corrosion in Post-Tensioned Members	28
2.8 Grouts for Bonded Post-Tensioning	30
2.9 Level of Prestress	31
2.10 Unanticipated Loss of Prestress	32
2.10.1 Construction Defects	33
2.10.2 Material Defects	34
2.10.3 Additional Factors	35
2.11 Code Provisions and Committee Recommendations	36
2.12 Summary	37
Chapter 3 Individual Strand Testing	40
3.1 Corroding of Strand Samples	41
3.2 Characterization and Measurement of Corrosion	46
3.3 Fatigue Test Setup, Test Parameters, and Test Results	55
3.4 Corrosion-Fatigue Relationship	61
3.4.1 Linear Elastic Fracture Mechanics Approach	64
3.4.1.1 Non-Corroded Strand	67
3.4.1.2 Corroded Strand – Modify Y	68

3.4.1.3 Corroded Strand – Modify Stress Range	70
3.4.2 Empirical Approach.....	71
3.4.3 Discussion.....	76
3.4.3.1 Seven Wire Strand versus Individual Wire.....	76
3.4.3.2 Fretting Fatigue.....	78
3.4.3.3 Defect Location, Pit Location, and Fracture Location.....	80
3.4.3.4 Hydrogen Embrittlement	82
3.4.3.5 Previous Fatigue Testing of Noncorroded Strand.....	83
3.5 Summary.....	83
Chapter 4 Beam Specimen Design and Construction	85
4.1 Beam Specimen Concept.....	85
4.2 Beam Specimen Test Matrix	89
4.3 Beam Specimen Design.....	95
4.3.1 Beam Tendon and Mild Steel Design.....	95
4.3.2 Local and General Zone Design	100
4.3.3 Deviator Design.....	102
4.3.4 Post-Tensioning Bar and Anchorage Design	104
4.3.5 Corbel Design.....	105
4.3.6 Beam Specimen Design Summary	106
4.4 Beam Specimen Construction.....	107
4.5 Beam Specimen Instrumentation.....	108
Chapter 5 Beam Specimen Testing.....	114
5.1 Determination of Strand Stress	114
5.1.1 Prior to Fatigue Testing.....	115
5.1.2 During Fatigue Testing.....	128
5.1.2.1 Moment-Curvature Analysis.....	129
5.1.2.2 Finite Element Analysis.....	132
5.2 Exposure Testing and Monitoring	136
5.3 Fatigue Testing and Observations	143
5.4 Summary.....	148
Chapter 6 Beam Specimen Forensic Investigation	152
6.1 General Findings from Forensic Investigation	152
6.1.1 Grout Coverage	153
6.1.2 Grout Cracking	154
6.1.3 Strand Location within Duct	156
6.1.4 Plastic Duct Performance at Deviators.....	159
6.2 Specific Findings from Forensic Investigation.....	161
6.2.1 Fatigue Reference Series	161
6.2.2 Anchor Zone Grout Void Series.....	162
6.2.3 Anchor Zone Grout Void Corrosion Series.....	163

6.2.4 Crown Grout Void Corrosion Series	164
6.3 Summary	167
Chapter 7 Findings, Conclusions, and Recommendations.....	170
7.1 Findings	170
7.2 Conclusions.....	174
7.3 Recommendations.....	177
Bibliography	179
Appendix A Accelerated Strand Corrosion Process	189
Appendix B Strand Protection for Individual Strand Testing.....	192
Appendix C Beam Specimen Construction Details	195
C.1 Formwork.....	195
C.2 Reinforcing Cage	197
C.3 Post-Tensioning Anchorage, Duct, and Deviator Hardware and Installation	199
C.4 Concrete Mix Design, Placement, and Curing.....	201
C.5 Prestressing Strand Stressing Operation	204
C.6 Tendon Grouting	206
C.7 Prestressing Bar Stressing Operation.....	208
C.8 Beam Specimen Material Property Testing	212
C.8.1 Concrete Testing	212
C.8.2 Grout Testing	213
Appendix D Vibrating Wire Strain Gauges	216
Appendix E Strain Gauge Measurements	221
Appendix F Longitudinal Cracking Finite Element Analysis.....	223
Appendix G Beam Specimen Crack Maps and Crack Width Measurements.....	229
Appendix H Beam Specimen Autopsy Procedure.....	246

LIST OF FIGURES

Figure 2-1: Prestressing Strand.....	12
Figure 2-2: Stress-Strain Curve for Grade 270 Prestressing Strand	14
Figure 2-3: Schematic of Corrosion Pit Propagation in Steel.....	18
Figure 2-4: Fatigue Capacity of Prestressing Wire as a Function of Pitting Corrosion. Nürnberg (2002) Reproduced with Permission	24
Figure 3-1: Non-Accelerated Corrosion Setup	42
Figure 3-2: Pitting Corrosion Attack	47
Figure 3-3: Crevice Corrosion Attack.....	47
Figure 3-4: Schematic of Typical Crevice Corrosion Attack	48
Figure 3-5: Wire Numbering Convention for Recording Corrosion Data in Table 3-1	52
Figure 3-6: Hydrogen Evolution During Localized Corrosion Attack.....	54
Figure 3-7: Strand Specimen Fatigue Test Setup	56
Figure 3-8: Strand Specimen Fatigue Test Setup	56
Figure 3-9: Strand Specimen End Treatment for Fatigue Testing	57
Figure 3-10: Cycles to Failure as a Function of Maximum Pit Depth.....	62
Figure 3-11: Cycles to Failure as a Function of Average Pit Depth.....	62
Figure 3-12: Cycles to Failure as a Function of Percentage Loss of Strand Area	63
Figure 3-13: Cycles to Failure as a Function of Percentage of Corroded Strand Surface	63
Figure 3-14: Cycles to Failure as a Function of Percentage Weight Loss of Strand ...	64
Figure 3-15: Cold Drawn Wire Defect Profile	67
Figure 3-16: Fatigue Crack Emanating from the Base of a Corrosion Pit.....	69
Figure 3-17: Cycles to Failure as a Function of Effective Stress Range	72

Figure 3-18: Cycles to Failure as a Function of Maximum Pit Depth.....	73
Figure 3-19: Cycles to Failure as a Function of Average Pit Depth.....	73
Figure 3-20: Individual Wire Break During Fatigue Testing	77
Figure 3-21: Wire Fracture Surfaces Observed During Fatigue Testing.....	80
Figure 3-22: Cycles to Failure as a Function of Percentage Loss of Strand Area	82
Figure 4-1: Beam Specimen Schematic and Internal Forces	87
Figure 4-2: Three-dimensional Schematic of Beam Specimen	89
Figure 4-3: Beam Specimen Design	96
Figure 4-4: Beam Specimen Design Details.....	101
Figure 4-5: Photograph Showing Location of Steel Deviation Pipe.....	103
Figure 4-6: Beam Specimen Reinforcing Cage	107
Figure 4-7: Completed Specimen Setup Ready for Concrete Placement	108
Figure 4-8: A Set of Three Completed Beam Specimens.....	109
Figure 4-9: Vibrating Wire Strain Gauge Locations at Midspan of Beam Specimens	111
Figure 4-10: Vibrating Wire Strain Gauge Orientation on Beam Specimens	111
Figure 4-11: Vibrating Wire Strain Gauge Installed on Prestressing Bar Coupler.....	112
Figure 5-1: Beam Specimen FR-1 Strain Gauge Measurements as a Function of Force in the Stressing Jack	116
Figure 5-2: Beam Specimen FR-1 Measured versus Calculated Concrete Strains During Jacking Operation.....	119
Figure 5-3: Beam Specimen AZ-1 Measured versus Calculated Concrete Strains During Jacking Operation.....	122
Figure 5-4: Beam Specimen AZC-1 Measured versus Calculated Concrete Strains During Jacking Operation.....	124
Figure 5-5: Beam Specimen GVC-1 Measured versus Calculated Concrete Strains During Jacking Operation.....	125

Figure 5-6: Beam Specimen Internal Forces During Load Application	127
Figure 5-7: Stress-Strain Curve for Grade 270 Prestressing Strand	131
Figure 5-8: Finite Element Model for Determining Strand Stress During Fatigue Testing	134
Figure 5-9: Anchor Zone Grout Void Corrosion Specimens Undergoing Exposure Testing	137
Figure 5-10: Exposed Grouted Tendon After Plastic Duct Removal	139
Figure 5-11: GVC-1 Grout Crack Map.....	139
Figure 5-12: GVC-2 Grout Crack Map.....	140
Figure 5-13: GVC-3 Grout Crack Map.....	140
Figure 5-14: Exposed Grouted Tendon for GVC-1 Showing Signs of Corrosion.....	141
Figure 5-15: Beam Specimen GVC-2 After Six-Month Duration of Exposure Testing	142
Figure 5-16: Beam Specimen Fatigue Test Setup.....	144
Figure 5-17: Beam Specimen Fatigue Test Setup.....	145
Figure 5-18: Longitudinal Cracking of Beam Specimens	146
Figure 5-19: Typical Crack Pattern for Partially Prestressed Specimens	147
Figure 6-1: Exposed Grouted Tendon After Plastic Duct Removal for <i>In Situ</i> Inspection.....	154
Figure 6-2: Close-Up of Air Pockets Along Peaks of Duct Ribs	155
Figure 6-3: Beam Specimen FR-1 Grouted Tendon with Schematic End View	157
Figure 6-4: Beam Specimen FR-1 Grouted Tendon with Schematic End View	157
Figure 6-5: Beam Specimen AZ-3 Grouted Tendon with Schematic End View.....	158
Figure 6-6: Beam Specimen AZ-3 Grouted Tendon with Schematic End View.....	158
Figure 6-7: Gouges in Plastic Duct from Strand Stressing, Beam Specimen FR-3.....	160
Figure 6-8: Strand Corrosion within Void Behind Anchor Head.....	163

Figure 6-9: Strand Corrosion Within and Away from Grout Void.....	165
Figure 6-10: Strand Corrosion at Anchor Head Opposite to Grout Void.....	166
Figure 6-11: Strand Corrosion Experienced by GVC Beam Specimens	166
Figure 6-12: Strand Corrosion of GVC Beam Specimen at Grout Crack.....	167
Figure A-1: Accelerated Corrosion Setup.....	190
Figure A-2: Artificially Dense Pitting Structure.....	191
Figure B-1: Strand End Treatment for Fatigue Testing	194
Figure C-1: Basic Formwork for Casting Specimens	196
Figure C-2: Completed Reinforcing Cage	198
Figure C-3: VSL Type EC Stressing Anchorage.....	199
Figure C-4: Completed Specimen Setup Ready for Concrete Placement.....	201
Figure C-5: Prestressing Tendon Stressing Operation.....	206
Figure C-6: Tendon Grouting Setup	207
Figure C-7: Grouting Setup for Anchor Zone Grout Void	209
Figure C-8: Prestressing Bar Stressing Setup.....	211
Figure C-9: Set of Three Specimens After Stressing of Post-Tensioning Bar	211
Figure D-1: Measured versus Calculated Concrete Strains for a Standard 6"x12" Cylinder	218
Figure D-2: Measured versus Calculated Concrete Strains for a Standard 6"x12" Cylinder	218
Figure D-3: Coupler Load-Strain Data for Fatigue Reference Series.....	219
Figure D-4: Coupler Load-Strain Data for Anchor Zone Grout Void Series	219
Figure D-5: Coupler Load-Strain Data for Anchor Zone Grout Void Corrosion Series.....	220
Figure D-6: Coupler Load-Strain Data for Crown Grout Void Corrosion Series.....	220
Figure F-1: Finite Element Model for Longitudinal Cracking	224

Figure F-2: Stresses Perpendicular to Longitudinal Plane During Jacking	226
Figure F-3: Typical Longitudinal Cracking of Beam Specimens	226
Figure G-1: Beam Specimen FR-1 Crack Map.....	230
Figure G-2: Beam Specimen FR-2 Crack Map.....	231
Figure G-3: Beam Specimen FR-3 Crack Map.....	232
Figure G-4: Beam Specimen AZ-1 Crack Map	234
Figure G-5: Beam Specimen AZ-2 Crack Map	235
Figure G-6: Beam Specimen AZ-3 Crack Map	236
Figure G-7: Beam Specimen AZC-1 Crack Map	238
Figure G-8: Beam Specimen AZC-2 Crack Map	239
Figure G-9: Beam Specimen AZC-3 Crack Map	240
Figure G-10: Beam Specimen GVC-1 Crack Map.....	242
Figure G-11: Beam Specimen GVC-2 Crack Map.....	243
Figure G-12: Beam Specimen GVC-3 Crack Map.....	244
Figure H-1: Removed Center Portion of Tendon	248
Figure H-2: Saw Cutting of Concrete Above Tendon	248
Figure H-3: Concrete Removed to Expose Tendon.....	249
Figure H-4: Saw Cutting of Concrete Above Tendon and Anchorage.....	251
Figure H-5: Beam Specimen After Anchorage Removal	251
Figure H-6: Anchor Head and Strand After Removal from Anchorage.....	252

LIST OF TABLES

Table 2-1: Summary of Code Provisions and Committee Recommendations	38
Table 3-1: Strand Specimen Corrosion Data	50
Table 3-2: Strand Specimen Corrosion Data	53
Table 3-3: Fatigue Results for As-received Strand.....	59
Table 3-4: Fatigue Results for Corroded Strand.....	60
Table 4-1: Beam Specimen Test Matrix	94
Table 4-2: Specimen Cross-Sectional Properties at Midspan.....	98
Table 4-3: Maximum Calculated Stresses and Code Allowable Stresses at Midspan	99
Table 5-1: Strand Stresses for Fatigue Reference Series	117
Table 5-2: Strand Stresses for Anchor Zone Grout Void Series.....	121
Table 5-3: Strand Stresses for Anchor Zone Grout Void Corrosion Series.....	123
Table 5-4: Strand Stresses for Crown Grout Void Corrosion Series	124
Table 5-5: Revised Specimen Loading Based on Actual Effective Prestress.....	128
Table 5-6: Summary of Findings from Beam Specimen Testing	150
Table 7-1: Summary of Findings for Full-Scale Beam Specimens	171
Table C-1: PennDOT Class A Mix Design Proportions Per Cubic Yard.....	203
Table C-2: Concrete Material Properties	213
Table C-3: Post-Tensioning Grout 7-Day Compressive Strengths.....	214
Table E-1: Calculated and Measured Concrete Strains for Beam Specimen FR-1	221
Table E-2: Calculated and Measured Concrete Strains for Beam Specimen AZ-1	221
Table E-3: Calculated and Measured Concrete Strains for Beam Specimen AZC-1	222

Table E-4: Calculated and Measured Concrete Strains for Beam Specimen GVC-1.....	222
Table G-1: Crack Widths for Fatigue Reference Series	233
Table G-2 Crack Widths for Anchor Zone Grout Void Series	237
Table G-3: Crack Widths for Anchor Zone Grout Void Corrosion Series	241
Table G-4: Crack Widths for Crown Grout Void Corrosion Series	245

ACKNOWLEDGEMENTS

As I write this final section of my dissertation, I am reminded of a quote from T. S. Eliot. “It's strange that words are so inadequate. Yet, like the asthmatic struggling for breath, so the lover must struggle for words.” I find myself struggling for words as, in the end, no matter how well thought out, they are destined to fall short of exactly how I feel about those that have meant so much.

To my advisor, Dr. Andrea Schokker, I want to say how enjoyable the process has been and how much I have learned and grown under her wing. She is a unique individual that offers just the right amount of freedom and restraint to her students so that they have every opportunity to succeed and yet a safety net should they fall. The most telling thing that I can say is that I will miss her terribly.

To Dr. Andrew Scanlon, who somehow avoided being a member of committee, I want express my appreciation and thanks for his help and encouragement over the years. I will always remember our talks while we shared an office at CTL during one of his sabbaticals, and his sage advice while I contemplated returning to school in pursuit of my doctoral degree.

To my committee, Drs. Jeffrey Laman, Daniel Linzell, and Howard Pickering, I want to express my sincere appreciation for their thorough and exacting review of my dissertation. Although Drs. Laman and Linzell are “steel guys,” their contributions helped us to look at prestressed concrete from a different point of view and added valuable insight and ideas about the research work. I am also indebted to Dr. Pickering, who somehow managed to teach electrochemistry to a structural engineer. I now understand

so much better the material from my freshman chemistry class. I also want to thank the committee for reviewing my dissertation and attending my defense during the summer, which is not the most convenient time of year.

I am also very thankful to VSL for donating all of the post-tensioning hardware, prestressing strand, and grouting equipment for the full-scale specimens. In particular, I would like to thank Mr. John Crigler, Senior Vice-President of VSL, and Dr. Zuming Xi, Project Engineer for VSL, for their advice and ideas related to my research. Their input was invaluable in helping us to develop a very realistic and practical approach to our research project.

To my fellow graduate students, Andy, Brian, Carlos, Dan, Dave, Emily, Eric, Ed, Melissa, Nick, and Shaun, thank you for all of your help and camaraderie during my time at Penn State. Thanks also to Dan Fura for his help and guidance in the construction and testing of my specimens. He is an invaluable asset to the CITEL Laboratory.

My sincere gratitude also extends to two individuals that formed the foundation of my education as a structural engineer and teacher, Drs. Louis Geschwindner and Harry West. Although they have very different styles of teaching, they were hands down the two finest teachers I ever had while a student at Penn State. More importantly, they both continued to guide me throughout my professional and academic career. If I can be half as successful an educator as either of them, I will consider myself to be a great success. I am but one of many that they have touched over the years, and I am sad that they have both retired and will no longer be able to mold the minds of young Penn State engineers to come.

Last, but in no way least, I want to thank my family for their help, support, guidance, and, most importantly, love. To Tyler, my dear son and the miracle in my life, thanks for keeping me grounded and always making sure I understood what was important in life. You are my best buddy, and I look forward to many years of you teaching me about life. To Kathy, my beloved wife and dearest friend, thank you for believing in me. You were the only one who thought I could do this, and I would not have been able to do it without your love and undying support, particularly during the darkest times. Yet none of these words are adequate to express exactly how I feel. All my love, today and each day forward.

Chapter 1

Introduction

1.1 Background and Motivation

Freyssinet's original design concept for prestressed concrete maintained the concrete in compression under full service load (Billington 2004, D'Arcy *et al.* 2003). In fact, Billington (2004) notes that "for Freyssinet, 'the fields of prestressed concrete and reinforced concrete have no common frontier.' Either a structure is fully prestressed or it is not to be called prestressed concrete." Prestressed concrete design has evolved over time to allow a nominal amount of tension in the concrete under full service load. Even with this nominal amount of tension, the design is still considered fully prestressed provided the tensile stresses do not exceed the modulus of rupture for the concrete.

As part of the evolution of prestressed concrete, designers, code writers, and researchers have begun to examine the potential for utilizing even lower levels of prestressing that allow the concrete to crack under full service load. This type of prestressing is often referred to as partial prestressing. One of the primary reasons for the potential use of partial prestressing is that ultimate strength generally never governs the design of fully prestressed sections. Instead, the design is controlled by tension stress limits at full service load. However, that approach may be overly conservative, even with respect to serviceability concerns, if the full live load is infrequently reached during the life of the structure.

The advantages of partial prestressing over fully prestressed designs include increased ductility, increased energy absorption, decreased cost, decreased camber, and decreased anchor zone congestion (Lin and Burns 1981, Nilson 1987). However, design codes have been slow to adopt provisions for the design of partially prestressed concrete because of concerns over fatigue and corrosion.

The current edition of the ACI Building Code (ACI 318 2008) now recognizes three classes of prestressed flexural members, U, T, and C. Under full service load, Class U members are considered uncracked, Class C members are considered cracked, and Class T members represent a transition between cracked and uncracked behavior (ACI 318 2008). The dividing lines between the three classes are based on nominal tensile stresses in the precompressed tensile zone of $7.5\sqrt{f'_c}$ and $12\sqrt{f'_c}$ (ACI 318 2008). Since they will crack under service load, Class C members and some Class T members are, in essence, partially prestressed flexural members. Consequently, these members are susceptible to fatigue and corrosion.

In order to properly design partially prestressed flexural members in aggressive environments, research is required to understand the role of fatigue and corrosion on these types of members. Furthermore, repair of existing prestressed concrete members damaged due to corrosion requires an understanding of the remaining capacity of the section prior to designing a fix, such as fiber-reinforced plastic (FRP) composites or external prestressing.

1.2 Problem Statement

This research program proposed to investigate the viability of partially post-tensioned concrete members in an aggressive environment, including the impact of cyclic loading. Corrosion of the nation's transportation infrastructure is a widespread and costly problem (Koch *et al.* 2001). Structures are deteriorating at a faster rate than they can be repaired or replaced. The most prevalent form of corrosion in highway structures is chloride-induced corrosion of steel. Limited research has been performed in the area of cyclic loading in post-tensioned members, and the addition of a corrosive environment to this problem has not been studied significantly.

Post-tensioning has many potential benefits, including crack control and rapid construction with minimal traffic interference when combined with precast members. Although the concept of post-tensioning is not new, post-tensioning as it stands today is a relatively new form of construction, having been used in bridge structures in the United States for less than 50 years. At this stage in development, construction practices and materials are continuously improving. And, it is important that durability of the structure be considered during this development process. In particular, chloride-induced corrosion is a very real concern for all types of bridges.

An additional concern for bridge members is fatigue. Repeated loadings can cause fatigue damage of the reinforcement as well as increased crack widths and deflections (Balaguru 1981, Naaman 1982). Traditional fully prestressed members are uncracked at service loads and fatigue would not typically be a problem with these sections. However, the economic benefits of partially prestressed members are now becoming ap-

parent. Unfortunately, partially prestressed members may be cracked at service loads and are therefore more susceptible to fatigue than fully prestressed members or cracked non-prestressed members.

Partially post-tensioned members are more susceptible to fatigue due to two reasons. First, they experience higher stress changes in the steel as compared to fully post-tensioned members or cracked non-prestressed member (Naaman 1982). Second, post-tensioned members have the additional concerns of fretting between the strands and fretting between the strands and duct (Rigon and Thurlimann 1985, Wollman *et al.* 1988).

Fully post-tensioned members may also be susceptible to durability and fatigue problems due to excessive loss of prestress. This unanticipated prestress loss can occur due to a number of factors, such as construction defects, material defects, overload, corrosion, and retrofitting. This loss of full prestress does not necessarily condemn the structure. In truth, the structure typically still possesses sufficient strength to support load over some service life – although likely not the full service life that was originally intended. However, no design guidelines exist to assist the engineer in determining what that safe service life is.

Larger crack widths from fatigue loading combined with aggressive agents such as chlorides must be investigated in order for partially post-tensioned members to be a safe and viable option in bridges and to provide guidance for fully post-tensioned structures with a loss of prestress beyond traditional losses. Corrosion protection of the post-tensioning system is vital to the integrity of the structure because loss of post-tensioning can result in catastrophic failure.

1.3 Scope of Study

This research program proposed to investigate the viability of partially post-tensioned concrete members in an aggressive environment, including the impact of cyclic loading. This objective was investigated within a limited scope to reduce the number of variables to a manageable level. One of the most important limitations was that the experimental program followed the specific sequence of exposure (corrosion) followed by fatigue to failure. The experimental program included both individual strand testing and full-scale, post-tensioned beam specimens.

The individual strand testing examined the effect of corrosion on the fatigue capacity of prestressing strand for the specific sequence of corrosion followed by fatigue to failure. The methodology developed for this portion of the study involved the following steps: (1) corrode the strand samples to different amounts of section loss; (2) characterize the amount and disposition of the corrosion; (3) test the strand samples under cyclic loading until failure; and (4) determine a relationship between the amount of strand corrosion and the resulting fatigue capacity. Both analytical and empirical approaches were studied to develop this corrosion-fatigue relationship. The strand testing used Grade 270, low-relaxation strand taken from the same spool.

The full-scale beam testing also examined the effect of corrosion on the fatigue capacity of prestressing strand for the specific sequence of exposure (corrosion) followed by fatigue to failure. After construction, the specimens were loaded under full service load and exposed to chlorides for a period of 6 months. At that point, the specimens were placed into a load frame and tested in fatigue to 2,000,000 cycles or failure, whichever

came first. Following testing, the specimens were autopsied for signs of corrosion and fatigue damage.

Full-scale beam specimens were necessary in order to evaluate actual post-tensioning hardware and the effect of multi-strand tendons. The full-scale beam test variables included the level of prestress, condition of the post-tensioning system, and exposure to saltwater. The full prestress design was based on a nominal tensile stress in the precompressed tensile zone of $3\sqrt{f'_c}$ (psi). The partial prestress design was based on 67 percent of the force required for full prestress, with one specimen using fewer strands and the other using a lower prestressing force. The specimen with the lower prestressing force was to mimic a fully prestressed design that experienced excessive prestress losses or overload.

The post-tensioning system for the full-scale specimens followed current design practice and construction standards. The beams used a multi-strand tendon within a plastic duct filled with a prepackaged grout. The tendon followed a two-point drape profile with steel deviator pipes and Grade 270, low-relaxation strand. All anchorage hardware was supplied by a post-tensioning hardware manufacturer, and stressing of the tendons was accomplished with a standard, multi-strand tensioning jack. As part of the study, imperfections in the grout were introduced to determine their effect on durability and fatigue behavior of the tendon.

Finally, findings were presented, and conclusions and recommendations were developed based on the scope of the research program.

1.4 Objectives and Scope of Work

The overall objective of this study was to determine the viability of partially post-tensioned concrete members in an aggressive environment, including the impact of cyclic loading. This goal was accomplished by achieving the following specific objectives:

1. Develop a relationship between the amount of corrosion on the prestressing strand and the resulting fatigue capacity for the specific sequence of corrosion followed by fatigue until failure.
2. Determine the potential of the relationship developed in Item 1 to predict the response of full-scale, partially post-tensioned beam specimens for the same sequence of corrosion followed by fatigue until failure.
3. Characterize the performance of the tendon – duct, grout, and strand – under exposure to chlorides followed by cyclic testing of full-scale, partially post-tensioned beam specimens.
4. Quantify the behavior of flexural cracks under exposure to chlorides followed by cyclic testing of full-scale, partially post-tensioned beam specimens.
5. Determine the role of grouting defects on the durability and fatigue performance of prestressing strand for full-scale, partially post-tensioned beam specimens.
6. Develop a set of best practices for the durability of partially post-tensioned concrete members in an aggressive environment, including cyclic loading.

The following scope of work was used to pursue these research objectives: (1) review of the applicable literature; (2) development of a research plan; (3) testing of individual strand specimens and development of a predictive model for the response; (4) design, construction, and testing of full-scale, partially post-tensioned beam specimens; (6) forensic investigation of the full-scale beam specimens; (7) development of findings, conclusions, and recommendations; and (8) preparation of this dissertation documenting the results of the research study.

1.5 Research Plan

The research plan necessary to accomplish the objectives discussed in Section 1.4 involved individual strand testing and full-scale beam testing, and also included the use of several analytical tools during the evaluation of the test results. It is important to note that to narrow the study to a manageable number of variables, the testing followed the specific sequence of exposure (corrosion) followed by fatigue to failure. Research has shown that the fatigue capacity of prestressed concrete is a function of either the fatigue capacity of the prestressing strand or the mild steel. Therefore, it was necessary to examine the strand alone and to evaluate its response to fatigue and the sequence of corrosion followed by fatigue to failure. The second experimental aspect involved testing of full-scale beam specimens. Full-scale beam specimens were necessary in order to evaluate actual post-tensioning hardware and the effect of multi-strand tendons. In support of the experimentation, various analytical tools were applied during evaluation of the ex-

perimental test results, including statistical methods, Linear Elastic Fracture Mechanics (LEFM), and Finite Element Analyses (FEA).

1.6 Thesis Organization

In this investigation, experimental and analytical procedures were performed in order to develop a better understanding of the interaction of corrosion and fatigue on partially post-tensioned concrete members. The different tasks conducted during this study are organized as chapters in this dissertation. Chapter 1 presents an introduction to the subject, highlighting the problem, objectives, and scope. Chapter 1 also presents the research plan deemed necessary to achieve these objectives. Chapter 2 presents a literature review of the current body of knowledge pertaining to partially post-tensioned concrete members. Chapter 3 presents the testing of individual strand specimens, including evaluation of the results. Chapter 4 presents details on the design and construction of full scale, post-tensioned beam specimens. Chapter 5 presents the exposure and fatigue testing of the full scale, post-tensioned beam specimens. Chapter 6 presents the subsequent autopsy results of the full scale, post-tensioned beam specimens. The findings, conclusions and recommendations are presented in Chapter 7.

1.7 Prestressing Terminology

Prestressed concrete refers to the construction method by which a compressive stress is placed on the concrete prior to the application of load. Precompression is ex-

tremely beneficial to concrete, which is inherently strong in compression but relatively weak in tension. There are two categories of prestressed concrete, pretensioned and post-tensioned. The fundamental difference between the two involves the sequence of strand stressing and concrete placement. In pretensioned concrete, the strand is stressed in tension prior to placement and curing of the concrete. In post-tensioned concrete, the concrete is placed and cured prior to tensioning of the strand.

Although the two prestressed categories behave in almost identical ways to the application of load, post-tensioned concrete has numerous variations in the way the prestressing force is applied to the concrete through the tendon. These tendon variations include the following: (1) grouted versus ungrouted; (2) internal versus external; and (3) bonded versus unbonded.

The difference between grouted and ungrouted tendons involves the method of protection of the tendon. Grouted tendons are placed within either a steel or plastic duct that has been cast into the concrete section. Once the concrete reaches sufficient strength, the tendons are tensioned, and then a cementitious grout is pumped into the duct to protect the tendon from the elements. Ungrouted tendons are greased and sheathed in a plastic coating during manufacture. Ungrouted tendons are placed within the concrete formwork on site. After the concrete is placed and reaches sufficient strength, the ungrouted tendons are tensioned. The grease and plastic sheathing provides protection of the tendon from the elements.

The difference between internal and external tendons involves their location relative to the concrete cross-section of the prestressed member. Internal tendons are located within the confines of the concrete cross-section, while external tendons are located out-

side of the concrete cross-section. External tendons include those that are located within the open area inside a concrete box, even though they are not visible “externally.”

The difference between bonded and unbonded tendons significantly affects the strain in the tendon during application of load. Bonded tendons are continuously connected to the concrete cross-section such that the tendon and concrete experience the same strain at each cross-section of the beam (strain compatibility). An unbonded tendon is only connected to the concrete cross-section at intermittent locations. Consequently, the strain in an unbonded tendon as a function of load is member-dependent, not section-dependent. When friction loss is excluded, the strain in an unbonded tendon due to load is uniformly distributed along the tendon length.

The final prestressed concrete term discussed in this section involves the difference between fully prestressed and partially prestressed. For the purposes of this study, the dividing line between fully prestressed and partially prestressed is based on a nominal tensile stress in the precompressed tensile zone of $7.5\sqrt{f'_c}$. This value corresponds to the modulus of rupture for concrete (ACI 318 2008).

Chapter 2

Literature Review

In this investigation, experimental procedures were performed in order to determine the viability of partially post-tensioned concrete members in an aggressive environment, including the impact of cyclic loading. The following sections discuss important findings from references and studies directly related to this goal.

2.1 Fabrication of Prestressing Strand

Prestressing strand, shown in Figure 2-1, has a significant impact on the overall behavior of a prestressed concrete member (ACI 423.5R 1999). The fabrication process for prestressing strand, in turn, significantly affects the performance of the material under static, dynamic, and corrosive conditions (Jones 1996). It is therefore prudent to first discuss the way in which prestressing strand is fabricated.



Figure 2-1: Prestressing Strand

Prestressing strand is fabricated through a multi-step production process involving both chemical and physical alterations to the original base material. The first step in the production process begins with a high-carbon steel billet produced by continuous casting (Klein 2006). This billet contains four to five times as much carbon as that used for mild reinforcing steel (Preston 1990). The higher carbon content greatly increases the tensile strength but significantly decreases the ductility. The billet is then hot rolled to the desired rod diameter and cooled in a controlled process that results in a homogeneous pearlitic grain structure (Klein 2006).

The next step is drawing. The rod is cold-drawn through a series of eight or nine carbide dies that progressively reduce the rod's diameter (Sumiden 2006). Besides reducing the rod to the desired wire diameter, the cold drawing process alters the microstructure of the steel (Klein 2006). The drawing process aligns the grain structure into a fibrous geometry, increasing the tensile strength of the steel from approximately 170 to more than 270 ksi (Sumiden 2006).

The next step is stranding. A prestressing strand is formed by helically wrapping six wires around a seventh, center wire that has a slightly larger diameter than the other six. Seven spools of wire are loaded into the stranding machine, which then wraps the wires at the required rate and pitch (Sumiden 2006). The stranding machine wraps the helical wires very tightly around the center wire to prevent slip (Podolney 1967).

The final step is stress relieving and stabilization (Preston 1990). In this thermo-mechanical process, the strand is heated to approximately 700° F while under a tension stress of approximately 40 percent of the strand tensile strength. This process relieves the residual wire drawing stresses, permanently elongates the strand, increases yield strength,

increases the ductility, and decreases relaxation losses in service (Preston 1990, Sumiden 2006). While still at 700° F, the strand is then quenched in a water bath, to lock in the permanent elongation and remove residual drawing lubricants from the strand surface (Sumiden 2006). After drying, the strand is wound onto spools for shipping.

As a result of this production process, prestressing steel exhibits a stress-strain relationship significantly different than mild steel. A detailed stress-strain diagram for Grade 270 prestressing strand is shown in Figure 2-2 (*e.g.*, Lin and Burns 1981, Nilson 1987).

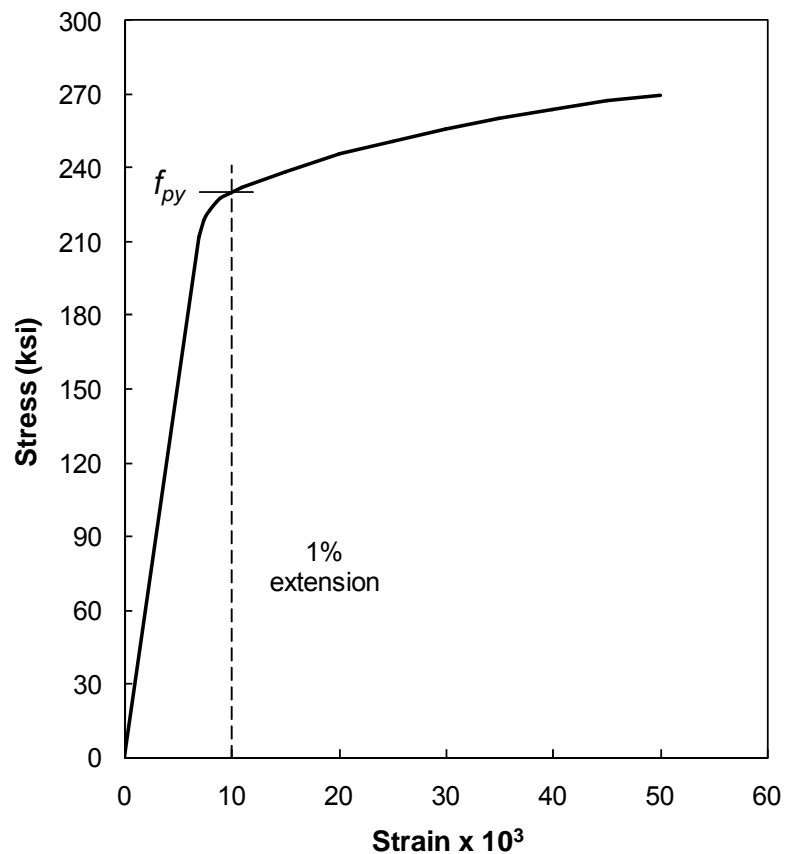


Figure 2-2: Stress-Strain Curve for Grade 270 Prestressing Strand

The most apparent feature of this stress-strain diagram is that prestressing strand does not possess a well defined yield point, but instead exhibits a proportional limit between 210 and 215 ksi. Between the proportional limit and a stress of about 230 ksi, the strand has a distinctly nonlinear region. After that point, the strand shows gradual yielding, but the curve continues to rise monotonically until the steel fractures at a stress of 270 ksi. As a result of this behavior, the yield point for prestressing strand is defined as the stress at which a total strain of one percent is reached (Nilson 1987). Another critical feature to take note of is the decreased ductility of prestressing strand compared to mild steel. Prestressing strand has a strain at failure of about 50 percent of that for Grade 60 mild steel.

The important findings from the discussion presented in this section are that the fabrication process for prestressing strand results in a unique macrostructure and microstructure that will impact the performance of the material under static, dynamic, and corrosive conditions. For instance, the unique make-up of seven individual wires for a single strand complicates the fatigue behavior as compared to a solid specimen. Furthermore, the unique grain structure results in a material that is distinctly anisotropic, which will impact fatigue crack growth and the nature of corrosion formation.

2.2 Corrosion of Prestressing Strand

Steel located in a high-pH environment, such as concrete or grout, is protected from corrosion by the formation of an oxide film (Jones 1996). This thin (~10 nm), dense film strongly adheres to the steel surface and prevents further metal ions from dis-

solving (Bentur *et al.* 1997). The corrosion process is not halted, but is reduced to a negligible amount (Bentur *et al.* 1997). Composed of both ferrous oxide, Fe(OH)₂ or FeO, and ferric oxide, FeOOH or Fe₂O₃, this film is chemically stable in concrete (Bentur *et al.* 1997). However, ferric oxide is the most stable and, over time, the ferrous oxide is slowly converted to ferric oxide, thus increasing the “strength” of the oxide film (Bentur *et al.* 1997). This film develops chemically in the sequence indicated by Eqs. 2.1 through 2.3.



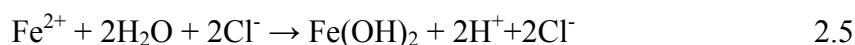
In the presence of chlorides in sufficient concentration, this stable passive film breaks down locally, and pitting occurs. The exact mechanism of pit formation (nucleation) is not completely understood (Jones 1996). However, based on extensive experimentation, it is believed that the chlorides react with the ferrous oxide portions of the passive film and produce a soluble complex as shown in Eq. 2.4 (Bentur *et al.* 1997).



This soluble complex, likely in the form FeCl₂, dissolves in the surrounding solution and fails to protect the strand (Bentur *et al.* 1997). Because this reaction competes with the conversion of ferrous oxide to ferric oxide, Eq. 2.3, it occurs more readily in the absence

of dissolved oxygen (Bentur *et al.* 1997). In other words, pit nucleation is more likely to occur in regions of low dissolved oxygen within the electrolyte.

The process of pit propagation, shown in Figure 2-3, is well understood (*e.g.*, Jones 1996, Broomfield 1997). Once failure of the passive film occurs, the iron is free to dissolve. The release of positively charged ferrous ions produces a potential gradient within the electrolyte, causing the chloride ions to migrate to the initiation site, resulting in the electrochemical hydrolysis reaction shown in Eq. 2.5.



The formation of hydrochloric acid (HCl), which readily dissociates, lowers the pH level at the initiation site. The result is a self-propagating or autocatalytic pit growth mechanism (Jones 1996). A lower pH at the initiation site increases the rate of iron dissolution, which increases the potential gradient within the electrolyte, which increases the migration of negatively charged chloride ions, which form additional hydrochloric acid, which lowers the pH further, which increases the rate of iron dissolution, *et cetera*.

Some of the ferrous ions migrate from the pit and oxidize at the pit mouth to form an insoluble, porous cap as shown in Figure 2-3. This cap reduces the further escape of dissolved iron but allows the smaller chloride ions to penetrate to the pit interior (Jones 1996). The chloride ions sustain the acid solution within the pit and result in the continued dissolution of iron (Jones 1996). The anodic reaction within the pit couples with a cathodic reaction on the strand surface, where oxygen is reduced to form hydroxyl ions, which increases the pH at these cathodic sites (Jones 1996).

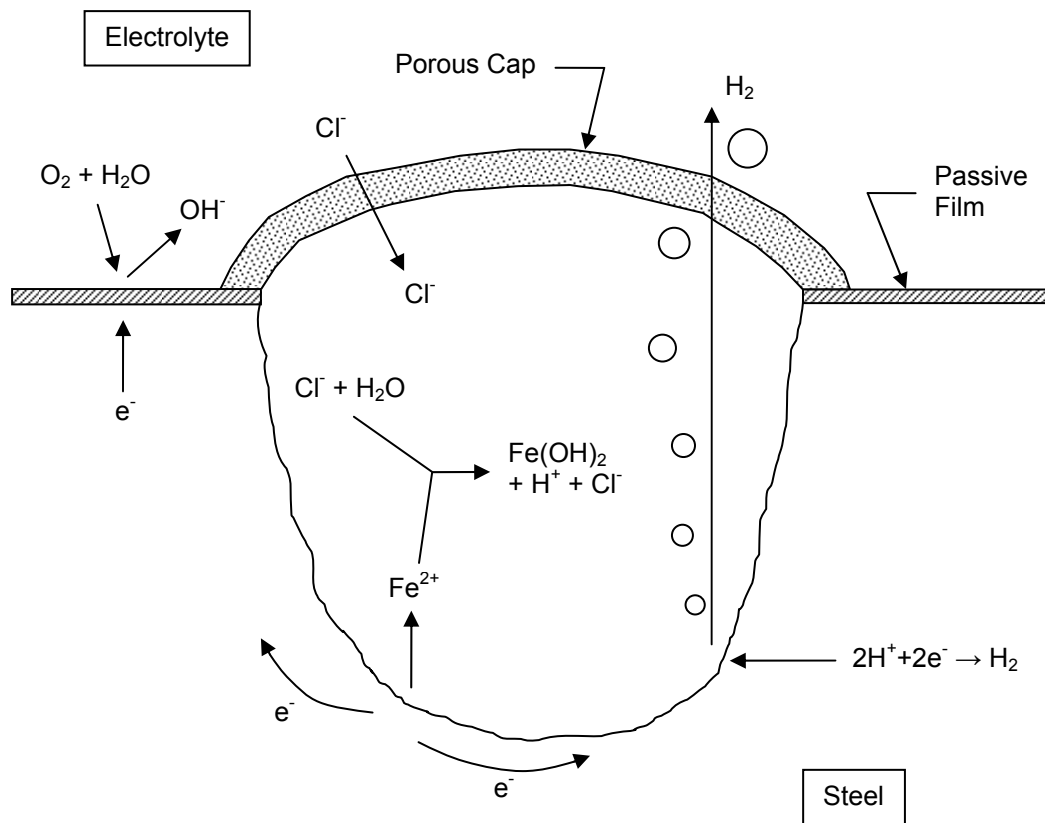


Figure 2-3: Schematic of Corrosion Pit Propagation in Steel

One additional important point to note is the formation of atomic hydrogen within the pit at some point during the corrosion process (see Figure 2-3). Due to the processes discussed previously, the environment within the pit is significantly different than that within the remainder of the electrolyte. The formation of hydrochloric acid (H^+) significantly reduces the pH within the pit. Dissolved ferrous ions also accumulate within the pit, due to formation of the cap. However, as shown in Figure 2-3, once the dissolved oxygen within the pit is depleted, water within the pit dissociates and combines with the ferrous ions to form ferrous hydroxide and hydrogen ions (ACI 222.2R 2001).

Electrons released during the dissolution of iron then combine with the hydrogen ions to form hydrogen atoms, which are adsorbed on the steel surface (Bentur *et al.* 1997). In most cases, atomic hydrogen will combine to form hydrogen gas molecules that bubble harmlessly out of the pit (Bentur *et al.* 1997). However, in a neutral or acidic solution, such as that occurring within the confines of the pit, atomic hydrogen resides on the steel surface for a significant time (Jones 1996). During this period, and because of atomic hydrogen's comparatively small size, atomic hydrogen may enter the metal crystal lattice and result in hydrogen embrittlement (Jones 1996). In general, atomic hydrogen diffuses through the metal crystal lattice of carbon steels at rates comparable to the diffusion of most ions through aqueous solutions, on the order of 10^{-6} in²/s (Krom *et al.* 1999, Pickering 2008).

The important finding from the discussion presented in this section involves the process of strand corrosion. Specifically, that pitting corrosion is the likely form of degradation for strand within a cementitious grout due to the ability of chloride ions to break down the protective oxide film. Pitting corrosion is also potentially more serious than general corrosion due to the highly localized loss of material. Furthermore, the pitting corrosion process results in the formation of hydrogen, which can readily diffuse through the metal lattice and potentially embrittle the steel.

2.3 Corrosion-Induced Failure of Prestressing Strand

Mild steel and prestressing strand can behave very differently under the effects of corrosion. Corrosion-induced damage to mild steel typically involves a loss of material

cross-section to the point that the reinforcing bar fails due to yielding (Bentur *et al.* 1997). This mode of failure is ductile and, although there is a loss of strength, the failure mode is identical to that which is experienced by non-corroded reinforcing bars. On the other hand, prestressing strand exposed to corrosion can fail in two very brittle ways. These two failure modes are referred to as: (1) stress corrosion cracking (SCC) and (2) hydrogen embrittlement (HE) (Jones 1996).

Both SCC and HE require a number of specific conditions in order to occur. Both require a material at a relatively high constant stress, which nearly always occurs with prestressing strand in service. Both require a material with a susceptible metallurgical structure, which occurs for prestressing strand because of its unique manufacturing process. Both also require an active corrosion state (Jones 1996). HE requires an acidic to neutral environment, since it requires the presence of an abundant amount of hydrogen, preferably in atomic or ion form (Jones 1996). As noted previously, pitting corrosion results in a localized environment conducive to the formation of atomic hydrogen at the steel surface.

The exact mechanisms involved in SCC and HE have been the subject of a great deal of research and much debate (Jones 1996). Complicating the issue is that the exact mechanisms for each type of failure can vary with the particular alloy under attack; the two failure modes often overlap; and it is often impossible to distinguish between the two (Bentur *et al.* 1997, Jones 1996). Nonetheless, they have one thing in common: they both cause the steel to fail in a brittle manner at a stress well below what would normally cause the material to fail.

It is generally believed that SCC is an extreme form of localized corrosion resulting in a micro-pit (Bentur *et al.* 1997). The stress is highly concentrated at the crack/pit tip at the same time that the material at the tip is dissolving (Bentur *et al.* 1997). This combination results in rapid crack growth and subsequent brittle failure (Jones 1996). Some researchers propose that hydrogen plays a role in SCC by weakening interatomic bonds at the crack tip (Jones 1996). As discussed previously, hydrogen is often present within a corrosion pit, even for a material in a high pH environment.

It is generally believed that HE is a result of the hydrogen atoms pinning dislocations within the material and thus preventing plastic deformations, the result of which is to embrittle the material (Bentur *et al.* 1997). This results in both decreased static and dynamic capacity. One type of hydrogen embrittlement, often referred to as hydrogen-induced cracking, occurs under constant stress and is very similar to SCC; the only difference is the definitive presence of hydrogen within the steel (Jones 1996). Another type of hydrogen embrittlement involves the fatigue capacity of a material. In this instance, it is believed that the embrittlement process can occur either prior to or concurrently with the fatigue loading (ACI 222.2R 2001, Nürnberger 2002).

The important finding from the discussion presented in this section involves the role of corrosion on the failure of prestressing strand under static and dynamic loading. This information is important because during the proposed experimental program, the strand will undergo exposure within the full-scale specimens while under a relatively high constant stress. Furthermore, the role of hydrogen embrittlement is critical to understanding the fatigue behavior of the strand for both the individual strand tests and the full-scale beam tests.

2.4 Individual Strand Fatigue Testing

Research has shown that the fatigue life of a partially prestressed member can be predicted from the lesser of the reinforcing steel or prestressing strand fatigue lives (ACI 423.5R 1999). Thus, the fatigue capacity of the prestressing strand itself is significant in understanding the fatigue behavior of the member as a whole. The following section discusses research on individual strand testing, including tests on both “clean” and corroded strand.

Paulson (1983) completed the most extensive study to date on the fatigue capacity of “clean” prestressing strand. This study compiled over 700 data points collected from 20 different researchers. Paulson also completed 50 fatigue tests to include with the data. Based on a statistical analysis, Paulson proposed a lower 5th percentile fracture design model, as shown in Eq. 2.6; where N is the number of cycles to failure, and S_r is the stress range in ksi.

$$\text{Log } N = 11 - 3.5 \text{ Log } S_r \quad 2.6$$

Also included in Paulson’s report is a mean fatigue life model (excluding grip failures), as shown in Eq. 2.7, with the variables as defined previously.

$$\text{Log } N = 12.67 - 4.23 \text{ Log } S_r \quad 2.7$$

Considerable research has been performed on “clean” prestressing strand (*e.g.*, Paulson *et al.* 1983, Tide and VanHorn 1966, Warner and Hulsbos 1966). However, only limited research has been performed on the mechanical properties of strand subjected to

corrosion or hydrogen embrittlement. With increasing concerns over durability, researchers have begun to study this issue.

MacDougall and Bartlett (2002) investigated the static mechanical behavior of corroded, monostrand tendons. Their method of corrosion involved unwinding the prestressing strand and spraying it with a salt solution. This approach generally leads to uniform corrosion as opposed to pitting corrosion. However, it was appropriate for a study of ungrouted, monostrand tendons. MacDougall and Bartlett found that the tendon lift-off test currently recommended by ACI Committee 423 does not always reveal the presence of broken wires because of the increased interwire friction from corrosion.

Siegwart (2006) investigated the impact of electrochemical chloride extraction (ECE) on the static and fatigue properties of prestressing strand. ECE is a method of removing chlorides from an existing structure in order to extend its service life. As discussed previously, chlorides initiate and propagate corrosion of embedded steel in concrete. Siegwart found that the ECE process temporarily reduced the fatigue life of prestressing strand due to hydrogen embrittlement.

Lopes and Simoes (1999) investigated the fatigue resistance of corroded prestressing strand and recommend a reverse bend test to study degradation of the strand. The method of strand corrosion in this study consisted of either a salt spray or immersion in a pH neutral, salt solution. Uniform corrosion, sometimes including uniform pitting, occurred in all of their strand specimens. The bend test recommended by the researchers concentrates the highest stress change at only one point along the strand.

Nürnberg (2002) summarized a significant amount of work performed in Europe concerning corrosion damage to prestressing strand. The paper discusses the causes

and mechanisms of corrosion, methods of preventing corrosion, and the results of corrosion on the behavior of prestressing strand. Nürnberger concludes that local corrosion is the most detrimental form of corrosion experienced by prestressing strand. Figure 2-4 is a plot from Nürnberger that shows the degradation in fatigue capacity of cold drawn prestressing wire as a function of pitting corrosion (based on 2,000,000 cycles).

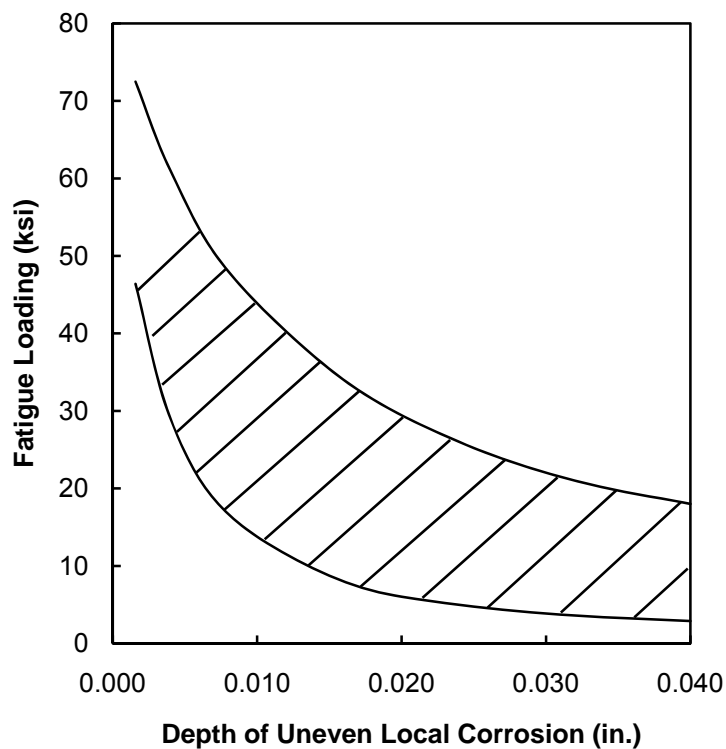


Figure 2-4: Fatigue Capacity of Prestressing Wire as a Function of Pitting Corrosion. Nürnberger (2002) Reproduced with Permission.

The important findings from the discussion presented in this section involve the previous testing performed on both “clean” and corroded prestressing strand. Paulson (1983) offers the most comprehensive treatment of fatigue testing of “clean” prestressing steel, summarizing over 700 data points collected from 20 different researchers spanning the last 50 years. With regard to tests on corroded prestressing steel, Nürnberger (2002)

offers the most comprehensive treatment by summarizing the work performed in Europe. The other researchers discussed in this section dealt with corrosion and fatigue situations that have limited applicability to the current study.

2.5 Corrosion Fatigue

Corrosion fatigue is a complex phenomenon that involves the simultaneous action of corrosion and cyclic stress (Shipilov 2005, Wang 2000). In general, true corrosion fatigue results when the two individual processes of corrosion and fatigue act in concert and result in failure of the material in less time than either action acting alone. The mechanism of corrosion fatigue involves one of two possible modes: anodic slip dissolution or hydrogen embrittlement. Anodic slip dissolution involves the following process after initial crack nucleation: rupture of oxide film, dissolution of metal, crack advance under cyclic stress, oxide growth, rupture of oxide film, dissolution of metal, *et cetera*. Hydrogen embrittlement, on the other hand, involves the reduction, adsorption, and diffusion of hydrogen from the corroding site to preferential locations within the metal lattice. The subsequent embrittling of the steel results in an increased rate of crack growth.

Actual situations of corrosion fatigue are highly complex and involve the interaction of multiple variables and mixed modes of crack propagation (Wang 2000). These variables include environmental, such as temperature, pressure, impurities, electrolyte pH, potential, and conductivity, mechanical, such as mean stress, frequency, and waveform, and metallurgical, such as impurity composition, microstructure, and cyclic deformation modes (Wang 2000). Furthermore, both true corrosion fatigue modes may occur

within the material under attack, and there is also a potential for stress corrosion cracking (SCC) to occur simultaneously with corrosion fatigue (Shipilov 2005).

The type of corrosion has a significant impact on the corrosion fatigue behavior of a particular alloy (Wang 2000). For instance, localized corrosion in the form of pitting often acts as a favorable location for crack nucleation and growth. However, pitting is not the only potential initiation site and is not a necessary precursor to failure (Shipilov 2005, Wang 2000).

The particular situation of pitting corrosion and fatigue crack nucleation and growth has been studied extensively in the aircraft industry (*e.g.*, Anderson 1995, Fett and Munz 1997). One particular variable that complicates this situation is the competing nature of corrosion and fatigue crack growth during the anodic slip dissolution mode of corrosion fatigue. Corrosion dissolves material but generally blunts the crack tip and reduces the fatigue crack growth rate (Chen *et al.* 1997). Chen *et al.* developed a rate competition criterion where the time-based crack growth rate has to exceed the pit growth rate for pit-to-crack transition.

The important findings from the discussion presented in this section involve the nature of true corrosion fatigue and the myriad complexities involved in this phenomenon. True corrosion fatigue results when the two individual processes of corrosion and fatigue act in concert and result in failure of the material in less time than either action acting alone. In addition, there are two modes of corrosion fatigue – anodic slip dissolution and hydrogen embrittlement – and both can occur simultaneously within a given material and set of conditions. Furthermore, actual situations of corrosion fatigue are highly

complex and involve the interaction of multiple variables and mixed modes of crack propagation.

2.6 Fatigue in Post-Tensioned Concrete Members

Fatigue loading on pretensioned members has been the focus of considerable research (Abeles *et al.* 1969, Foo and Warner 1986, Naaman 1982, Overman *et al.* 1984, Rabbat *et al.* 1978, Warner and Hulsbos 1966). Research on fatigue in post-tensioned members has been more limited, but has shown that fatigue life can be substantially shorter for post-tensioned members than for pretensioned members (Rigon and Thurlimann 1985, Ryals *et al.* 1992, Shahawi and Batchelor 1986, Wollman *et al.* 1988).

The shorter fatigue life of post-tensioned members is due to strand-against-strand fretting fatigue and strand-against-duct fretting fatigue. While in-air tests and small-scale tests of specimens with a single strand have been used successfully to investigate pretensioned members (Wollman *et al.* 1988), larger multi-strand specimens are necessary to capture the types of fretting fatigue common to post-tensioned members. Key variables in fatigue resistance of post-tensioned members include the duct type, strand type, stress range, and the curvature of the tendon. In studies on fretting fatigue in post-tensioned members (Rigon and Thurlimann 1985, Wollman *et al.* 1988), researchers found that the predominant mode of failure for metal ducts was strand-duct fretting, while the predominant failure mode for plastic ducts was strand-strand fretting. The use of epoxy-coated strand in Wollmann's studies reduced both types of fretting. However, Wollmann points

out that only a very limited number of plastic duct and epoxy-coated strand specimens were tested.

The important findings from the discussion presented in this section involve both the limited amount of research of fatigue in post-tensioned members and the phenomenon of fretting fatigue that is particular to post-tensioned concrete. Because of the limited amount of work performed to date, additional research is required in the area of fatigue and post-tensioned concrete, particularly if partial post-tensioning is to become a viable alternative. The other important finding is that fretting fatigue is a condition particular to post-tensioned concrete, and this characteristic will significantly alter the fatigue performance of the strand. Also, several of the key variables mentioned were incorporated into the test matrix for this study: duct type, stress range, and curvature of the tendon.

2.7 Chloride-Induced Corrosion in Post-Tensioned Members

Research in the area of chloride-induced corrosion for post-tensioned bridges is limited in part due to the long-term nature of durability studies. The development of new post-tensioning materials and systems in recent years has made some durability research obsolete. A large, long-term project was initiated in 1961 by Schupack and O'Neil (1997) to investigate end anchorage protection. Unfortunately, many of the post-tensioning materials used in the study are no longer used today. Because of this, there is limited data available on the susceptibility of current post-tensioning materials and systems to chloride-induced corrosion.

Perenchio *et al.* (1989) investigated different strand, end anchorage, grout, and duct types through a year-long exposure study of small-scale specimens. The epoxy-coated strand and plastic ducts were found to have better performance than uncoated strand and a traditional galvanized duct. Addition of silica fume or corrosion inhibitor (calcium nitrite) to the grout contributed little to corrosion performance. Even under laboratory grouting conditions, voids were found in the duct.

A large-scale research program at the University of Texas at Austin involved exposure testing of twenty-seven large-scale beam specimens and ten large-scale column specimens to investigate numerous combinations of variables for durable post-tensioned substructure design (Schokker 1999a, 1999b). Beam variables included prestress level, loading, grout type, concrete type, strand type, duct type, duct splices, and end anchorage protection. Column variables included foundation connection, post-tensioning protection, concrete type, and loading. The research included a comprehensive study on grouts for bonded post-tensioning, including fluidity testing, accelerated corrosion testing, and field-testing in a large-scale clear parabolic duct. Interim design guidelines were developed and long-term exposure testing is ongoing. Recommendations for immediate implementation from this project include the use of plastic duct, plastic chairs, fly ash concrete, and high performance grout. Specimens with higher levels of prestressing are generally showing less corrosion over time (Turco *et al.* 2007).

The important finding from the discussion presented in this section is that results from previous durability studies have limited value due to the constantly evolving nature of construction and the long-term requirements for this type of testing. Nonetheless, the recent study at the University of Texas offers data on the critical variables involved with

durability of post-tensioning systems. These critical variables include prestress level, loading, grout type, concrete type, strand type, duct type, duct splices, and end anchorage protection. Consequently, some of these key variables were incorporated into the test matrix for this study.

2.8 Grouts for Bonded Post-Tensioning

Portland cement grout is often used in post-tensioned structures to provide bond between internal tendons and the surrounding concrete, to discretely bond external tendons at diaphragms and deviators and as corrosion protection for the tendons. Grout for post-tensioning is usually a combination of Portland cement and water, along with any admixtures necessary to obtain required properties such as fluidity, thixotropy, and reduced permeability.

Voids can form in the post-tensioning duct from incomplete grouting, trapped air pockets, or from the evaporation of bleed water pockets. Bleed lenses that form as a result of the separation of water from the cement are accentuated by the addition of seven-wire strand, which acts as a water-transport mechanism (Schupack 1971). Ducts with vertical rises will typically experience more bleed due to the increased pressure within the grout column. By far the most common problem found in corroded post-tensioning tendons is poorly grouted or completely ungrouted tendons. In response to the need for proper grouting, the Post-Tensioning Institute completed the *Guide Specification for Grouting of Post-Tensioned Structures* (2003). This specification includes recommenda-

tions on grout materials and design based on research findings in this area (Schokker *et al.* 2001, 2002a, 2002b).

Voided areas in the duct leave a small section of strand unbonded and may have an effect on the fatigue properties of the member. While the effect of voids on the corrosion protection of the strand has been studied (Hamilton 1995, Schokker 1999a, Schupack 1974), this effect has not been studied with relation to fatigue. Key areas for voids are at high points (such as crests in draped tendons) and end anchorages. Larger voids may be less of a problem from a fatigue point of view, since the stress in the voided area will be distributed along that part of the tendon (acting as an unbonded tendon in the voided area). However, small voids or cracks in the grout may become problem areas. Voids at the end anchorage may allow significant movement causing fatigue concerns at the strand-wedge interface, particularly if corrosion has started in this area.

The important findings from the discussion presented in this section are that grouting defects impair the corrosion protection of the strand and may also impair the fatigue performance of the post-tensioning tendons. These defects may be in the form of voids, bleed water pockets, and bleed lenses. The typical locations for these voids are at the high points in the strand profile and at the end anchorages.

2.9 Level of Prestress

The subject of varying levels of prestressing has been a topic of much discussion (ACI 423.5R 1999, Bennett 1986, Cohn 1986, Freyermuth 1986, Ivering and Trost 1990, Naaman 1986). One serious concern about the use of sections with lower prestress levels

is reduced durability. A traditional fully prestressed section will be uncracked at service loads. As the percentage of post-tensioning decreases, the number of cracks in the loaded structural member tends to increase. Completely uncracked sections resist aggressive agents more effectively than cracked sections and are also more resistant to fatigue. However, there may be economic benefits to using sections with lower levels of prestressing. Even sections designed as uncracked may end up as cracked sections due to overload, excessive loss of prestress, or shrinkage stresses. The member should have a level of prestressing sufficient to provide adequate corrosion protection for the given application. The combination of cyclic loading and an aggressive environment for partially prestressed members needs to be investigated prior to widespread use of these sections in bridge applications.

The important finding from the discussion presented in this section is that partially prestressed sections are susceptible to cracking and thus raise concerns about corrosion and fatigue performance. Cracking of the concrete removes one of the levels of protection enjoyed by a fully prestressed element. Cracking of the concrete also results in a higher stress range for the tendon during the application of live load to the element. These two concerns are the critical issues of this study.

2.10 Unanticipated Loss of Prestress

If a fully prestressed element experiences an excessive loss of prestress, it will behave as a partially prestressed design, which will crack during the application of live load. Excessive loss of prestress can occur due to a number of factors, such as construc-

tion defects, material defects, overload, corrosion, and retrofitting. This loss of full prestress does not necessarily condemn the structure. In truth, the structure typically still possesses sufficient strength to support load over some service life – although likely not the full service life that was originally intended. However, no design guidelines exist to assist the engineer in determining what that safe service life is.

During his tenure as a forensic engineer for Construction Technology Laboratories, Inc. (CTL), the author encountered a wide variety of projects involving unintentional loss of full prestress. These projects dealt with both new and existing construction and both pretensioned and post-tensioned concrete structures. Problems so encountered are described in a general sense in the following sections.

2.10.1 Construction Defects

Construction defects likely account for the largest unintentional loss of prestress in post-tensioned concrete structures. These defects are common to almost all construction projects to some degree. However, in many field cases, these defects led to serious concerns about the integrity and service life of the structure. Typical construction defects that result in less than full prestress include: improper tendon profile, improper tendon location, honeycombing at end anchorages and low points in the tendon profile, and lack of full tensioning of the tendons.

A typical improper tendon profile involves a slight to pronounced reverse curvature of the tendon near the low point or high point of the drape. This reverse curvature induces forces opposite to the intended prestress, thus adding to the stresses due to load-

ing instead of counteracting them. The overall affect is equivalent to a reduced level of prestress in the member.

Improper tendon location involves either misplacement of the tendon within the formwork or movement of an improperly secured tendon during concrete placement. An improper tendon location, well beyond any acceptable construction tolerance, alters the stress distribution of the cross section. Any loss of tendon eccentricity reduces the pre-compression of the tension zone of a member.

Honeycombing at end anchorages and low points in the tendon profile is not an uncommon problem in post-tensioned concrete construction. Due to its internal location, the honeycombing often goes unnoticed prior to the stressing operation. In the majority of instances, the stressing operation reveals the defect when it occurs at the end anchorages. However, in some instances, the end anchorage has slipped well after the stressing operation yet prior to tendon grouting. If this goes unnoticed, the result is a reduction in the level of prestress. Honeycombing at low points in the tendon profile typically results in localized straightening of the tendon during stressing, which is equivalent to the affect of an improper tendon profile or tendon location.

2.10.2 Material Defects

Although not nearly as common as construction defects, material defects have been known to result in less than full prestress of post-tensioned concrete structures. In essence, the material defects resulted in significantly greater than anticipated prestress losses, thus reducing the effective prestress. The two most common defects are increased

creep and shrinkage of the concrete. Both defects are usually related to greater than specified water-cement ratios in the concrete. However, in a few cases, inadequate curing resulted in excessive premature drying of the concrete and contributed to the excessive losses.

2.10.3 Additional Factors

Exceeding the design load of a prestressed structure can result in cracking of the cross section. Such cracks, due to the small gauge length and local debonding of the tendon, can result in local yielding of the prestressing tendon. Excessive overload of a post-tensioned bridge in New Jersey initiated yielding in the prestressing tendon that reduced the level of effective prestress (Oesterle and Volz 1994).

Tendon corrosion may occur in a fully prestressed section causing a loss of prestress force due to wire breakage. Corrosion issues are discussed in more detail in Sections 2.2 and 2.3.

One research aspect of the FHWA Jointless Bridge Project involved retrofitting existing jointed bridges (Oesterle *et al.* 2007). A jointless bridge is subjected to internal restraint strains, continuity strains, and longitudinal restraint strains that typically do not exist in a jointed bridge. These additional secondary stresses may add to the stresses due to dead and live loads and need to be included in the original design approach. However, the amount of prestress in a retrofitted bridge is already set. As a result, a retrofitted jointed bridge is essentially partially prestressed, and fatigue of the prestressing tendons becomes a design issue.

The important finding from the discussion presented in Section 2.9 is that a fully prestressed element that experiences an excessive loss of prestress will behave as a partially prestressed design. Thus, the guidelines developed as part of this study will be directly applicable to this situation, for which no current guidelines exist.

2.11 Code Provisions and Committee Recommendations

The AASHTO LRFD Bridge Design Specifications (2008) limit both the allowable stress range and maximum curvature for a prestressing strand. The minimum radii of curvature for a strand is set at 20 feet, except in anchorages areas where a minimum of 12 feet is permitted. The allowable stress range is 18 ksi when the strand radius is equal to or greater than 30 feet and 10 ksi when the radius is equal to 12 feet, with a linear interpolation allowed between these limits. These values correspond to 0.067 and 0.037 times the guaranteed ultimate tensile strength (GUTS), f_{pu} , for Grade 270 strand, respectively. For conditions where the strand radii exceed the limits stated or where there is concern over metal-to-metal fretting fatigue, the designer is directed to consult the applicable literature to determine revised fatigue limits.

Some researchers (Ryals *et al.* 1992, Wollman *et al.* 1988) have proposed applying the AASHTO LRFD Fatigue Categories B and C to the design of prestressing strand for fatigue. Although these were originally developed for structural steel weldments, comparison with a significant amount of test data reveals good agreement with the fatigue design curves for these categories.

The CEB-FIP Model Code (1990) limits the allowable stress range for prestressing strand based on a minimum fatigue life of 2,000,000 cycles. The allowable stress range is equal to $0.15f_{pu}$, with a minimum applied stress not to exceed $0.75f_{pu}$.

Although ACI 318 Building Code Requirements for Structural Concrete (2008) does not contain any specific limitations, ACI Committees 215 and 423 have recommendations for fatigue limits of prestressing strand. As in the CEB-FIP Model Code, these recommendations are based on a minimum fatigue life of 2,000,000 cycles. The allowable stress range recommended in ACI 215R (1997) is equal to $0.06f_{pu}$, with a minimum applied stress not to exceed $0.60f_{pu}$. However, in locations of tendon curvature where fretting fatigue may be an issue, ACI 215R limits the stress range to $0.054f_{pu}$. The allowable stress range recommended in ACI 423.5R (1999) is equal to $0.10f_{pu}$, with a minimum applied stress not to exceed $0.60f_{pu}$. However, ACI 423.5R also recommends Paulson's equation discussed in Section 2.4.

The code provisions and committee recommendations discussed previously are summarized in Table 2-1.

2.12 Summary

The goal of this study was to develop a better understanding of the interaction of corrosion and fatigue on partially post-tensioned concrete members. In order to pursue that goal, the author needed to investigate the current body of knowledge associated with

each critical aspect of this study, from prestressing strand performance to design code provisions and industry committee recommendations.

Table 2-1: Summary of Code Provisions and Committee Recommendations

Reference	Allowable Fatigue Stress Range	Minimum Stress Upper Limit	Remarks
AASHTO	$0.067f_{pu}$ $0.037f_{pu}$	- -	≥ 30 ft. radii 12 ft. radii
CEB-FIP	$0.15f_{pu}$	$0.75f_{pu}$	-
ACI 215	$0.06f_{pu}$ $0.054f_{pu}$	$0.60f_{pu}$ $0.60f_{pu}$	typical condition fretting concerns
ACI 423	$0.10f_{pu}$	$0.60f_{pu}$	also Paulson's eqn.

This investigation began by studying the single most important component of the system – the prestressing strand. Prestressing strand undergoes a very particular manufacturing process that involves both chemical and physical alterations to the original base material. These alterations affect the static, dynamic, and corrosive performance of the strand. In general, prestressing strand has excellent fatigue properties but is susceptible to corrosion, hydrogen embrittlement, and stress-corrosion cracking.

After investigating the prestressing strand, the author focused on durability of post-tensioned systems. Two major strengths of a post-tensioned structure for fighting corrosion are crack control and multiple levels of corrosion protection. These levels of protection can include the duct, grout, and strand coatings. However, construction de-

fects can occur that reduce the level of protection and lead to potential problems, particularly since the prestressing strand is usually inaccessible to view.

The next area of review involved the effect that different levels of prestressing have on the overall behavior of a post-tensioned member subjected to fatigue and corrosion. A fair amount of research has been performed on the fatigue performance of pre-tensioned, partially prestressed concrete members. However, very little research has been performed on post-tensioned, partially prestressed concrete members. A significant amount of research has also been performed on corrosion of post-tensioned concrete members. However, no research had been performed on the combination of fatigue and corrosion on the behavior of partially post-tensioned concrete members.

Finally, the investigation touched on the various code provisions and committee recommendations pertaining to fatigue of prestressed concrete members. These provisions were summarized in Table 2-1.

The results of this literature review then served as the starting point for this research endeavor.

Chapter 3

Individual Strand Testing

This chapter discusses the exposure, fatigue testing, and analysis of individual strand specimens for the specific sequence of corrosion followed by fatigue to failure. The objective of this testing was to develop a relationship between the amount of corrosion on the strand and the resultant fatigue capacity. Research has shown that the fatigue life of a partially prestressed member can be predicted from the lesser of the reinforcing steel or prestressing strand fatigue lives (ACI 423.5R 1999). Thus, the ultimate intent was to determine whether this strand corrosion-fatigue relationship could then predict the response of full-scale beam specimens undergoing the same sequence of exposure to chlorides followed by fatigue until failure. Testing of the full-scale beam specimens is discussed in Chapter 5.

The methodology developed for this corrosion fatigue study of prestressing strand involved the following steps: (1) corrode the strand samples to different amounts of section loss; (2) characterize the amount and disposition of the corrosion; (3) test the strand samples under cyclic loading until failure; and (4) determine a relationship between the amount of strand corrosion and the resulting fatigue capacity.

The author investigated both analytical and empirical approaches to develop this corrosion-fatigue relationship. The analytical approach involved Linear Elastic Fracture Mechanics (LEFM), which included several variations on how to treat the corrosion pit as either an initial defect, stress concentrator, or simply a reduction in effective strand area.

The empirical approach examined the relationship between the number of cycles to failure and the following corrosion measurements: maximum pit depth, average pit depth, percentage loss of strand area, percentage of corroded strand surface, and percentage weight loss of strand. In the end, an empirical relationship proved the most reliable.

3.1 Corroding of Strand Samples

This section discusses the method of corroding the individual strand samples. The most important consideration with respect to corroding the strand samples is to mimic the exact conditions encountered in the field. Steel located in a high pH environment, such as concrete or grout, is protected from corrosion by the formation of an oxide film (Böhni 2000). However, if chloride ions in sufficient concentration come in contact with this film, the passivating layer will break down, resulting in pitting corrosion (Böhni 2000). Pitting corrosion is potentially more dangerous to the integrity of the strand than uniform corrosion because the corrosion cell is concentrated at a few locations, resulting in a highly localized loss of material.

To mimic this mechanism, strand samples were placed in a simulated concrete pore water solution containing five percent by mass of NaCl salts. The pore water solution consisted of deionized water mixed with the following concentrations of hydroxides (Christensen *et al.* 1992):

0.32 mol/L of KOH,

0.17 mol/L of NaOH,

0.07 mol/L of Ca(OH)₂

The author placed the strand samples within the above solution and allowed them to corrode at their own natural pace, as shown in Figure 3-1. (Initial testing accelerated the degradation process by applying an electrode potential to the strand sample. However, as discussed in Appendix A, this method was subsequently abandoned.) A plastic container measuring 26.5"x 15.8"x 6.5" was used to contain the pore water and NaCl salt solution. A 1/2" diameter hole was drilled in the short sides of the container through which the strand sample was placed. These holes were subsequently sealed with a rubber-silicone caulk. This arrangement was used to limit the exposed portion of the strand to the center two-thirds, eliminating corrosion within the vicinity of the attachment points to the fatigue frame.



Figure 3-1: Non-Accelerated Corrosion Setup

Due to potential wicking affects, the strand regions outside of the plastic container underwent additional protective measures. Prior to placing the solution in the container, the strand end regions were first dipped into low-viscosity oil and then coated in high-viscosity grease. The oil penetrated between the individual wires, and the grease coated the exterior surfaces and sealed in the oil. Post-fatigue testing examination revealed excellent protection of the strand end regions through this method.

As shown in Figure 3-1, some of the calcium hydroxide does not go into solution (the white material on the strand and bottom of the container). When the above concentrations of hydroxides are added to the deionized water, the mixture becomes saturated. Because calcium hydroxide has the lowest solubility of the three hydroxides, a portion of the calcium hydroxide remains in suspension and eventually settles to the bottom of the solution. The pH of the solution was tested at three separate times: immediately after mixing of the water and hydroxides; immediately after the undissolved portion of the calcium hydroxide settled to the bottom of the solution; and, finally, two months after mixing. At all three times, the pH measured approximately 13.3, which is consistent with values for concrete and grout and facilitated the formation of an oxide film on the strand.

However, due to the length of time required to corrode many of the samples, pH testing of the solution continued at two-month intervals. For the majority of measurements, the pH remained at 13.3 due to periodic addition of solution to compensate for evaporation. However, at certain times of the year when the evaporation rate slowed and the solution was not replenished as often, the pH fell to values of 10 to 12. The likely cause of the drop in pH is carbonation of the solution due to carbon dioxide (CO_2) in the air, similar to carbonation of concrete although occurring much faster in an aqueous solu-

tion. Subsequent adjustments to the testing protocol maintained the pH above 13 for all samples throughout the immersion period.

The author also investigated the following non-electrochemical techniques to decrease the time to corrosion of the strand samples:

1. periodic agitation of the solution;
2. active aeration of the solution;
3. sealing of the setup; and
4. varying the NaCl salt concentrations.

Even with the inherently variable nature of pitting corrosion, the author was able to identify which characteristics were most favorable to initiating and propagating the process. The optimum conditions consisted of a stagnant solution, open to the air, and containing five percent by mass of NaCl salts. The stagnant solution conclusion is consistent with other pitting corrosion research studies (Böhni 2000). Consequently, active aeration of the solution, meant to provide an abundance of dissolved oxygen, actually increased the time to corrosion due to its agitating effect. It is also likely that the initial amount of dissolved oxygen within the solution was sufficient to passivate the strand and induce pitting in the presence of chlorides (Jones 1996). Thus, sealing the container had no influence on the process. With respect to the NaCl salt concentration, levels above five percent did not shorten the time to initiation.

Partial immersion of the strand will also accelerate pit formation due to the formation of differential aeration cells (Jones 1996). Cathodic areas naturally form at the waterline due to the abundance of dissolved oxygen near the surface of a stagnant solution (Jones 1996). Anodic areas, on the other hand, form nearby but lower down in the solu-

tion where oxygen is not as readily replaced (Jones 1996). The anodic site also favors a location as close as possible to the cathodic site, in order to reduce distance (resistance) within the electrolyte, yet still within an area of decreased dissolved oxygen (Jones 1996). In other words, in a partially submerged horizontal section of strand, pitting will form very near, but not at, the waterline. Initially, the author employed this technique, as opposed to full immersion, to accelerate the corrosion process. However, considerable care is required to prevent uniform corrosion on portions of the strand located above the waterline, and this method may force the pitting to occur at predetermined locations. Instead, the author fully immersed the strand but located it very near the surface of the solution, which also tended to accelerate the corrosion process but eliminated the problems mentioned above.

Pitting corrosion is inherently unpredictable (Böhni 2000, Jones 1996). During the corrosion step of the process, the author found little consistency between the amount of time within the solution and the resulting amount and distribution of corrosion. Some strand samples started corroding within two weeks after placement within the solution, while many others did not start corroding until two months after placement. A few samples did not start corroding for over a year. Furthermore, the number of pitting locations varied between strand samples, even between those samples that started corroding at approximately the same time after placement within the solution. Nevertheless, with time and patience, the author was able to obtain a series of samples that represented various levels of pitting corrosion.

3.2 Characterization and Measurement of Corrosion

This section discusses the characterization and measurement of the corrosion experienced by the individual strand samples. In general, the strand experienced two types of localized attack – pitting corrosion and crevice corrosion – in approximately equal amounts. Figure 3-2 shows the typical pitting corrosion attack of the strand, and Figure 3-3 shows the typical crevice corrosion attack of the strand. Both types of corrosion are typical for an alloy in a high pH and salt enriched environment (Jones 1996).

While pitting corrosion and crevice corrosion share similar mechanisms, crevice corrosion is controlled more by geometric constraints, such as those that occur due to the seven-wire make-up of the strand (see Figure 2-1). The interstitial spaces created by the six helically wrapped wires provide a geometry that is conducive to the formation of crevice corrosion. However, because of the non-traditional crevice shape formed by the wires (*i.e.*, variable thickness instead of constant thickness), the corrosion experienced within these interstitial spaces is more pitting-like and less crevice-like in its morphology.

The morphology of classic crevice corrosion is shown in Figure 3-4 (Jones 1996). The shape of the section loss within the crevice follows the shape of the active and passive regions of the anodic polarization curve (Pickering 2003). However, studies have shown that pitting can form near the mouth of very tight crevices (Jones 1996), such as those that occur between adjacent wires of the strand. Furthermore, research has shown that the presence of chlorides in the electrolyte can promote the formation of pitting near the mouth of a crevice (Cho and Pickering 1991).



Figure 3-2: Pitting Corrosion Attack



Figure 3-3: Crevice Corrosion Attack

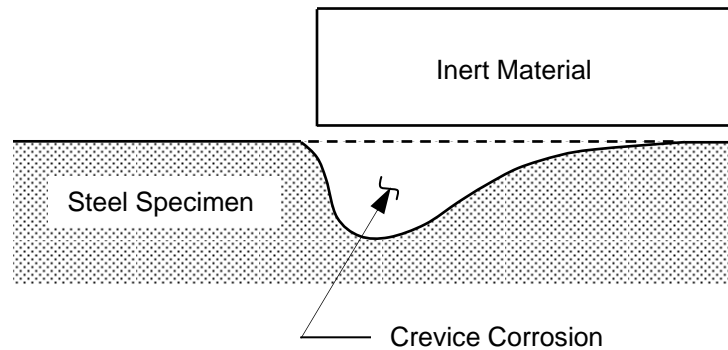


Figure 3-4: Schematic of Typical Crevice Corrosion Attack

Examination of the corrosion that occurred within or very near the interstitial wire spaces revealed a section loss that resembled an elongated pit, both in shape and in surface texture. The interior surface of the crevice corrosion appeared virtually identical to the interior surface of the pitting corrosion experienced by the strand. This finding is very critical because research has shown that pitting corrosion typically results in open and polished hemispherical pits, while crevice corrosion can result in etched crack-like shapes (Böhni 2000). Crack-like shapes would tend to exhibit a much higher stress concentrating affect during the subsequent fatigue loading. It would appear that the geometry of the interstitial spaces promoted pit formation that, once reaching a certain hemispherical shape, had its growth pushed parallel to the adjacent wires, resulting in an elongated pit shape. Consequently, the two types of localized corrosion were treated identically in determining a relationship between the amount of corrosion and the resulting fatigue capacity.

Tables 3-1 and 3-2 contain the results of the strand corrosion mapping and measurements for the strand samples. Table 3-1 contains the specimen designation, depth of localized corrosion, type of localized corrosion ('P' for pitting, 'C' for crevice), and wire location. The six outer wires were numbered clockwise from one to six, as shown in Figure 3-5. Prior to mapping, the specimens were thoroughly cleaned with a degreaser, wire brush, and steel wool pad. All localized corrosion visible to the unaided eye was included in the corrosion mapping. Pit depths were measured with a digital pit depth gauge having a range of 0 to 0.5 in. and a resolution of 0.0005 in. The measurements recorded in Table 3-1 represent the maximum depths measured for each individual pit.

Table 3-2 contains the specimen designation, net area, percentage of corroded strand surface, and percentage weight loss. The net area calculation was based on the minimum remaining area for all seven wires. In other words, if a particular wire had more than one corrosion pit, the area calculation for that wire was based on the largest pit depth. The percentage of corroded strand surface was based on the total strand area exposed to the solution, and the percentage weight loss was based on before and after weight measurements of each strand sample.

Autopsies performed after fatigue testing revealed no pitting of the center seventh wire. However, some samples exhibited a very light uniform corrosion of the center wire. For all specimens tested, the center wire never failed due to fatigue loading but instead suffered either a traditional cup-cone fracture or pulled out of the chuck due to failure of the six outer wires. In other words, the center wire only failed after a sufficient number of outer wires failed due to fatigue such that the stress in the center and remaining wires exceeded the ultimate tensile strength.

Table 3-1: Strand Specimen Corrosion Data

Specimen	Depth of Local Corrosion (in.)	Type of Local Corrosion	Wire Location
SC-1	0.002	P	6
	0.003	P	3
	0.003	C	1
	0.004	P	6
	0.005	C	1
	0.005	P	2
	0.009	C	4
	0.010	C	4
SC-2	0.003	C	4
	0.005	C	6
	0.007	C	6
	0.007	P	5
	0.009	C	1
	0.010	P	1
	0.010	C	2
	SC-3	0.010	C
0.011		C	5
0.011		P	3
SC-4	0.012	P	2
	0.013	P	6
	0.015	C	3
	0.016	P	3
	0.016	P	1
	0.016	C	4
SC-5	0.012	P	2
	0.012	P	2
	0.013	C	5
	0.014	C	6
	0.016	P	3
	0.017	C	4
	0.022	P	3

Table 3-1: Strand Specimen Corrosion Data (cont'd)

Specimen	Depth of Local Corrosion (in.)	Type of Local Corrosion	Wire Location
SC-6	0.008	C	3
	0.012	C	2
	0.014	P	4
	0.020	P	4
	0.020	C	2
	0.022	P	1
SC-7	0.024	C	5
	0.025	P	5
	0.025	C	4
SC-8	0.006	P	4
	0.019	C	2
	0.027	P	5
	0.030	P	4
	0.030	C	1
	0.033	C	1
	0.035	P	3
	0.035	C	3
SC-9	0.019	C	6
	0.023	C	1
	0.024	P	3
	0.029	P	3
	0.033	P	5
	0.035	C	4
SC-10	0.018	C	5
	0.028	C	5
	0.031	C	1
	0.033	C	6
	0.036	P	4
	0.037	C	3
	0.039	P	3
	0.050	P	2

Table 3-1: Strand Specimen Corrosion Data (cont'd)

Specimen	Depth of Local Corrosion (in.)	Type of Local Corrosion	Wire Location
SC-11	0.025	C	4
	0.037	P	2
	0.040	C	5
	0.040	C	6
	0.043	P	1
	0.048	P	2
SC-12	0.035	C	6
	0.035	C	2
	0.040	C	2
	0.046	P	5
	0.050	P	3

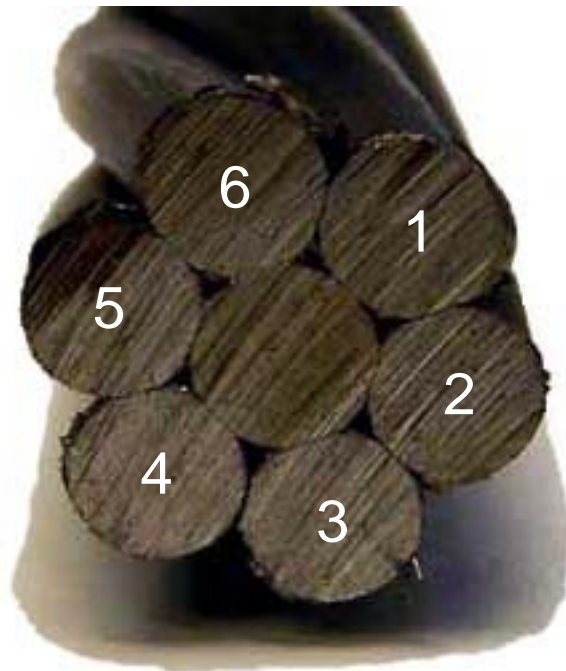


Figure 3-5: Wire Numbering Convention for Recording Corrosion Data in Table 3-1

Table 3-2: Strand Specimen Corrosion Data

Specimen	Net Area (in. ²)	Percentage of Corroded Strand Surface	Percentage Weight Loss
SC-1	0.1515	0.0032	0.0002
SC-2	0.1513	0.0043	0.0002
SC-3	0.1514	0.0028	0.0002
SC-4	0.1502	0.0087	0.0006
SC-5	0.1499	0.0169	0.0022
SC-6	0.1498	0.0138	0.0015
SC-7	0.1500	0.0137	0.0017
SC-8	0.1456	0.0619	0.0126
SC-9	0.1459	0.0381	0.0055
SC-10	0.1403	0.0836	0.0184
SC-11	0.1406	0.0699	0.0130
SC-12	0.1415	0.0788	0.0197

In addition to characterizing and measuring the localized corrosion experienced by the strand, it is important to note that hydrogen evolution occurred during the corrosion process. Figure 3-6 is a photograph of a strand sample undergoing pitting corrosion while in the simulated pore water and salt enriched solution. Mass spectrometer analysis of the bubbles shown in the figure indicated predominantly hydrogen gas, with trace amounts of nitrogen and oxygen. As shown in the figure, all of the bubbles coincide with

active pitting and, based on the mass spectrometry, support the theory put forth by numerous researchers (*e.g.*, Novokshchenov 1994, Bentur *et al.* 1997, Broomfield 1997) concerning hydrogen formation within a corrosion pit.



Figure 3-6: Hydrogen Evolution During Localized Corrosion Attack

These researchers postulated that with the production of free acid (H^+) within the pit, the lower pH results in a shift in the corrosion potential below the reversible hydrogen potential and the subsequent formation of atomic hydrogen. This process begins once the dissolved oxygen within the pit is depleted. At this point, water within the pit dissociates at the anode site to form H^+ protons. These protons migrate to the cathode site, which has moved inside of the pit, to combine with electrons released during the dissolution of iron to form hydrogen atoms.

Equally important as the presence of hydrogen is the fact that this corrosion process was allowed to occur at its own natural pace, without an artificially applied potential. This atomic hydrogen can either combine to form hydrogen gas, which bubbles harmlessly out of the pit (see Figure 3-6), or, in some instances, it can reside on the steel surface and eventually enter the metal lattice structure and embrittle the steel. It is impossible to observe whether any atomic hydrogen entered the strand samples.

3.3 Fatigue Test Setup, Test Parameters, and Test Results

This section discusses the fatigue test setup, test parameters, and test results for the individual strand specimens. To test the strand specimens in fatigue, they were placed in a supplemental frame within a 220 kip, servo-hydraulic, four-post, fatigue rated frame. A drawing of the test setup is shown in Figure 3-7, with a photograph of the test setup shown in Figure 3-8. Reusable chucks anchored the strand at each bearing plate. The author used chucks manufactured for 0.6" diameter strand because of the supplemental protection required to prevent the wedge teeth from biting into the strand, and thus causing a severe stress concentration and probable failure within the anchorage. This protection is shown in Figure 3-9 and discussed in more detail in Appendix B. To prevent the helically wrapped wires from unwinding during the test, the author installed an anti-rotation device as part of the supplemental test frame (see Figure 3-8). Essentially a vertical roller, the anti-rotation device allowed free vertical movement during the fatigue loading but restrained rotation of the actuator head.

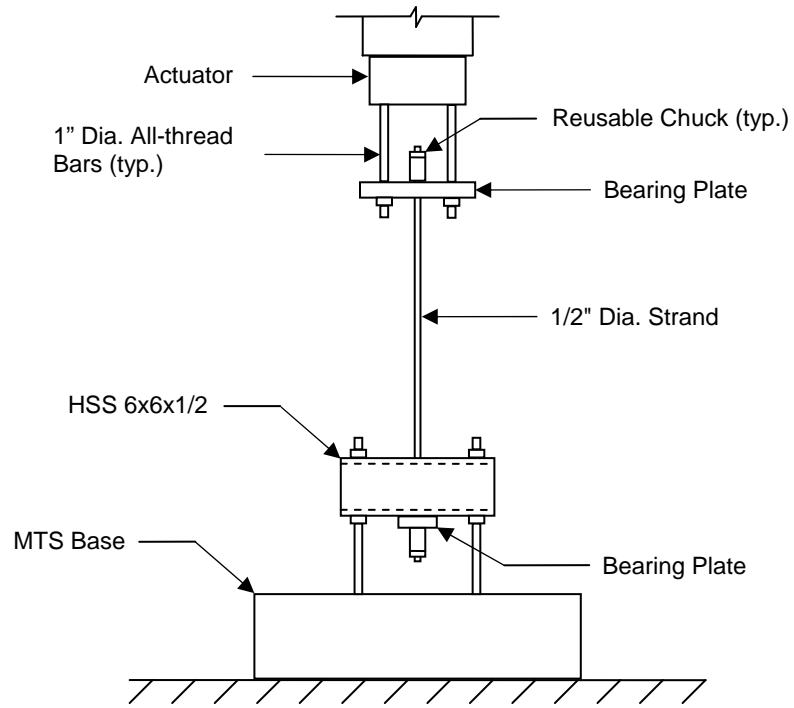


Figure 3-7: Strand Specimen Fatigue Test Setup

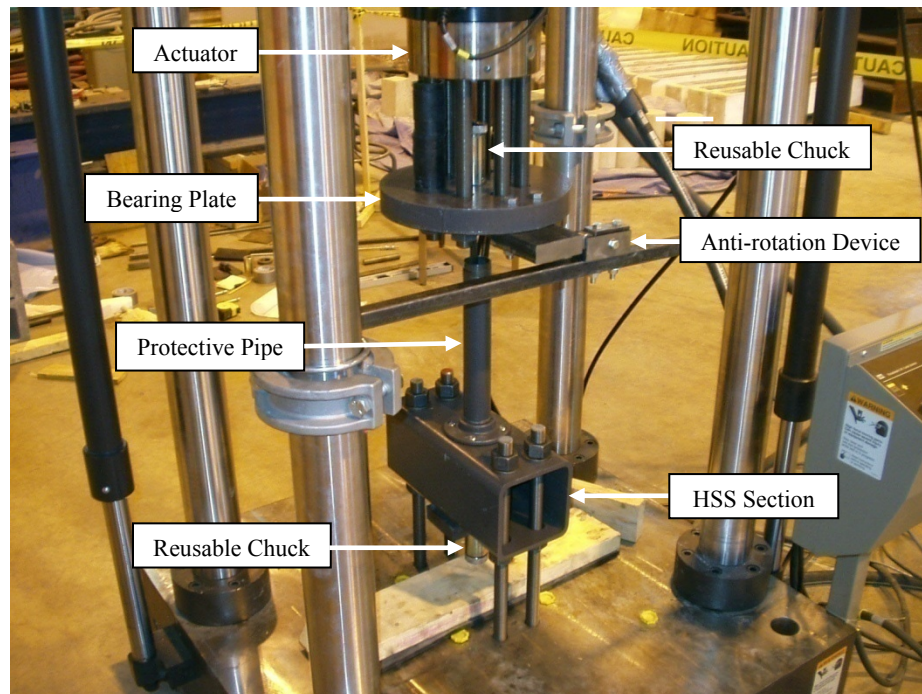


Figure 3-8: Strand Specimen Fatigue Test Setup



Figure 3-9: Strand Specimen End Treatment for Fatigue Testing

The author selected a 36" gage length for the 1/2"-diameter strand specimens. ASTM A416 (2005) prefers a minimum test length of 60 times the nominal strand diameter, although it also allows 40 times the nominal strand diameter. Consequently, a minimum gage length of 30" would satisfy ASTM A416. ACI 423.7 (2007) requires a minimum gage length of 36" for tendon fatigue testing. To account for the end anchorage treatments discussed previously, all strand specimens were cut to a length of 46". ASTM A370 (2005) cautions against applying significant heat to a strand test specimen, thus the author cut all specimens with an abrasive saw as opposed to torch cutting. All of the fatigue specimens were taken from the same spool of prestressing strand.

For the fatigue testing, the author chose $0.60f_{pu}$ as the minimum applied stress and $0.75f_{pu}$ as the maximum applied stress. Thus, for a strand area of 0.153 in.^2 and an ultimate tensile strength of 270 ksi, these stresses correspond to minimum and maximum loads of 24.8 and 31.0 kips, respectively. The value of $0.60f_{pu}$ represents a reasonable lower bound for the effective prestress after losses due to anchor seating, creep, shrinkage, friction, and steel relaxation (*e.g.*, ACI 318 2008, ACI 215R 1997, Paulson 1983). The value of $0.60f_{pu}$ is also the traditional lower bound used in 95 percent of the strand fatigue studies performed in the last 50 years (Paulson 1983).

For the upper bound, both AASHTO LRFD (2008) and ACI 318 (2008) limit the maximum applied strand stress to a value of $0.80f_{pu}$, although this limit applies during the jacking operation. Immediately after transfer, both codes currently limit the maximum strand stress to a value of $0.74f_{pu}$. For a partially prestressed concrete section, the stress increase due to live load, which represents the cyclic portion of the fatigue loading, will primarily vary as a function of the dead-to-live-load ratio and the level of partial prestressing chosen by the designer. Therefore, the author performed a parametric study of typical partially prestressed designs and found the strand stress to vary between 0.65 and $0.75f_{pu}$ during the application of live load. Thus, the upper bound was chosen as $0.75f_{pu}$. However, it is important to mention that the actual stress range selected was not critically important, as the intent of the strand study was to determine how corrosion reduced the fatigue capacity for a given stress range.

The author used load-controlled sequencing for this study. Fatigue testing requires a load sequencing method, either in the form of a stress-controlled or displacement-controlled approach. For strand fatigue testing, all previous research used load controlled sequencing (Paulson 1983). For typical “solid” test specimens, load-controlled sequencing would be equivalent to stress-controlled sequencing, as the entire section participates in resisting the applied load during the entire test. However, for a strand specimen, individual wire breaks will usually occur during the fatigue test, but often these do not result in the instantaneous failure of the specimen. Multiple wire breaks are usually required before the specimen fails. Furthermore, in an actual beam section, due to internal force equilibrium, the strand is required to resist the same force even after some of the

individual wires fail. Consequently, load-controlled sequencing is the normal method of controlling a strand fatigue test, and thus it was the method chosen for this study.

These load-controlled tests were run at a frequency of 2 Hz, which was the maximum capacity for the MTS system with a strand specimen in place. This frequency is well below any value that would cause significant heating of the specimen during the test, which would subsequently alter the test results. Excessive heating alters the properties of the strand from what which would be encountered in practice, particularly the fatigue properties (ASTM A370 2005).

To ensure proper operation of the fatigue setup and end anchorage method outlined previously, three as-received (“clean”) strand specimens were tested to failure in the fatigue frame. The results of the tests are shown in Table 3-3. The test results averaged 743,607 cycles with a standard deviation of 95,501 cycles and a coefficient of variation of 12.8 percent. Most importantly, none of the three specimens failed within the end anchorages, with all wire breaks occurring within 6” of the strand centerline.

Table 3-3: Fatigue Results for As-received Strand

Specimen	Cycles to Failure
S-1	734,088
S-2	653,222
S-3	843,512

These test results were also compared to the value predicted from Paulson's mean fatigue life equation (1983), given in Section 2.4, which was based on over 700 individual strand fatigue tests performed over the last 50 years. For a stress range of $0.15f_{pu}$ and an ultimate tensile strength of 270 ksi, Paulson's equation gives a mean fatigue life of 742,105 cycles, which compared very well with the test average of 743,067 cycles. Therefore, based on this favorable comparison with previous testing, failure of the strand specimens away from the end anchorages, and the relatively low coefficient of variation for the test results compared to most strand fatigue testing (Paulson 1983), the test frame and anchorage method were deemed acceptable, and the author proceeded with fatigue testing of the corroded prestressing strand specimens.

The results of the fatigue tests of the corroded strand are shown in Table 3-4. The specimen designations are the same as those used in Tables 3-1 and 3-2.

Table 3-4: Fatigue Results for Corroded Strand

Specimen	Cycles to Failure	Specimen	Cycles to Failure
SC-1	537,444	SC-7	355,712
SC-2	656,026	SC-8	202,758
SC-3	348,889	SC-9	376,388
SC-4	300,018	SC-10	269,172
SC-5	512,078	SC-11	148,800
SC-6	444,922	SC-12	240,084

3.4 Corrosion-Fatigue Relationship

This section discusses the analytical and empirical approaches used by the author to develop a predictive relationship between the amount of strand corrosion and the resulting fatigue capacity. The analytical approach involved Linear Elastic Fracture Mechanics (LEFM), which included several variations on how to treat the corrosion pit as either an initial defect, stress concentrator, or simply a reduction in effective strand area. The empirical approach, on the other hand, examined the relationship between the number of cycles to failure and the following corrosion measurements: maximum pit depth, average pit depth, percentage loss of strand area, percentage of corroded strand surface, and percentage weight loss of strand. Following the predictive approaches is a discussion of the complex factors that influence the fatigue capacity of corroded prestressing strand as well as prestressing strand in general.

The strand test results are presented in Figures 3-10 through 3-14. The independent variables are maximum pit depth, average pit depth, percentage loss of strand area, percentage of corroded strand surface, and percentage weight loss of strand, respectively. The dependent variable is number of cycles to failure. The data is contained in Tables 3-1 through 3-4. For the plot of average pit depth, Figure 3-11, the independent variable represents the numerical average of the pit depths recorded in Table 3-1 for a particular strand specimen. The data presented in Figures 3-10 through 3-14 was used as the basis for the LEFM and empirical studies that follow.

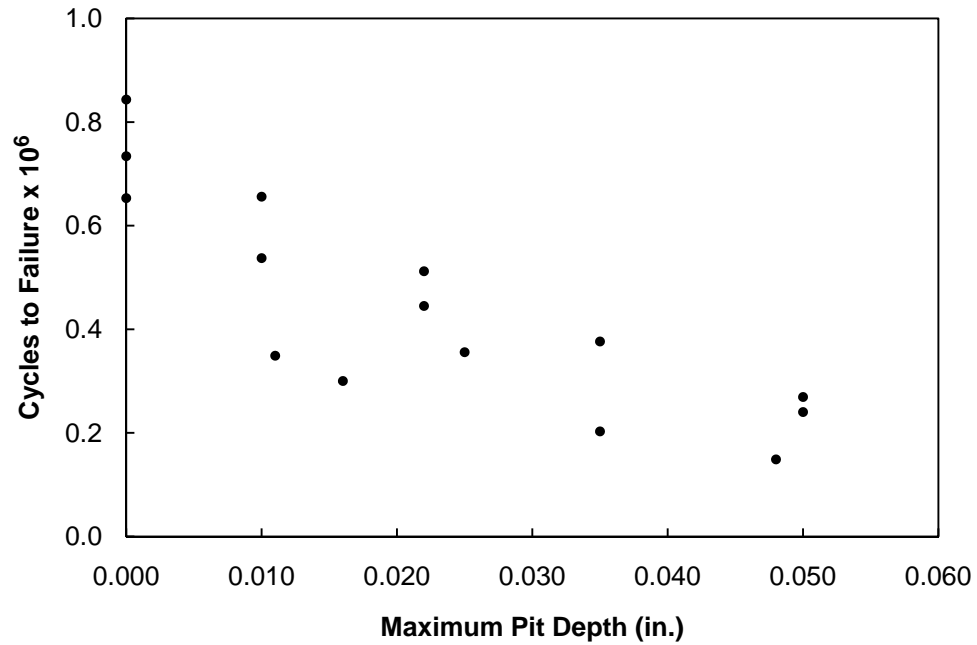


Figure 3-10: Cycles to Failure as a Function of Maximum Pit Depth

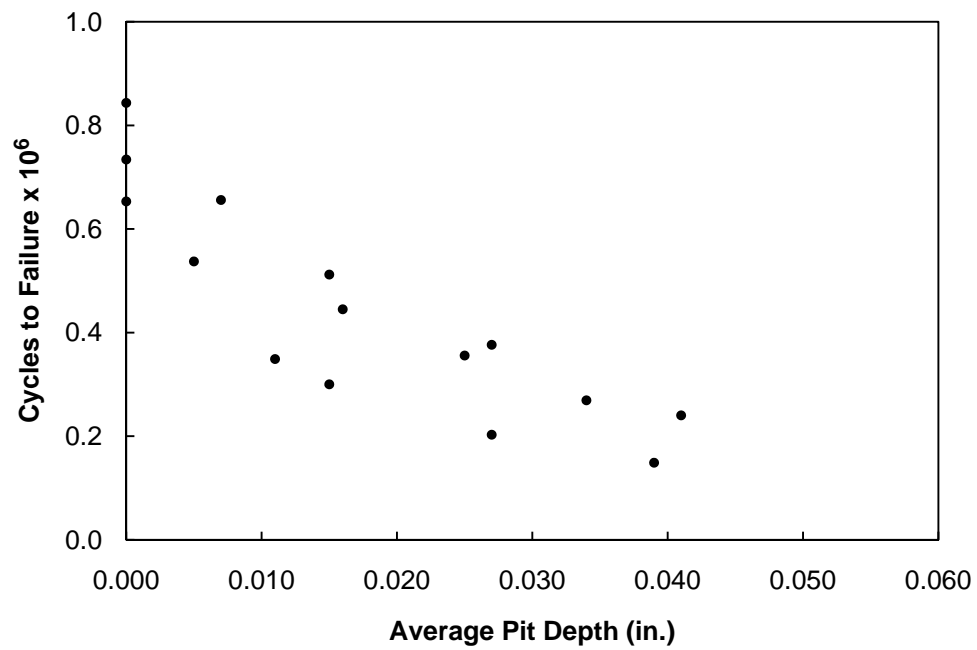


Figure 3-11: Cycles to Failure as a Function of Average Pit Depth

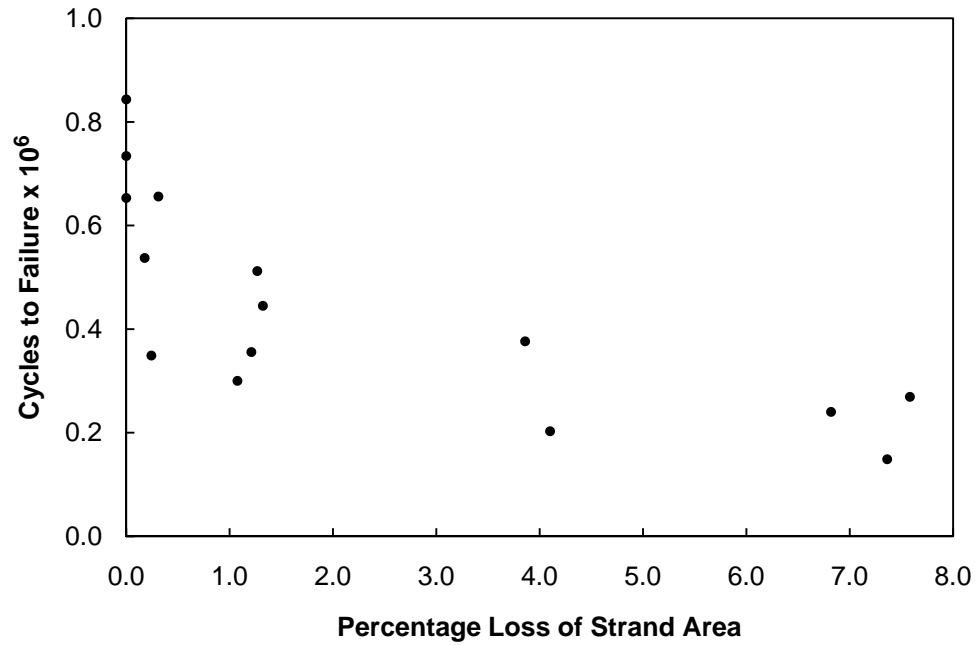


Figure 3-12: Cycles to Failure as a Function of Percentage Loss of Strand Area

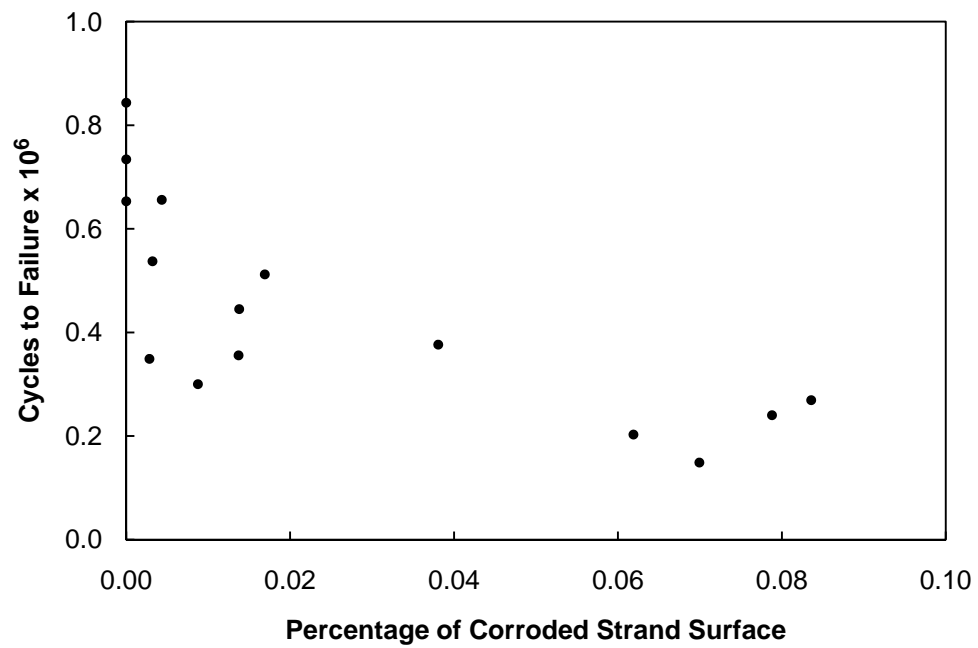


Figure 3-13: Cycles to Failure as a Function of Percentage of Corroded Strand Surface

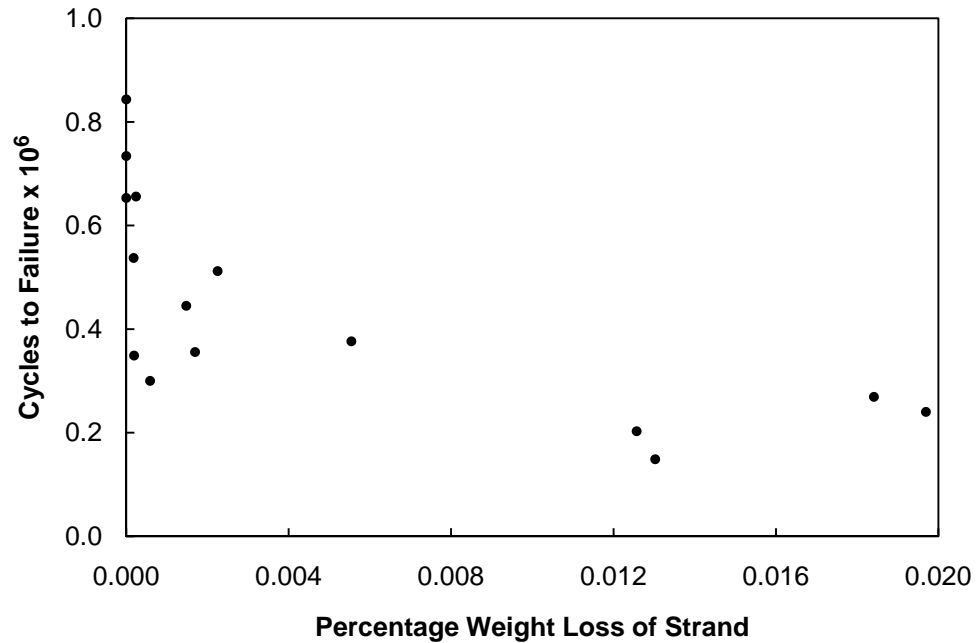


Figure 3-14: Cycles to Failure as a Function of Percentage Weight Loss of Strand

3.4.1 Linear Elastic Fracture Mechanics Approach

This section discusses the application of Linear Elastic Fracture Mechanics (LEFM) to predict the fatigue behavior of corroded prestressing strand. First, background is given as to the formulation and material constants necessary for the analysis. Next, the author applied LEFM to non-corroded strand to determine its ability to predict the fatigue response of prestressing strand. Finally, the author looked at several variations on how to treat the corrosion pit as either an initial defect, stress concentrator, or simply a reduction in effective strand area.

The typical LEFM approach is to assume that Stage II crack growth covers the entire range from the threshold value to the point of failure (Pook 2000). In State II, for a metallic material, the Paris equation governs the rate of crack growth (da/dN), which is shown in Eq. 3.1.

$$\frac{da}{dN} = C(\Delta K)^m \quad 3.1$$

where a = crack length,

N = number of cycles,

C, m = empirical constants for a given material,

ΔK = range of stress intensity factors.

For a constant amplitude fatigue loading, the general expression for the range of stress intensity factors is given by Eq. 3.2.

$$\Delta K = Y\Delta\sigma\sqrt{\pi a} \quad 3.2$$

where Y = geometric and loading correction factor,

$\Delta\sigma$ = fatigue loading stress range.

Combining Eqs. 3.1 and 3.2 and solving for N , the number of cycles to failure, gives the expression shown in Eq. 3.3, where a_i and a_f are the initial and final crack lengths, respectively.

$$N = \int_{a_i}^{a_f} \frac{1}{CY^m(\Delta\sigma)^m\pi^{m/2}a^{m/2}} da \quad 3.3$$

Solving Eq. 3.3 will yield an expression for the number of cycles to failure for a given material and set of conditions. In Eq. 3.3, C , m , $\Delta\sigma$, and π are all constants and although Y can vary as a function of a , it is often treated as a constant for preliminary analyses (Pook 2000). Therefore, integrating Eq. 3.3 gives the result shown in Eq. 3.4.

$$N = \frac{2}{(m-2)CY^m(\Delta\sigma)^m\pi^{m/2}} \left(\frac{1}{a_i^{(m-2)/2}} - \frac{1}{a_f^{(m-2)/2}} \right) \quad 3.4$$

Equation 3.4 will serve as the general expression for the following studies of both non-corroded and corroded prestressing strand.

Equation 3.4 requires the empirical constants C and m as well as initial and final defect lengths, a_i and a_f , respectively. For cold drawn, eutectoid steel wires, Llorca and Sanchez-Galvez (1989) determined values of 1.107×10^{-11} for C and 2.417 for m . These values were based on units of m/cycle for da/dN and $\text{MPa}\sqrt{\text{m}}$ for ΔK . Llorca and Sanchez-Galvez also found that the cold drawing process resulted in surface flaws in the wires due to inclusions, cavities, and cracks associated with cavities. Although the flaws varied in profile, the most common defect had an aspect ratio, a/c , equal to 0.5, as shown in Figure 3-15, and a length, a_i , of 55 to 57 μm .

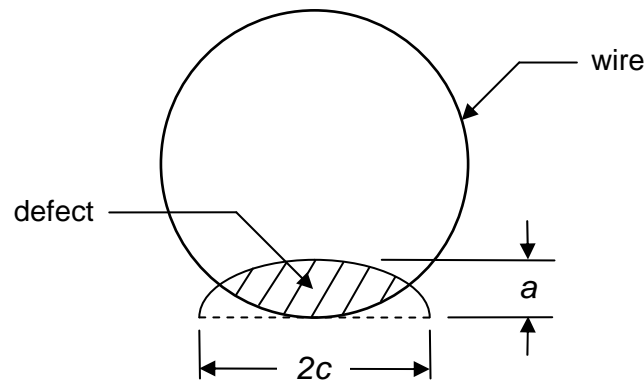


Figure 3-15: Cold Drawn Wire Defect Profile

3.4.1.1 Non-Corroded Strand

The author applied Eq. 3.4 to the prestressing strand by treating the seven individual wires as a single wire of equivalent area. The only remaining variable in the LEFM equation is Y , the geometric and loading correction factor. For Mode I crack surface movement, the surface defect in a cold drawn, eutectoid steel wire has been treated in two ways. Llorca and Sanchez-Galvez (1987) treated the defect as an equivalent surface crack in the edge of a semi-infinite plate due to the defects small size relative to the wire diameter, and for this condition, Y is equal to a value of 1.12. Beretta and Matteazzi (1996), on the other hand, treated the defect as a semi-circular edge crack in a semi-infinite solid, where the semi-circle is oriented perpendicular to the direction of the applied load, and for this condition, Y is equal to a value of 0.728.

Both approaches for treating the wire defects resulted in reasonable estimates of the fatigue life, but both require slightly different applications. In treating the defects as

surface cracks in the edge of a semi-infinite plate, the author assumed that the final crack length was very large compared to the initial crack length, which is a common assumption in LEFM (Pook 2000), and thus the second term within the brackets of Eq. 3.4 is negligible. For a stress range of $0.15f_{pu}$, this approach resulted in a value for N of 780,053 cycles to failure, compared with Paulson's (1983) mean fatigue life prediction equation value of 742,105.

In treating the defects as semi-circular edge cracks in a semi-infinite solid, Eq. 3.4 significantly overestimated N when neglecting the second term within the brackets. Consequently, the author set Eq. 3.4 equal to Paulson's mean fatigue life value of 742,105 cycles and calculated a required final crack length of 398 μm (0.016 in.). Using this value for the final crack length, the author then compared Eq. 3.4 to Paulson's mean fatigue life equation at other stress ranges, and found reasonable agreement. For example, at a stress range of 35 ksi, Paulson's equation predicted 1,375,917 cycles to failure and Eq. 3.4 predicted 1,157,196 cycles to failure. Based on these favorable results, the author applied LEFM to the corroded prestressing strand.

3.4.1.2 Corroded Strand – Modify Y

To apply LEFM to corroded strand requires a modification to the geometric and loading correction factor, Y . The physical situation is shown in Figure 3-16, where a fatigue crack nucleates and grows from the base of a corrosion pit. This particular situation has been studied extensively in the aircraft industry (*e.g.*, Anderson 1995, Fett and Munz 1997). The general approach is to apply a stress concentration factor, based on pit shape,

to the stress intensity factor, based on the particular crack shape. For example, Chen *et al.* (1997) modeled pitting-induced cracking in aluminum airframe components as an equivalent surface crack in the edge of a semi-infinite plate multiplied by the stress concentration factor for a circular hole. This approach results in an effective geometric and loading coefficient. Extensive calculations have confirmed this approach as a special case for radial cracks emanating from elliptical holes (Murakami 1987).

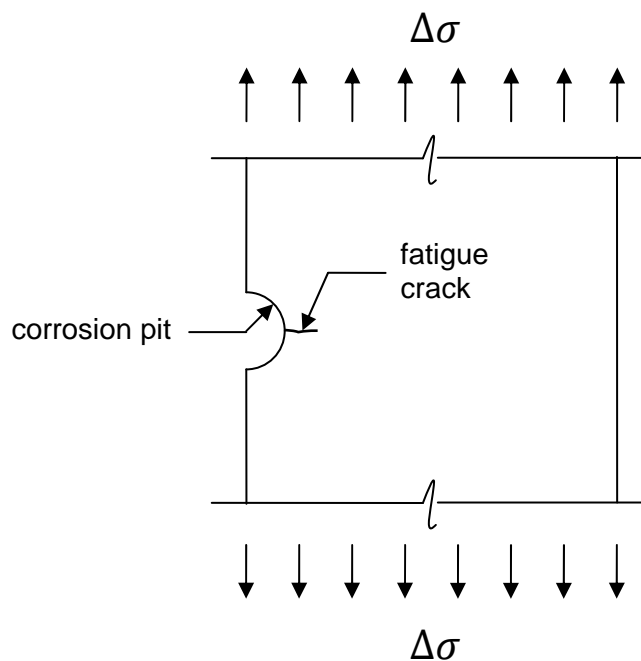


Figure 3-16: Fatigue Crack Emanating from the Base of a Corrosion Pit

The author determined an effective geometric and loading correction factor, Y , of 3.36 for the case of a surface crack in the edge of a semi-infinite plate that emanates from the base of a circular hole (Figure 3-16). This value results from the previous value for Y of 1.12 multiplied by a stress concentration factor of 3.0 for a circular hole (or semicircu-

lar edge hole). For a stress range of $0.15f_{pu}$ and again treating the second term within the brackets of Eq. 3.4 as negligible, this approach resulted in a value for N of 54,860 cycles to failure. This value is well below all of the test values for corroded prestressing strand and, more importantly, is independent of pit size. In other words, this approach would predict that all strand having a pit, of any depth, would fail at the same number of cycles, or very nearly so, which is inconsistent with the test data.

The author also determined an effective geometric and loading correction factor, Y , of 2.184 for the case of a semi-circular crack in the edge of a semi-infinite solid that emanates from the base of a hemispherical hole (Figure 3-16 in three dimensions). This value results from the previous value for Y of 0.728 multiplied by a stress concentration factor of 3.0 for a spherical hole (or hemispherical edge hole). For a stress range of $0.15f_{pu}$ and first treating the second term within the brackets of Eq. 3.4 as negligible, this approach resulted in a value for N of 155,398 cycles to failure. This value is well below all but one of the test values for corroded prestressing strand and, more importantly, is again independent of pit size. Consequently, the method of modifying Y for a fatigue crack emanating from a corrosion pit failed to accurately predict the test results for corroded prestressing strand.

3.4.1.3 Corroded Strand – Modify Stress Range

Another approach developed by the author for applying LFM to corroded strand involved modifying the stress range as a function of the reduced strand area. For this application, the author neglected the stress concentration approach of Section 3.4.1.3 and

only modified the stress range for the reduced strand area. The fatigue crack was then modeled as either an edge crack in a semi-infinite plate or as a semi-circular edge crack in a semi-infinite solid, as discussed in Section 3.4.1.1.

Figure 3-17 is a plot of the test results as a function of stress range based on the reduced strand area. Also included in the plot is Eq. 3.4 with the stress range also based on the reduced strand area. Either method of treating the fatigue crack results in approximately the same equation. As shown in the plot, the LEFM equation does not decrease at a fast enough rate to match the test data. Furthermore, the LEFM equation is essentially linear in the range of data shown on the plot, while the test data is markedly nonlinear, particularly between 40.5 and 41.0 ksi. Consequently, the method of modifying the stress range as a function of the reduced strand area failed to accurately predict the test results for corroded prestressing strand.

3.4.2 Empirical Approach

Of the data displayed in Figures 3-10 through 3-14, the plots of maximum pit depth and average pit depth appear to offer the greatest potential for developing a statistically valid relationship between the amount of corrosion and the resulting fatigue capacity. Both plots exhibit data over their full range of values and also display definitive trends. On the other hand, the plots shown in Figures 3-12 through 3-14 exhibit vacancies (gaps), clustering, more scatter, and less recognizable trends in their data (Cleveland 1994). As a result, the author evaluated the data for maximum pit depth and average pit

depth to derive an empirical relationship between the amount of corrosion and the resulting fatigue capacity.

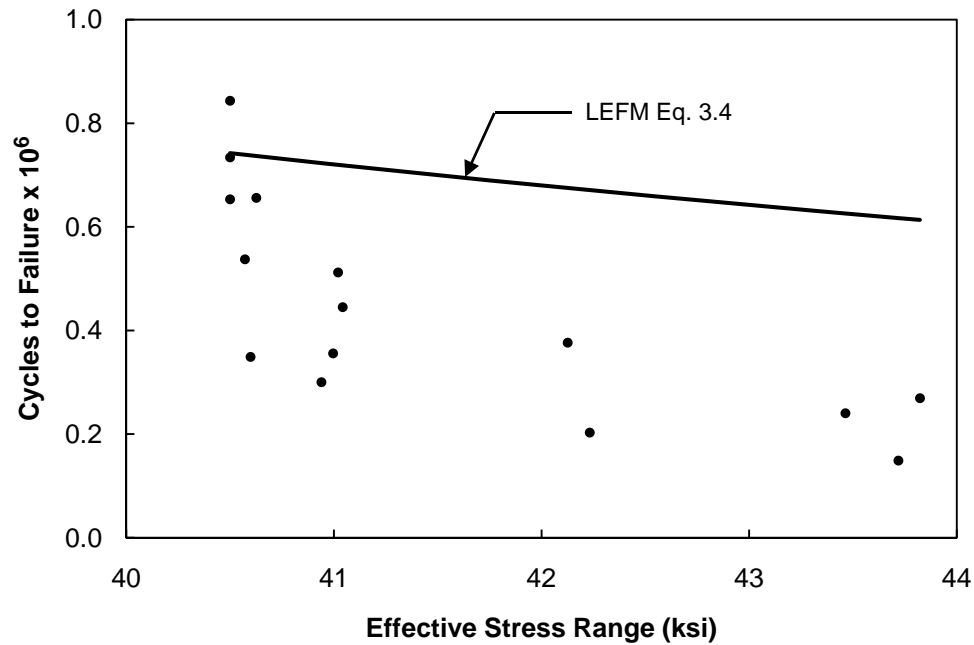


Figure 3-17: Cycles to Failure as a Function of Effective Stress Range

The author performed nonlinear regression analyses of the data relating maximum and average pit depth to number of cycles to failure. The data is replotted in Figures 3-18 and 3-19 along with the equations deemed most appropriate to characterize the relationships. These equations were based on an exponential decay function of the form shown in Eq. 3.5, where y_o is the value of y at x equal to zero and k is the decay rate.

$$y = y_o e^{(-kx)} \quad 3.5$$

This form of an exponential decay function assumes a plateau value of zero (*i.e.*, y equals zero at x equal to infinity).

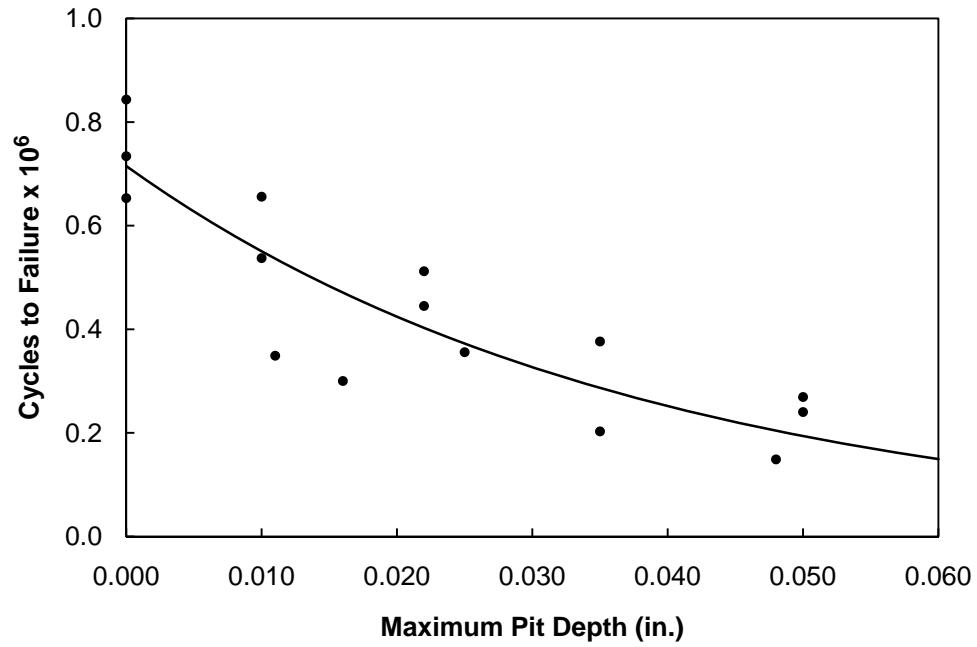


Figure 3-18: Cycles to Failure as a Function of Maximum Pit Depth

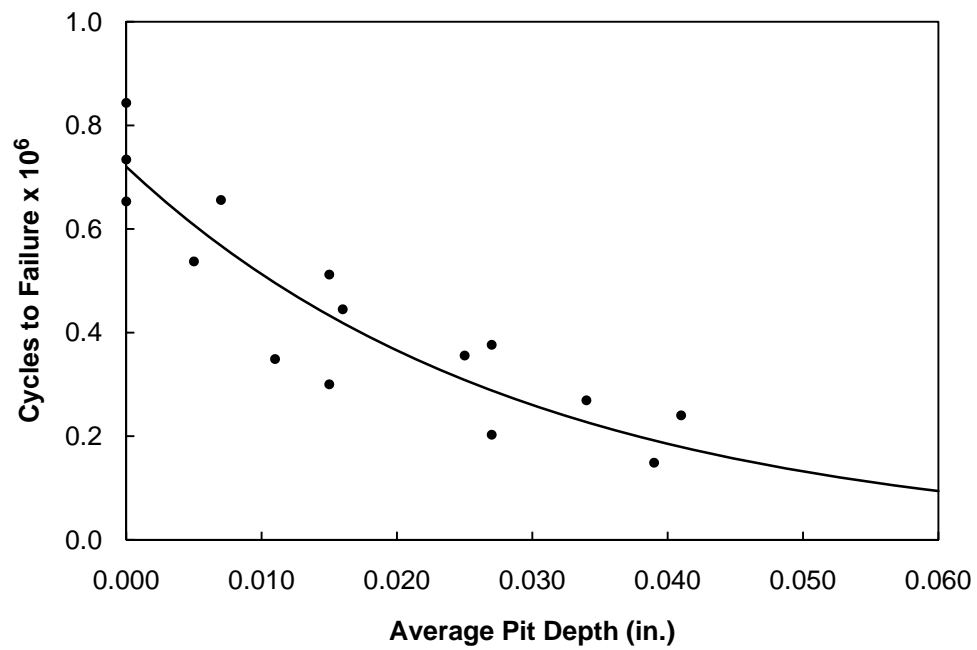


Figure 3-19: Cycles to Failure as a Function of Average Pit Depth

The choice of an exponential decay function for the model was based on several criteria. First, visually, where the plotted data trends in the form of a function that starts at a peak value and trails off at a decreasing rate. Next, the purpose of developing a model is not necessarily to fit the best curve to the data but, instead, to use an equation that mimics the physiological behavior of the process (Box *et al.* 1978). An exponential decay function models many chemical, biological, and physiological processes found in nature (Box *et al.* 1978) and maps very well with the test data. Next, the equation should predict the response beyond the limits of the testing. In this case, an equation that best fits the given data, such as a polynomial, would begin to plateau around 250,000 cycles. Physically, this cannot occur, as the strand will eventually have no fatigue limit as the pitting depth approaches the full thickness of the specimen. Finally, the exponential decay function possessed goodness-of-fit statistics that were negligibly less than those that resulted from the best curve that could be fit to the data.

Both equations had positive indicators that they represented a good fit for the data. Both functions had good D'Agostino & Pearson omnibus K2 values. These values determine whether or not the data scatter follows a Gaussian (normal) distribution, which is a necessary assumption in a nonlinear regression analysis (Seber and Wild 2003). Furthermore, a visual inspection of the curves shows that the data points randomly bounce above and below the curves, and the distance of points from the curves is also random. These visual clues support the adequacy of the given model to represent the data (Seber and Wild 2003).

However, of the two, the data plots closer to the curve when the independent variable is average pit depth, Figure 3-19, as compared to maximum pit depth, Figure 3-18.

Not only visually, but the goodness-of-fit statistics are also better for the exponential decay function that used average pit depth as the independent variable. The R^2 value for the average pit depth curve in Figure 3-19 equaled 0.83, compared with a value of 0.77 for maximum pit depth, Figure 3-18. It is also important to note that these R^2 values are consistent with values obtained for fatigue tests of non-corroded strand (Paulson 1983). In other words, the scatter of the data is of the same order of magnitude as that found when testing “clean” prestressing strand.

Consequently, the author proposes the use of an exponential decay function with average pit depth as the best indicator of the reduced fatigue capacity due to corrosion. For the curve in Figure 3-19, the exponential decay function is given by Eq. 3.6; where N is the number of cycles to failure and d is the average pit depth for the strand in inches.

$$N = 720,327 e^{(-34d)} \quad 3.6$$

In terms of a generalized equation, the author proposes adjusting the model with the value for y_o based on Paulson’s mean fatigue life equation (1983). The result is given by Eqs. 3.7a and 3.7b; where N_o is the mean fatigue life predicted from Paulson’s equation (*i.e.*, with no corrosion), S_r is the stress range in ksi, and d is the average pit depth for the strand in inches.

$$N = N_o e^{(-34d)} \quad 3.7a$$

$$\text{Log } N_o = 12.67 - 4.23 \text{ Log } S_r \quad 3.7b$$

3.4.3 Discussion

This section discusses the many complex factors that influence the fatigue capacity of corroded prestressing strand as well as prestressing strand in general. These factors include: (1) behavior of a seven-wire strand versus an individual wire; (2) fretting fatigue; (3) variation in wire defect location, pit location, and fracture location; and (4) potential for hydrogen embrittlement. In addition, the results of previous testing of noncorroded prestressing strand are included as a basis of comparison for the testing of this study. The consequence of this complex behavior is that the most reliable method of predicting the response of corroded prestressing strand is an empirical relationship, as discussed and developed in Section 3.4.2.

3.4.3.1 Seven Wire Strand versus Individual Wire

On average, the fatigue capacity of prestressing strand is about 75 percent of the fatigue capacity of individual wire (ACI 215R 1997). Furthermore, the scatter of test data for prestressing strand is about 40 percent greater than that for individual wire. Part of the reason for this behavior is the complex interaction of seven “independent” wires acting in concert to support a single load, and the resulting mode of failure for the strand during a fatigue test.

For “solid” specimens, fatigue failure of a ductile material involves stable crack growth followed by fracture once the stress on the remaining portion of the cross-section exceeds the ultimate tensile strength (Bannantine *et al.* 1990). For the strand, composed of seven individual wires, a progressive failure occurs instead. First, for the stress range

used in this study, two of the wires fail in a traditional fatigue mode, most likely at separate times. Once the second wire fails, the remaining five wires are unable to support the test load near the peak of the cyclic loading. Rapid failure occurs as the remaining five wires fracture. These remaining five wires fail either in a fatigue fracture mode, having developed a partial fatigue crack before this point, or in a traditional cup-cone fracture.

The number of cycles between failure of the first wire and complete failure of the strand can be significant. Figure 3-20 is an example of a strand specimen where the first wire failed due to fatigue and the remaining six wires carried the cyclic test load for an additional 129,608 cycles until complete failure of the strand. Approximately 18 percent of the total specimen fatigue life occurred after the first wire break.

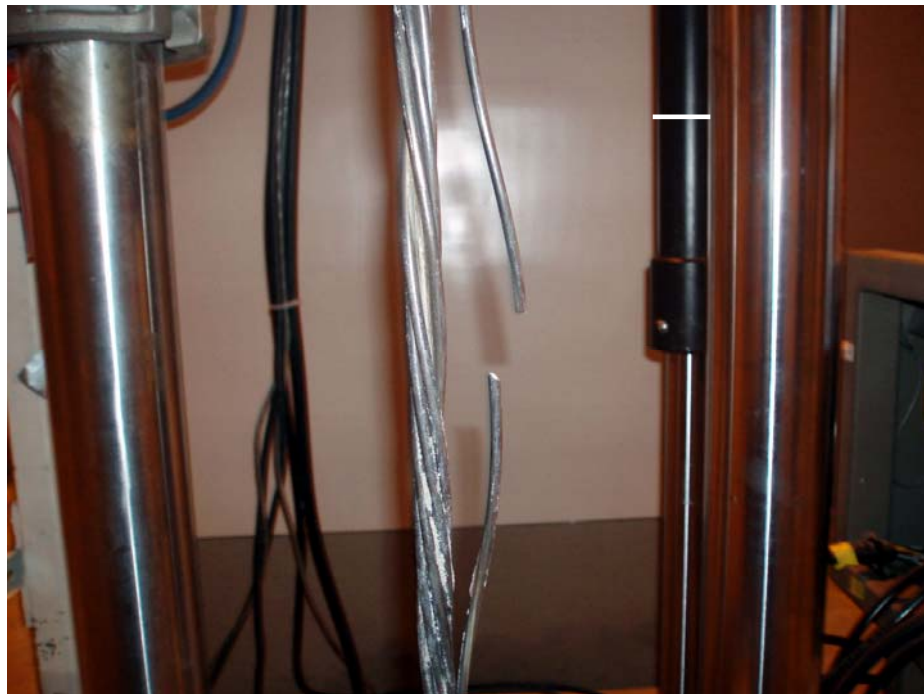


Figure 3-20: Individual Wire Break During Fatigue Testing

What this means for the test data is that the failure mode is quite complex and highly variable, which increases the scatter of the test data as well as the types of failures experienced by the strand. The failures are not only due to fatigue, as would be experienced in a “solid” specimen, because some of the wires fail in fatigue but some fail in fracture or a complex interaction of fatigue and fracture. Furthermore, the proportion of standard fatigue failures to standard fracture failures depends on both the particular cyclic test range and the statistical variation of the individual wire fatigue strengths. In other words, a lower stress range will require a larger number of fatigue failures of individual wires before the remaining wires fail in fracture due to the increased stress. The reverse is true for a higher stress range, where only one or two fatigue failures of individual wires are required before the remaining wires fracture at the increased stress.

3.4.3.2 Fretting Fatigue

Wire-to-wire fretting fatigue has a significant negative impact on the fatigue resistance of prestressing strand. On average, the fatigue capacity of prestressing strand is about 75 percent of the fatigue capacity of individual wire (ACI 215R 1997). Most researchers have attributed this decrease to wire-to-wire fretting fatigue (*e.g.*, ACI 215R 1997, Paulson 1983). Edwards and Picard (1972) also found that strand fatigue life decreased with increasing specimen length due to wire-to-wire fretting conditions.

Referred to as asperity contact initiation, Wollmann *et al.* (1988) discusses the phenomenon of fretting fatigue in prestressing strand in significant detail. The process involves the contact area between adjacent wires. When placed under tension, the heli-

cally wrapped outer wires can exert a lateral force on each other over a very small contact area. Localized plastic deformations at these contact points result in the material fusing in a process commonly referred to as cold welding. Under cyclic loading, relative slip at the contact points results in localized damage to the material, and the imposition of cyclic shear stresses. Combined with the fluctuating tension stress, these shear stresses cause a very complex stress state and serve as the driving force for crack initiation and propagation.

Figure 3-21 contains the types of wire fracture surfaces observed during the testing and subsequent autopsies. Figure 3-21a shows the typical cup-cone fracture surface for wires that exceeded the ultimate tensile strength but did not possess any fatigue cracks. Figures 3.21b through 3.21d display the range of fatigue fracture surfaces experienced by the strand. The failure surface for an ordinary fatigue fracture begins with an inclined crack that quickly transitions into a crack perpendicular to the axis of the member (Wollmann *et al.* 1988). This type of failure is shown in Figure 3.21b. A fretting fatigue failure, on the other hand, experiences a much longer inclined crack due to the lateral pressures and friction stresses caused by adjacent wires (Wollmann *et al.* 1988). This type of failure is shown in Figure 3.21d. Figure 3.21c shows an intermediate fracture surface between these two extremes.

What this means for the test data and failure modes is the addition of another random variable. Fretting fatigue reduces the fatigue capacity of prestressing strand (Wollmann *et al.* 1988). Furthermore, fretting fatigue may or may not occur, or even if it does occur, the extent can vary, as indicated by the varying angles of the fracture surfaces shown in Figure 3-21. Thus, both the location and impact of fretting fatigue is complete-

ly random. In addition, for corroded prestressing strand, fretting fatigue locations and corrosion pit locations will likely not coincide due to the random nature of both phenomena. Consequently, depending on the severity of the corrosion, a wire may fail due to fretting fatigue at a location away from a corrosion pit, and thus be independent of the affect of corrosion.

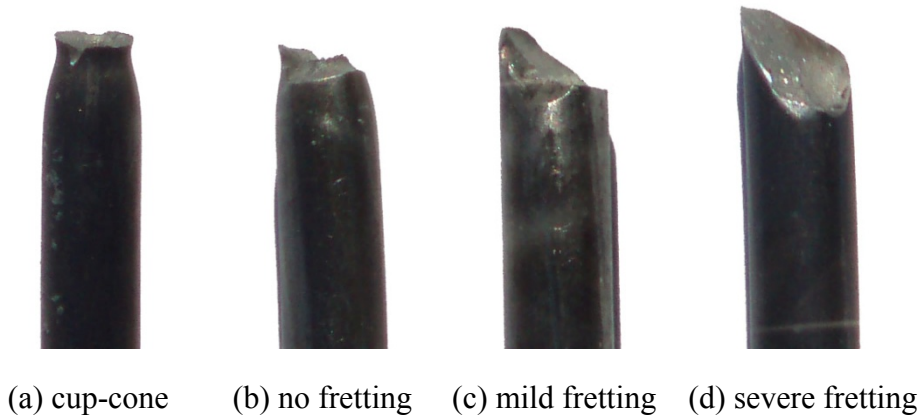


Figure 3-21: Wire Fracture Surfaces Observed During Fatigue Testing

3.4.3.3 Defect Location, Pit Location, and Fracture Location

Due to the nature of the cold drawing process, prestressing strand experiences surface flaws in the wires due to inclusions, cavities, and cracks associated with cavities (Beretta and Boniardi 1999, Llorca and Sanchez-Galvez 1989). Furthermore, the drawing and manufacturing process causes residual stresses within an outer ring of the wires, which has an effect on crack propagation. Without corrosion present, a wire will generally fail at the location of one of these inherent defects.

In addition to these defects, alloys are not homogeneous at the microscopic level. Most alloys contain grain boundaries, multiple phases, and varying potentials (Jones 1996). Corrosion tends to prefer these sites, yet these sites may or may not coincide with a normal wire defect, such as a dislocation or those due to the drawing process. In addition, the shape of a corrosion pit compared to the shape of a defect impacts the stress intensity at the front of a fatigue crack. Corrosion pits are generally hemispherical and relatively smooth. Defects, on the other hand, tend to exhibit a sharp crack front, which has a much higher stress intensity, and thus a much higher fatigue crack growth rate.

The effect of this interaction between the inherent defects and corrosion pitting is evident in the failure locations for the strand and the data plotted in Figure 3-22. At “smaller” pit depths, fatigue failures were essentially split between failing at or away from a pit location. At “larger” pit depths, the pitting began to dominate, where nearly 70 percent of the failures were at pit locations.

This trend is evident in Figure 3-22, which is a plot of number of cycles to failure as a function of percentage loss of strand area. Although not at the exact same percentage loss, there are definite groupings of the data for which the vertical spread decreases at increasing loss in strand area. The vertical spread of the data points clustered near 0.2 percent (3 data points), 1.3 percent (4 data points), 4.0 percent (2 data points), and 7.3 percent (3 data points), is 307,137 cycles, 212,060 cycles, 173,630 cycles, and 120,372 cycles. What this means is that as the pit sizes increase, they begin to override the inherent defects in the steel and thus dominate the response. However, at “smaller” pit depths, both the corrosion pits and the inherent defects play an equal role in the fatigue failure of the prestressing strand.

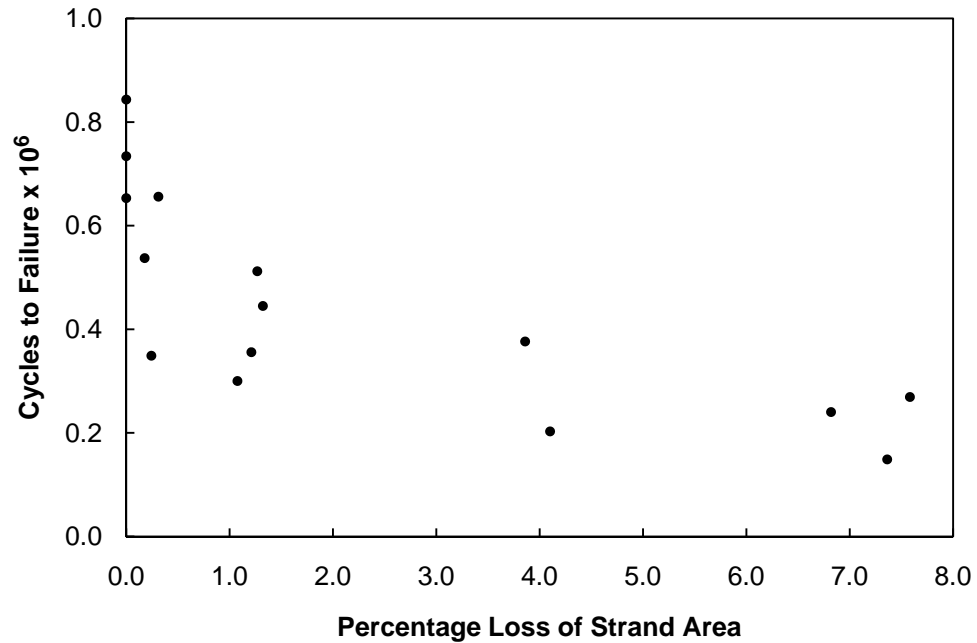


Figure 3-22: Cycles to Failure as a Function of Percentage Loss of Strand Area

3.4.3.4 Hydrogen Embrittlement

Another aspect that increases the complexity and variability of the fatigue behavior of corroded strand is the potential for hydrogen embrittlement. As discussed previously, atomic hydrogen forms within a pit during the corrosion process. Under the right circumstances, this atomic hydrogen will enter the metal lattice and embrittle the strand, resulting in a lower fatigue strength but one that is potentially independent of pit size. In addition, if the hydrogen does enter the metal lattice, it may diffuse away from the corrosion pit and “seek out and congregate” within defects within the metal lattice (Krom *et al.* 1999). The potential result is a brittle fracture that does not coincide exactly

with a pit location. Consequently, it may not be possible to conclude whether or not the corrosion decreased the fatigue capacity.

3.4.3.5 Previous Fatigue Testing of Noncorroded Strand

While it is important to note the significant scatter of the test data, the scatter is of the same order of magnitude as that found when testing “clean” prestressing strand. For example, from Figure 3-11, at an average pit depth of 0.015 in., there are test results with the number of cycles to failure equal to 300,018 and 512,078, a difference of 70 percent. Furthermore, from Figure 3-10, at a maximum pit depth of 0.011 in., there is a test result of 348,889 cycles to failure, and at a maximum pit depth of 0.010 in., there is a test result of 656,026 cycles to failure, a difference of 88 percent. By comparison, the test data on “clean” prestressing strand presented by Paulson (1983) shows consistent variations of up to 100 percent on the number of cycles to failure for the same stress range, with maximum variations of up to 800 percent.

3.5 Summary

Although this study was limited to the specific sequence of corrosion followed by fatigue to failure, it does offer some insight into the influence of corrosion on the fatigue capacity of prestressing strand. Specifically, that either due to the “notching” effect of the pits or hydrogen embrittlement, there is a significant drop off in fatigue capacity at

relatively small pit depths. This behavior is also well represented by an exponential decay function of the form shown by Eq. 3.7.

Chapter 4

Beam Specimen Design and Construction

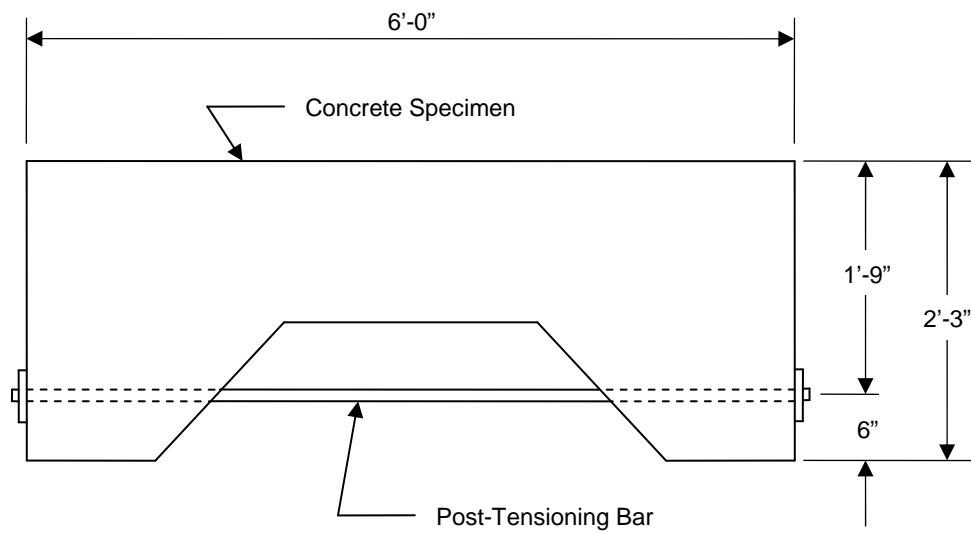
This chapter discusses the design and construction of the post-tensioned beam specimens used in this research study. Twelve full-scale beam specimens were included in the testing program, combining long-term static exposure testing with fatigue testing. Full-scale specimens were necessary in order to evaluate actual post-tensioning hardware and multi-strand tendons. The discussion also includes the rationale behind the test variables selected. These test variables included level of prestress, condition of post-tensioning system, and exposure to saltwater.

4.1 Beam Specimen Concept

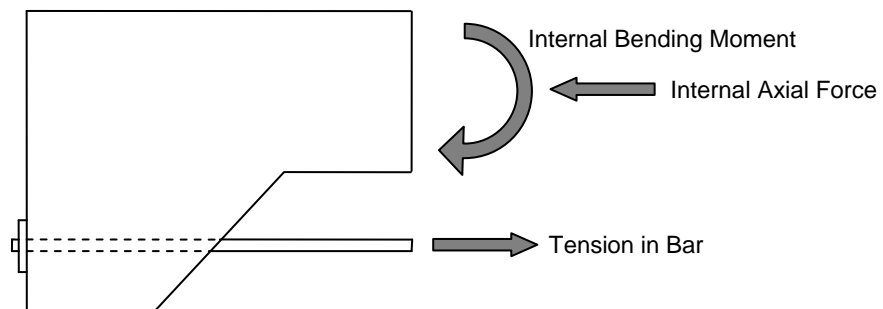
The main problem that the author confronted was how to feasibly place the beam specimens under full service load continuously for six months during the period of chloride exposure. This requirement is fundamental to evaluating the long-term durability of partially prestressed concrete, because these members crack under service load. Furthermore, for most designs, the cracks are only open during the application of live load. The benefit of prestressing, even partial prestressing, is that the cracks close once the live load is removed. Without continuous application of live load, the specimens would behave as if they were fully prestressed, negating the intent of this study.

The beam specimen concept for this research study was based on work done by Ahern (2005). His specimen design was entirely self-reacting and significantly shorter than the specimens used in previous durability studies (*e.g.*, Schokker 1999a, West 1999). In essence, Ahern added a corbel at each end of the beam through which an eccentric axial load was applied with a post-tensioning bar, as shown in Figure 4-1a. The eccentric axial load places the “beam” portion of the specimen under a uniform moment, as shown by the free-body diagram in Figure 4-1b. Thus, maximum flexural stresses occur throughout the “beam” portion of the specimen during loading, and the self-reacting nature of the specimen allows freedom of movement during the six to nine month exposure period.

The only negative feature of this specimen design was the “short” beam length, approximately six feet, which increased seating losses during post-tensioning of the beam. Seating losses are a function of the retainer plate for the stressing jack, which allows the same movement to seat the wedges regardless of the beam length. Therefore, as the beam length decreases, the strain loss due to seating increases. Nevertheless, the author determined that the benefits of this specimen design outweighed this negative, particularly since the problem of seating losses could be partially negated through an increase in jacking stress, as discussed in Chapter 5.



(a) Beam Specimen Schematic



(b) Beam Internal Forces

Figure 4-1: Beam Specimen Schematic and Internal Forces

Although Ahern's concept formed the basis for the beam specimens, the author made the following changes to accommodate the objectives of this study:

1. Use of a single, multi-strand tendon designed in accordance with AASHTO LRFD (2008) and ACI 318 (2008) recommendations.
2. Use of a partially external tendon that allowed visual examination of the tendon during testing, rapid exposure of the tendon to chlorides to accelerate the durability study, and the ability to easily mimic post-tensioning system imperfections.
3. Use of a plastic duct in accordance with the requirements of AASHTO LRFD for external tendons.
4. Addition of a reservoir in the center of the beam for the application of the sodium chloride solution during the durability testing.
5. Addition of a deviator pipe at the drape point in accordance with AASHTO LRFD recommendations. The pipe coincides with the transition from internal to external tendon.
6. Use of the AASHTO LRFD (2008) minimum bend radius for the tendon at the deviation point, which maximizes the localized bending stresses in the tendon at the deviator.

A three-dimensional schematic of the specimen layout for this research study is shown in Figure 4-2. The detailed design is contained in Section 4.3, and the construction details are discussed in Appendix C.

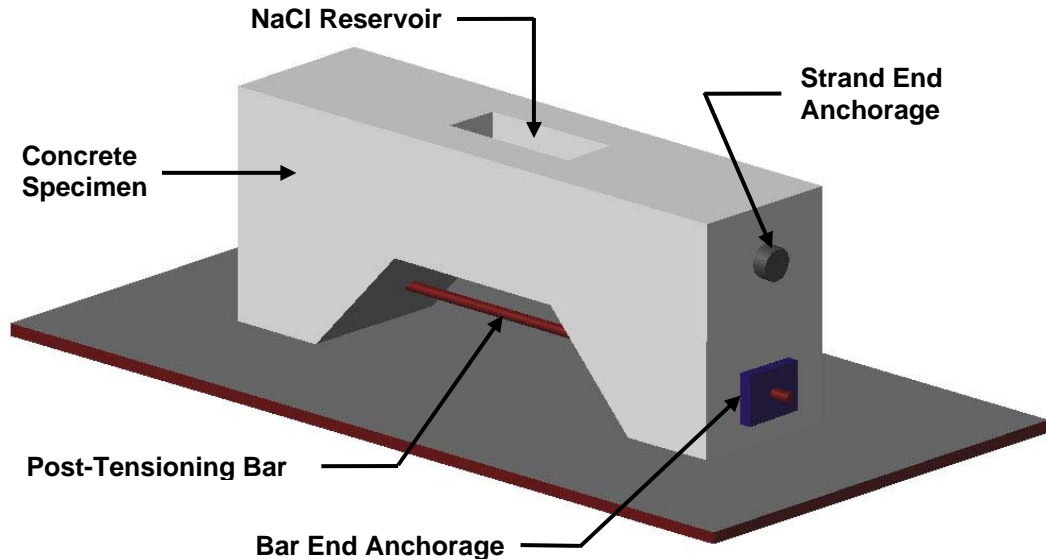


Figure 4-2: Three-dimensional Schematic of Beam Specimen

4.2 Beam Specimen Test Matrix

The following section discusses the types and combinations of full-scale beam test variables examined in this study. These variables included level of prestress, condition of the post-tensioning system, and exposure to NaCl salts. Dimensions, loading, and tendon curvature were constant for all specimens.

The most critical variable for the full-scale beam testing was the level of prestress. Two levels of prestressing were investigated, one representing a fully prestressed design, and one representing a partially prestressed design. In addition, the partially prestressed design was obtained in two ways, either with fewer strands or with a lower prestressing force. The fewer-strand option simulates a typical partially prestressed design, and the

lower-prestressing-force option simulates an unanticipated loss of prestress for a fully prestressed design.

The fully prestressed design was based on a maximum tensile stress in the concrete under full service load of $3\sqrt{f'_c}$, with units of pounds per square inch ($0.0948\sqrt{f'_c}$ with units of kips per square inch). As discussed previously, the dividing line between fully prestressed and partially prestressed is typically based on a nominal tensile stress in the precompressed tensile zone of $7.5\sqrt{f'_c}$ (psi), which corresponds to the modulus of rupture for concrete (ACI 318 2008). The more restrictive choice of $3\sqrt{f'_c}$ (psi) corresponds to the AASHTO (2008) tension stress limit for bridges with components subjected to severe corrosive conditions. This limitation represents the most conservative design condition for a fully prestressed concrete bridge member.

The partially prestressed design was initially based on a prestress force of 60 to 70 percent of that required for full prestress. During the detailed design, as discussed in Section 4.3, the partially prestressed design evolved to a value of 67 percent of the full prestress force. This percentage resulted from the whole number of strands required for each design. The fully prestressed design used six 1/2-inch-diameter strands. The partially prestressed design used four 1/2-inch-diameter strands. This ratio allowed a very realistic partially prestressed design, as shown in Section 4.3, with a nominal tensile stress under full service load of approximately $12\sqrt{f'_c}$ (psi).

The next test variable for the study involved potential post-tensioning system imperfections. The study initially considered three types of imperfections, one at the anchor

zone, one in the grout at the crown, and one in the plastic duct along the crown. However, based on the strand testing discussed in Chapter 3 and results from recent research at the University of Texas (Kotys 2003), the author determined that the imperfections in the grout at the crown and in the duct were not necessarily separate conditions. This conclusion was based on three important considerations: (1) the high variability in strand fatigue capacity both with and without the presence of corrosion; (2) the high likelihood that the grout will crack due to shrinkage; and (3) the low likelihood that the robust plastic duct will experience a naturally occurring breach during the finite exposure period for this research. (The PT-PLUS™ System manufactured by VSL was used in the construction of the beam specimens.)

Consequently, the author considered a duct breach with the naturally occurring cracking of the grout as a single post-tensioning system imperfection. It was highly likely that the grout would crack for all of the beam specimens due to shrinkage. Shrinkage cracks form very thin voids in the grout, resulting in very small free gauge lengths. In terms of fatigue, the smaller the free gauge length, the higher potential stress range in the strand during cycling. Larger, purposely created voids in the grout, due to the increased gauge lengths, are not as critical with respect to potential fatigue problems, provided the shrinkage cracks allow the relatively free passage of chlorides. In other words, a naturally occurring grout void in the form of a thin crack is more critical than a thicker, manufactured void in the grout. Furthermore, unless the plastic duct is purposely breached, it will prevent chlorides from gaining access to the strand during the exposure testing.

As a result, the research considered only two types of post-tensioning system imperfections. The first involved a moderate void in the grout immediately behind the anc-

hor head. This imperfection, prevalent in the Mid-Bay Bridge tendon failures (Corven 2001), allows chlorides to access the tendon and, in the case of cyclic loading, may allow localized bending stresses due to the lack of tendon support. The second imperfection involved a void in the grout (caused by cracking) combined with a breach in the plastic duct to allow chloride ingress. The methods of achieving these imperfections are contained in Appendix C.

The final test variable for the study involved chloride exposure. The main thrust of this research study was to investigate durability, which typically involves exposure to a high chloride environment. In an actual structure, this high chloride environment typically results from salting of roadways during winter storms, salt spraying onto structures located immediately above or adjacent to the ocean, or salt air blowing onto structures located proximate to the ocean. As a comparison, the test matrix must include identical series of specimens both with and without exposure to chlorides. Typically, unexposed specimens serve as nothing more than a baseline comparison for exposed specimens. However, because this study also investigated fatigue, some of the unexposed specimens were also important in order to determine whether any of the previously discussed grout defects affected fatigue performance.

The resulting beam test matrix is shown in Table 4-1. Specimens without exposure to chlorides were tested in fatigue to 2,000,000 cycles or failure, whichever came first. Because prestressing strand does not possess an endurance limit, a value of 2,000,000 cycles is generally taken as the fatigue life of a structure (ACI 215R 1997, ACI 423.5R 1999). Specimens exposed to chlorides underwent an initial fatigue loading of 10,000 cycles to initiate cracking in the partially prestressed members. Following this

initial loading, the specimens underwent exposure to chlorides for six months. The chloride exposure took the form of a five percent NaCl solution placed in a two-week-long, alternating wet-then-dry sequence. After the six months of continuous exposure, the specimens were placed in the fatigue frame and tested to 2,000,000 cycles or failure, whichever came first. The exposure specimens were visually examined throughout the six-month period.

Table 4-1: Beam Specimen Test Matrix

Series	Specimen	Level of Prestress ²	Post-Tensioning Condition ³	Exposure
Fatigue Reference	FR-1 FR-2 FR-3	Full Partial 1 Partial 2	Intact	None
Anchor Zone Grout Void	AZ-1 AZ-2 AZ-3	Full Partial 1 Partial 2	Grout void at anchor zone	None
Anchor Zone Grout Void with Corrosion	AZC-1 AZC-2 AZC-3	Full Partial 1 Partial 2	Grout void at anchor zone	Saltwater cycles during static loading
Crown Grout Void with Corrosion ¹	GVC-1 GVC-2 GVC-3	Full Partial 1 Partial 2	Grout void (due to cracking) with a breach in the duct	Saltwater cycles during static loading

Notes:

1. The fatigue reference serves as the baseline condition for a void in the grout due to shrinkage cracking.
2. Full prestress is based on a nominal tensile stress in the precompressed tensile zone of $3\sqrt{f'_c}$ (psi). Partial prestress is based on 67 percent of the force required for full prestress, with Partial Prestress 1 obtained using fewer strands and Partial Prestress 2 obtained using a lower prestressing force.
3. The post-tensioning system consisted of a plastic duct filled with a prepackaged grout.

4.3 Beam Specimen Design

Design, by its very nature, is an iterative process. This fact held during the evolution of the dimensions and layout for the full-scale beam specimen. Several competing interests shaped the final specimen design, including overall size and weight limitations; ease of testing; use of a single multi-strand tendon; desire to push the code limits for the concrete and strand stresses; and the construction methods and materials available in the lab. The result is shown in Figure 4-3.

4.3.1 Beam Tendon and Mild Steel Design

The structural design of the beam cross-section was based on both ACI 318 (2008) and AASHTO LRFD (2008) recommendations. This requirement was not overly difficult to attain as the two are in substantial agreement. However, if there was a disagreement, the more conservative approach was used in the design. The service load design was based on the following:

- Uncracked, gross section properties
- Linear-elastic material behavior
- $f'_c = 4,000$ psi
- Concrete 28 days old at stressing
- Allowable tensile stress in the precompressed tensile zone of

$3\sqrt{f'_c}$ (psi) for the fully prestressed design

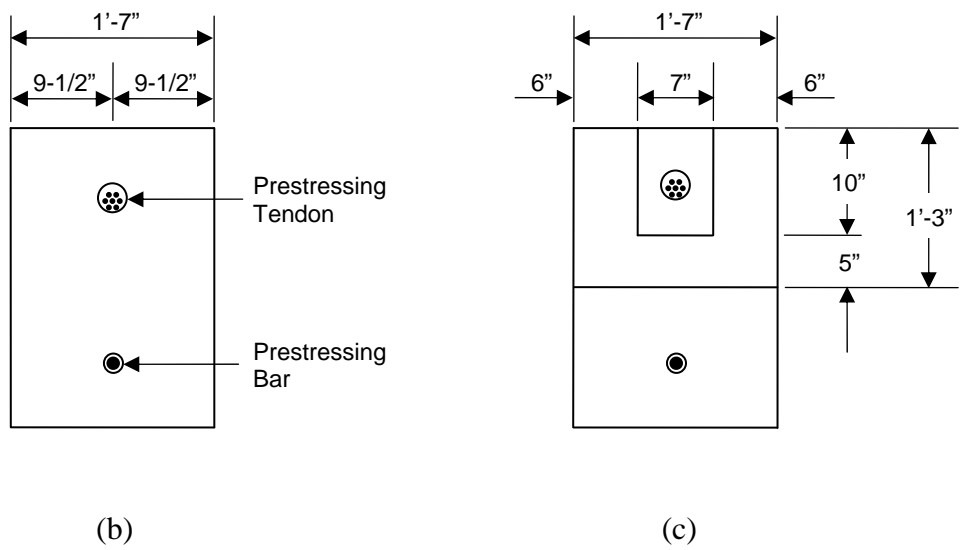
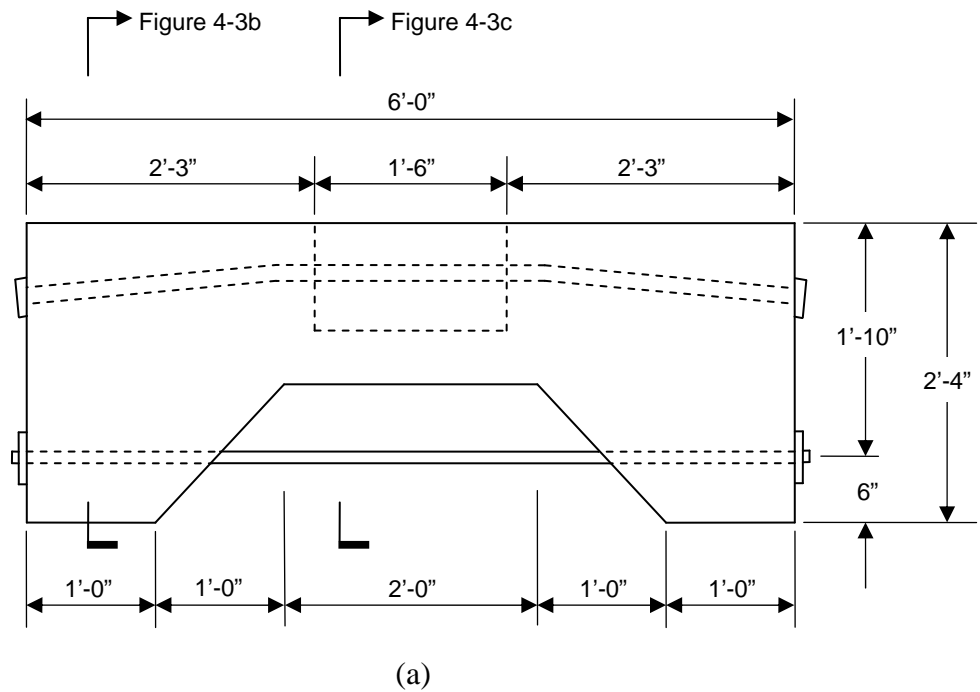


Figure 4-3: Beam Specimen Design

- Two-point drape strand profile with AASHTO LRFD minimum allowable bend radius of 20'-0"
- 1/2-inch-diameter, low-relaxation prestressing strand
- $f_{pu} = 270$ ksi, $f_{py} = 230$ ksi
- Grade 60 mild steel, $f_y = 60$ ksi
- 1-1/2" minimum concrete cover for prestressed and nonprestressed reinforcement
- Prestress losses in accordance with ACI and AASHTO recommendations

Stressing at 28 days reduced the effect of shrinkage on the prestress losses. As a comparison, most precast segmental concrete bridges and splice-girder bridges are at least 28 days old at the time of prestressing.

The tendon design focused on the two competing issues of stress in the concrete at transfer and stress in the concrete at full service load. The transfer stresses were particularly critical because the beam specimen has no dead load to counteract the prestressing force at transfer. One option for controlling the stresses at transfer was to install the post-tensioning bar, with a very small amount of force, prior to stressing the tendon. A more desirable option would be to stress the tendon without the post-tensioning bar in place; that would greatly simplify construction, handling, and testing of the specimens. Therefore, the author reduced the tendon eccentricity at midspan and the ends to control transfer stresses and allow stressing without the post-tensioning bar in place. The final design for the fully prestressed specimen used six 1/2-inch-diameter strands, and the final design

for the partially prestressed specimen used four 1/2-inch-diameter strands (or six strands at the same total force). Table 4-2 contains the section properties at midspan of the specimen. Table 4-3 contains the calculated stress checks at midspan for the two specimen designs as well as the code allowable values. All values are given as a function of f'_c . Refer to Figure 4-3 for the specimen dimensions.

Table 4-2: Specimen Cross-Sectional Properties at Midspan

Moment of Inertia, I	4,276 in. ⁴
Cross-sectional Area, A	220 in. ²
Distance from neutral axis to top of section, y_t	8.24 in.
Distance from neutral axis to bottom of section, y_b	6.76 in.
Eccentricity of tendon from neutral axis, e_p	2.60 in.
Eccentricity of prestressing bar from neutral axis, e_b	13.76 in.

Table 4-3: Maximum Calculated Stresses and Code Allowable Stresses at Midspan

Condition	Stress State	Fully Prestressed		Partially Prestressed	
		Calculated	Code ²	Calculated ³	Code ²
Jacking ¹	Tension	$0.63\sqrt{f'_c}$	$3\sqrt{f'_c}$	$0.42\sqrt{f'_c}$	$3\sqrt{f'_c}$
	Compression	$0.49f'_c$	$0.60f'_c$	$0.32f'_c$	$0.60f'_c$
Transfer	Tension	$0.48\sqrt{f'_c}$	$3\sqrt{f'_c}$	$0.32\sqrt{f'_c}$	$3\sqrt{f'_c}$
	Compression	$0.37f'_c$	$0.60f'_c$	$0.25f'_c$	$0.60f'_c$
Service	Tension	$3\sqrt{f'_c}$	$3\sqrt{f'_c}$	$11.3\sqrt{f'_c}$	see note 4
	Compression	$0.50f'_c$	$0.60f'_c$	$0.49f'_c$	$0.60f'_c$

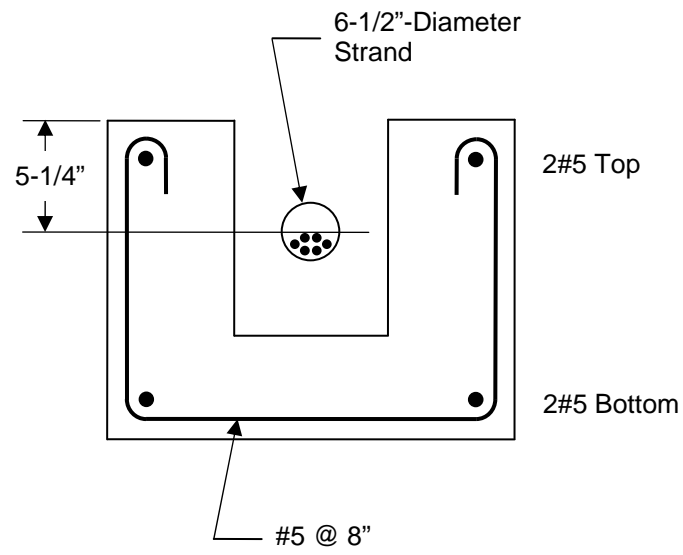
Notes:

1. ACI and AASHTO do not specifically address this condition, but the author determined that the use of a multi-strand jack necessitated a check of these stresses and compared them to allowable stresses at transfer.
2. Because the beam specimens were stressed at 28 days after casting the concrete, code allowable stress checks during jacking and at transfer are based on f'_c .
3. Calculated service stresses were based on uncracked section properties, which is consistent with the ACI code approach, with the values representing a nominal stress check.
4. ACI and AASHTO do not place a limit on the tensile stress in the precompressed tensile zone for partially prestressed members, but both codes require serviceability checks for deflection, crack control, and reinforcement stresses.

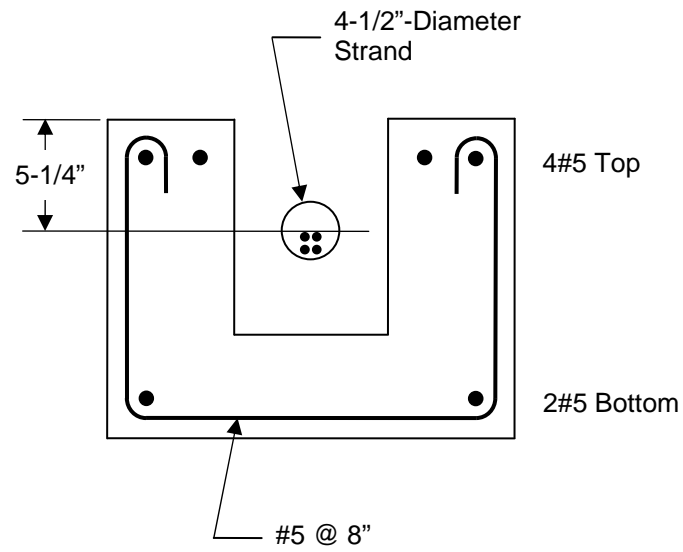
Reinforcement details for the center region of the fully prestressed and partially prestressed designs are shown in Figure 4-4 (see Figure 4-3 for specimen dimensions). Mild steel for the beam specimens was based on two requirements: (1) providing ACI and AASHTO minimum bonded reinforcement; and (2) providing approximately equal ultimate strength capacities for the two designs. Where the tendon is partially external to the concrete, it is partially unbonded from the section. As such, a minimum amount of bonded reinforcement is required to satisfy the design codes. This required the addition of two No. 5 bars at the tension face for both designs. To arrive at equal ultimate strength capacities, the partially prestressed specimen required another two No. 5 bars. Stresses in the tendon at ultimate strength were based on equations for unbonded tendons. With respect to stirrups, the beam specimens did not require any shear reinforcement because of the method of applying load through an eccentric axial force. However, the author provided minimum shear reinforcement for handling and unanticipated conditions.

4.3.2 Local and General Zone Design

For a successful post-tensioned design, the concentrated anchorage force must be dispersed over the entire cross-section of the member. This dispersion takes place within the disturbed region of the beam where plane sections no longer remain plane (AASHTO 2008). Design of the local zone is the responsibility of the post-tensioning hardware supplier and is usually based on extensive testing (VSL 1991). VSL provided the local zone reinforcement for their 5-7 Type EC Anchorage used in the construction of the beam spe-



(a) Full Prestress Design



(b) Partial Prestress Design

Figure 4-4: Beam Specimen Design Details

cimens. The 5-7 designation stands for 1/2-inch-diameter strand in a maximum seven-strand tendon. The local zone reinforcement consisted of a No. 4 spiral with a 9" diameter, 12" length, and 2" pitch.

Design of the general zone is the responsibility of the engineer. AASHTO allows three different methods for the design of the general zone. Due to the unusual geometry of the beam specimens, the author chose the strut-and-tie method. Furthermore, the specimen required a three-dimensional strut-and-tie model due to the unusual shape. The final design, based on AASHTO recommendations, required five No. 5 horizontal bars and three No. 5 vertical bars. The three vertical bars were changed to four for symmetry since the tendon was located in the center of the cross-section. These bars were located approximately 14" from the end of the beam, with the horizontal bars equally distributed over the 15" depth of the section and the vertical bars equally distributed over the 19" width of the section.

4.3.3 Deviator Design

Tendon curvature introduces both in-plane and out-of-plane forces on a prestressed concrete member. Tendon curvature also introduces localized bending effects on the prestressing strand. The author chose a two-point drape strand profile in order to investigate these localized bending effects when combined with a fatigue loading. To accentuate the effect, the researcher chose the minimum radius of curvature allowed by the AASHTO LRFD Code (2008) at the deviation point. The following section discusses the impact of the deviation point on the design of the prestressed concrete member.

In accordance with AASHTO requirements, the author installed a steel pipe at the tendon deviation point, as shown in Figure 4-5, which also coincided with the transition from internal to external tendon. The plastic duct of the tendon, with a maximum outside diameter of 2-7/8" at the ribs, passes through the steel pipe, which has an internal diameter of 3-1/8". The pipe measures 6" in length and was curved to a 20'-0" radius, the minimum value allowed by AASHTO. The steel pipe conforms to the requirements of ASTM A53, Type E, Grade B with a nominal wall thickness not less than 0.125" as specified by AASHTO.



Figure 4-5: Photograph Showing Location of Steel Deviation Pipe

In addition to the requirement for a steel deviation pipe, the tendon curvature introduces in-plane forces. These in-plane deviation forces were calculated in accordance with the AASHTO recommendations. The author again applied a strut-and-tie model to

determine the adequacy of the section to resist these forces. The design required the placement of one No. 5 bar to resist the tie force of the model. The bar was added in the form of a U-shaped stirrup since the tension is at the bottom of the cross-section, perpendicular to the longitudinal axis.

The tendon curvature also introduces out-of-plane forces due to wedging action of the strands against the duct. However, the deviation pipe resists this effect. Nonetheless, the author also examined whether the concrete section surrounding the pipe could resist these forces. The out-of-plane forces were again calculated in accordance with AASHTO recommendations. The author found the shear resistance of the concrete sufficient to resist these forces, so the addition of confining reinforcement was unnecessary.

4.3.4 Post-Tensioning Bar and Anchorage Design

The post-tensioning bar provided the static dead and live load to the beam specimens during the exposure cycles. The prestressing bar extended between the corbels located at each end of the beam (see Figure 4-3). When the bar was tensioned, it provided a uniform moment to the beam cross-section. For the tendon design and concrete cross-section chosen for the specimens, a prestress force of 74 kips was required to apply the full dead and live load service moment. The prestressing bars, manufactured in accordance with ASTM A722, had an ultimate tensile strength of 150 ksi. In accordance with ACI 318 (2008) and the manufacturer's recommendations, a prestressing force of 74 kips would require a 1-inch-diameter prestressing bar. However, because the bars were or-

dered well ahead of the final specimen design, a 1-1/4"-diameter bar was used in the construction of the specimens.

Anchorage of the prestressing bars was in the form of a bearing plate and nut, as the bars were threaded throughout their length. The dimensions of the bearing plate were chosen such that supplemental confining reinforcement would not be required in the anchorage zone. All concrete bearing stresses were checked in accordance with ACI 318 (2008). The bearing plate was constructed from ASTM A36 steel with a minimum yield stress of 36 ksi. Design of the bearing plate was in accordance with AISC (2005) recommendations and included a dish-shaped depression to allow for seating of the spherical hex nuts.

4.3.5 Corbel Design

The corbels at each end of the beam specimen provided the means of applying the static dead and live load during the exposure cycles and the fatigue loading during the cyclic testing. Design of the corbel was in accordance with the provisions of ACI 318 (2008) and ACI 215R (1997). The provisions of ACI 318 were used for the basic design, but the provisions of ACI 215R were used to evaluate the impact of fatigue on the concrete and reinforcing steel during the cyclic loading.

In order to evaluate fatigue in the corbels, the author needed to select a dead-to-live-load ratio for the beam specimens. Dead-to-live-load ratios for concrete bridges vary considerably, with the ratio increasing with span length. A review of the literature provided the following recommendations for typical dead-to-live-load ratios for bridges:

- FHWA Report HI-98-032 (Withiam *et al.* 1998) – 1.0 to 3.0
- NCHRP Report 368 (Nowak 1999) – 0.5 to 3.0
- NCHRP Report 454 (Moses 2001) – 1.0 to 3.0
- NCHRP Report 507 (Paikowsky 2004) – 2.0 to 2.5
- AASHTO Bridge Committee (AASHTO T-5 2007) – 0.5 to 3.0

Withiam *et al.* also suggest a convenient rule-of-thumb for the dead-to-live-load ratio as the span length in meters divided by 20.

Selection of the dead-to-live-load ratio affects the fatigue loading applied to the specimens. The lower the ratio, the higher the percentage of total load attributed to live load, which represents the cyclic portion of the total applied loading. The higher the cyclic portion of the total load, the lower the number of cycles to failure. The average of the five ranges given above is 1.0 to 2.9, or essentially 1 to 3. The author chose the mid-value of 2 for the dead-to-live-load ratio. The goal was not to examine the worst possible case, but to evaluate a very typical bridge dead-to-live-load ratio.

The final corbel design consisted of six No. 5 bars for the primary reinforcement and two No. 5 bars for the closed stirrup reinforcement. Particular care was taken during construction to adequately develop the primary reinforcement in accordance with recommendations from ACI 318 (2008).

4.3.6 Beam Specimen Design Summary

The final beam specimen design required a careful arrangement of all of the design elements discussed previously. For simplicity, the author used only No. 5 bars for

the mild steel. The only exception was the post-tensioning anchorage spiral provided by VSL, which was a No. 4 bar. All reinforcement was detailed in accordance with ACI 315, *Details and Detailing of Concrete Reinforcement* (1999). Figure 4-6 is a photograph of a finished reinforcement cage for the beam specimens highlighting the role of each aspect of the mild steel.

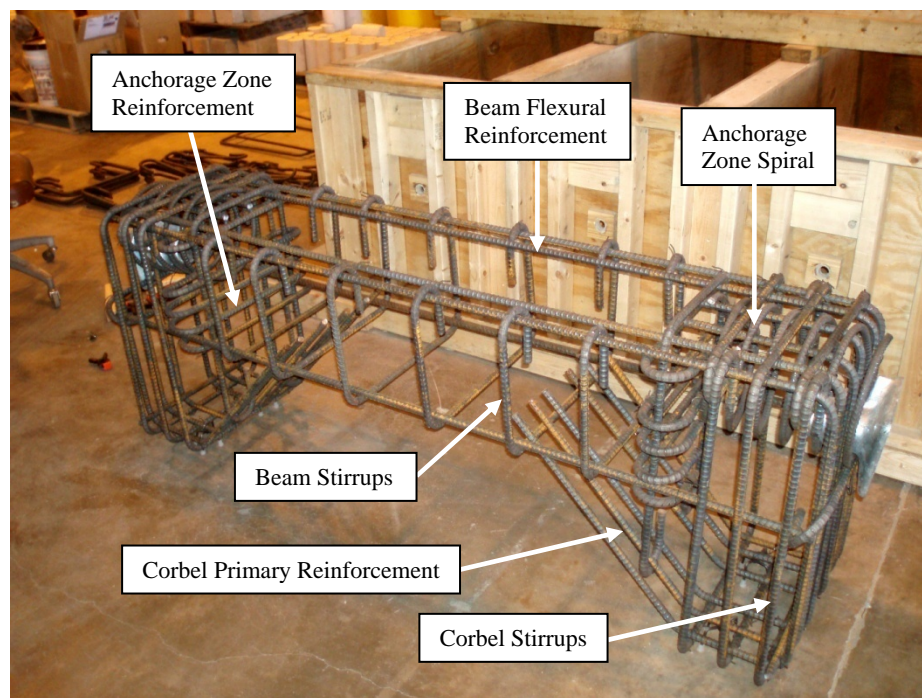


Figure 4-6: Beam Specimen Reinforcing Cage

4.4 Beam Specimen Construction

In general, fabrication of the beam specimens followed typical construction practices for construction of the formwork; fabrication of the reinforcing cages; placement and curing of the concrete; installation and stressing of the post-tensioning tendons; and

grouting of the tendons. Figure 4-7 shows the completed formwork, reinforcing cage, deviators, prestressing anchorages, and plastic duct ready for concrete placement. Figure 4-8 shows a set of three finished specimens. Details of the beam specimen construction are contained in Appendix C, including the concrete mix design and results of the material property testing.



Figure 4-7: Completed Specimen Setup Ready for Concrete Placement

4.5 Beam Specimen Instrumentation

Beam specimen instrumentation consisted of vibrating wire strain gauges installed on the concrete beam surface and the prestressing bar couplers. The choice of vibrating wire strain gauges was based on many factors. First, vibrating wire strain gauges have a

history of long-term reliability (*e.g.*, Barr *et al.* 2005, Burns *et al.* 1997). Due to the length of time required for the durability portion of the study, the gauges must remain stable for a period of six to nine months. Second, vibrating wire strain gauges have a history of successful use with reinforced and prestressed concrete (Burns *et al.* 1997). Third, due to the particular specimen design, only axial strains occurred within the concrete beam. Thus, a strain rosette was not required as these were the principal strains experienced by the specimens. Lastly, vibrating wire strain gauges offer simplicity of use and thus a decreased potential for error. Appendix D discusses the particular vibrating wire strain gauges chosen for the test specimens and the rationale for this choice.



Figure 4-8: A Set of Three Completed Beam Specimens

The critical element to monitor during the specimen testing was the prestressing strand. However, monitoring of the strand directly was extremely difficult due to the limited accessibility and very high strains experienced by the strand during stressing. Numerous researchers have attempted to monitor the stress in the strand with very limited to no success (*e.g.*, Barr *et al.* 2005, Ciolko and Tabataba 1999, Ryals *et al.* 1992, Wollman *et al.* 1988). Furthermore, breaching the duct and grout to monitor the strains in the strand offers a path for the chlorides that does not exist in an actual structure, and durability was a primary element of this study. Consequently, the strains in the strand were monitored indirectly.

Vibrating wire strain gauges were installed at midspan of the beam specimens at the locations shown in Figure 4-9 (see Figure 4-3 for specimen dimensions). Figure 4-10 is a photograph of an actual specimen showing the gauge orientation. These gauges served multiple purposes. First, the gauges allowed the beam specimens to function as giant load cells in order to determine the stress in the prestressing strands. During the strand stressing operation, the author recorded the changes in strain and calibrated these values to the overall tendon force measured by the stressing jack's pressure gage. Second, the gauges monitored the strains in the concrete during the strand stressing operation and during the prestressing bar stressing operation. Third, the gauges also monitored changes in concrete strain during the durability portion of the study. These changes in concrete strain, due to creep and shrinkage, caused long-term losses of the prestressing force in the strand. The specific procedure for monitoring the strand stress is discussed in detail in Chapter 5.

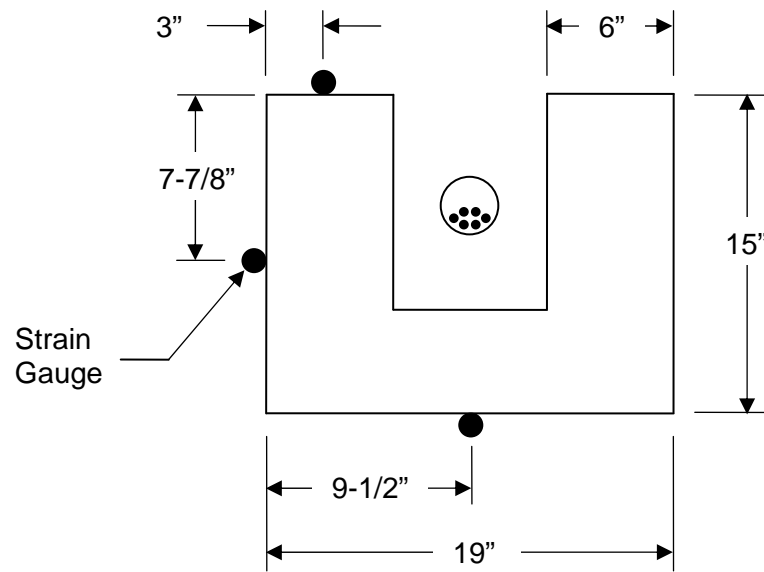


Figure 4-9: Vibrating Wire Strain Gauge Locations at Midspan of Beam Specimens



Figure 4-10: Vibrating Wire Strain Gauge Orientation on Beam Specimens

In addition to the gauges installed on the specimens, vibrating wire strain gauges were installed on the prestressing bars. These gauges were used to monitor the strain, and thus force, applied by the prestressing bar to the beam specimens. Because the bars are continuously threaded, the author cut the bars into two pieces and used a coupler to tie them back together. The strain gauges were installed on the smooth couplers, which then acted as load cells to determine the force in the prestressing bar at any given time. The “load cells” were calibrated during the prestressing operation through the use of a calibrated pressure gage attached to the hydraulic pump. A photograph of one of the prestressing bar couplers is shown in Figure 4-11. Appendix D contains the load versus strain behavior for the coupler “load cells.”

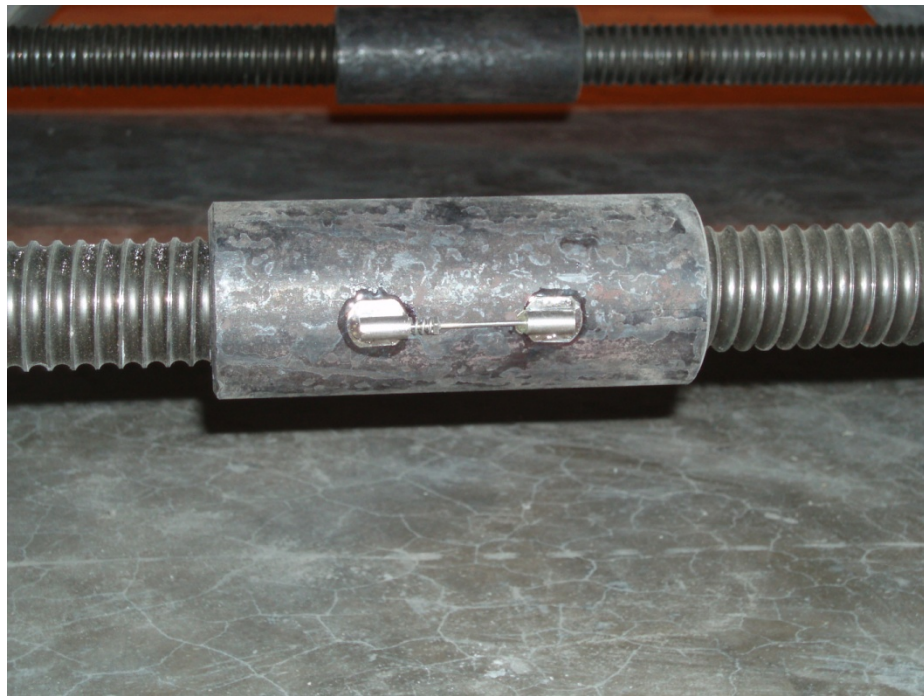


Figure 4-11: Vibrating Wire Strain Gauge Installed on Prestressing Bar Coupler

Periodic retensioning of the prestressing bars was required due to creep and shrinkage of the beam specimens. The prestressing bars were retensioned when they lost five percent of their initial force.

Chapter 5

Beam Specimen Testing

This chapter discusses the exposure and fatigue testing of the post-tensioned beam specimens. Discussed in detail in Section 4.2, the testing program included twelve full-scale beam specimens that combined long-term static exposure testing with fatigue testing. The exposure testing, performed on six of the twelve specimens, involved exposing the specimens to saltwater for a period of six months while under full service load. The fatigue testing, performed on all twelve specimens, involved loading the specimens for 2,000,000 cycles or until failure, whichever came first. A complete description of the test variables and the design, construction, and instrumentation of the beam specimens is contained in Chapter 4.

5.1 Determination of Strand Stress

The critical element to monitor during construction and testing of the beam specimens was the prestressing strand. However, as discussed in Section 4.5, monitoring of the strand directly was extremely difficult due to the limited accessibility and very high strains experienced by the strand during stressing. Consequently, the author developed a technique to determine the stress in the strand that combined experimental and analytical methods. From construction up to the point of fatigue testing, the strand stress was monitored indirectly through vibrating wire strain gauges installed on the surface of the con-

crete specimens. During fatigue testing, the stresses in the strand were calculated through two independent analytical methods: a moment-curvature analysis and a finite element analysis. This section discusses the methodology, rationale, and results for determining the stress in the prestressing strand at these different stages.

5.1.1 Prior to Fatigue Testing

The vibrating wire strain gauges installed on the surface of the concrete essentially allowed the beam specimens to function as giant load cells. During the strand stressing operation, the author recorded the changes in strain and calibrated these values to the overall tendon force measured by the stressing jack's pressure gage, as shown in Figure 5-1 for Specimen FR-1. Results from any of the three gauges could be used to determine the force in the strand. However, the gauge at the bottom of the beam offers the least reliability due to the very small strains experienced at this location during stressing. Following removal of the jacking force, and subsequent seating of the wedges, the author again recorded the changes in strain. These final values were used to determine the force in the prestressing strand at transfer from the relationship shown in Figure 5-1. This procedure was possible because of the use of a multi-strand stressing jack to stress the beam specimen tendons.

Using Beam Specimen FR-1 as an example, the strand stresses during jacking and at transfer were calculated by the following method. Preliminary design calculations indicated that, primarily due to seating losses, the tendon must be tensioned to the full code allowable value of 80 percent of the guaranteed ultimate tensile strength (GUTS) of the

strand, f_{pu} (AASHTO 2008, ACI 2008). With a six-strand-tendon and an ultimate tensile strength of 270 ksi, this equates to a force of 198.3 kips, which is the peak value plotted in Figure 5-1. With the tendon force applied in increments of 30 kips, the response of the strain gauges in Figure 5-1 is essentially linear. Following removal of the jacking force, and subsequent seating of the wedges, the author again recorded the strains, which measured $401\mu\epsilon$ for Gauge No. 1 and $169\mu\epsilon$ for Gauge No. 2. Using the relationship shown in Figure 5-1 results in a force in the strand at transfer of 144.8 kips based on Gauge No. 1 and 143.8 kips based on Gauge No. 2, essentially identical. This value represents a transfer stress of $0.58f_{pu}$. Both the jacking and transfer stresses are shown in Table 5-1.

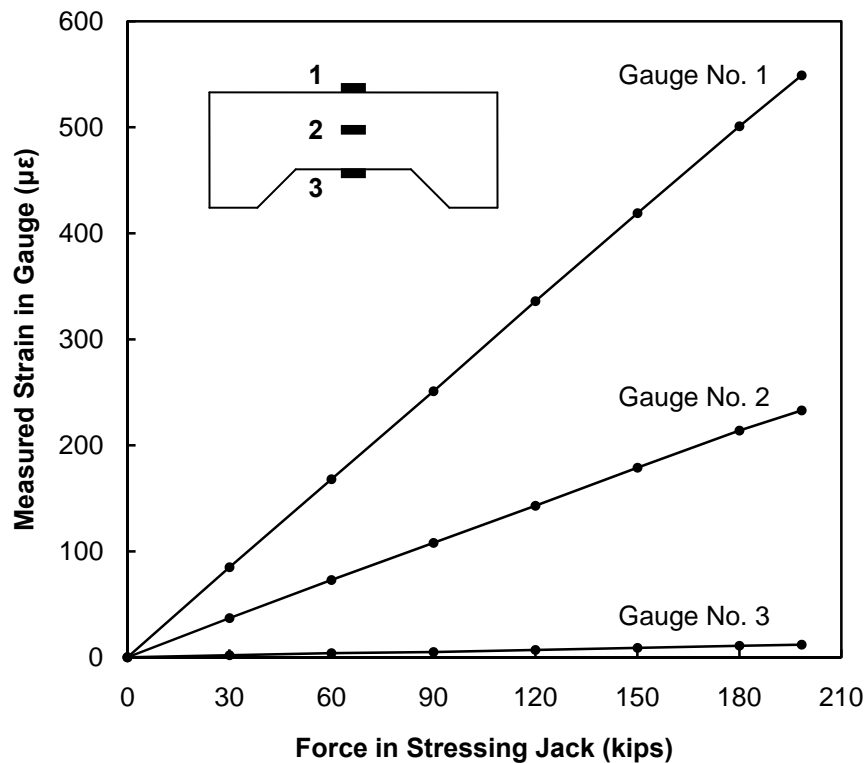


Figure 5-1: Beam Specimen FR-1 Strain Gauge Measurements as a Function of Force in the Stressing Jack

Table 5-1: Strand Stresses for Fatigue Reference Series

Specimen	Prestressing Strand Stress		
	Jacking	Transfer	Final
FR-1	$0.80f_{pu}$	$0.58f_{pu}$	$0.58f_{pu}$
FR-2	$0.80f_{pu}$	$0.58f_{pu}$	$0.58f_{pu}$
FR-3	$0.53f_{pu}$	$0.31f_{pu}$	$0.31f_{pu}$

The last value shown in Table 5-1 includes prestress losses due to creep and shrinkage during the time between transfer and fatigue testing. These losses were also determined by the use of the vibrating wire strain gauges. Using surface gauges to measure prestress losses due to creep and shrinkage is a very common technique (*e.g.*, Baran *et al.* 2005, Hale and Russell 2006). The change in strain experienced by the tendon is equal to the change in strain experienced by the concrete at the same vertical location in the specimen. Gauge No. 1 was located approximately 5-5/8" above the tendon, and Gauge No. 2 was located approximately 2-1/4" below the tendon. The author then determined the change in strain at the location of the tendon through linear interpolation (plane strain assumption).

A temperature correction to the measured creep and shrinkage strains was unnecessary, primarily since the specimens were inside a conditioned lab space. Nonetheless, the author monitored the specimen temperatures with an infrared thermometer and through the vibrating wire strain gauges. The strain gauges incorporate a thermistor in their housing, which could be read through the readout box. Final creep and shrinkage strain measurements were only taken if the beam specimen temperature fell within 2° Fa-

hrehnheit of the temperature during the initial strain measurement immediately following prestress transfer. Thus, any temperature effects were negligible.

For Beam Specimen FR-1, which underwent fatigue testing within a month of stressing, the prestress losses due to creep and shrinkage were minimal. The change in strain at the location of the tendon measured $33 \mu\epsilon$, which resulted in a prestress loss of 0.96 ksi based on a strand modulus of elasticity of 29,000 ksi. Therefore, the final strand stress prior to fatigue testing was equal to $0.58f_{pu}$, as shown in Table 5-1.

The losses from seating of the wedges were significant due to the relatively short length of the beam and the use of a stressing jack without power seating. For Beam Specimen FR-1, the seating losses amounted to 58.8 ksi. In general, losses due to anchor seating, creep, shrinkage, friction, and steel relaxation within an actual prestressed member do not exceed 20 percent of the guaranteed ultimate tensile strength, or 54 ksi for Grade 270 strand (*e.g.*, ACI 318 2008, ACI 215R 1997, Paulson 1983). Fortunately, the Fatigue Reference Series specimens were tested very soon after stressing, such that long-term prestress losses were negligible. For subsequent specimens, the author increased the jacking stress to partially compensate for the significant seating losses.

As a secondary check on the vibrating wire strain gauges, the author also compared the measured strains in the concrete during the jacking operation to calculated strains in the concrete. The calculated strains were based on the calculated stresses imposed by the jacking force converted to strains through the modulus of elasticity measured for the particular concrete placement (see Section C.8.1). Figure 5-2 is a plot of the measured strains versus the calculated strains. Compared to a one-to-one relationship,

which would indicate a perfect correlation, the strains have an R^2 value of 0.988. Therefore, the measured strains compared very well with the calculated strains and confirmed the accuracy of the measured results. The calculated and measured strain values are tabulated in Appendix E.

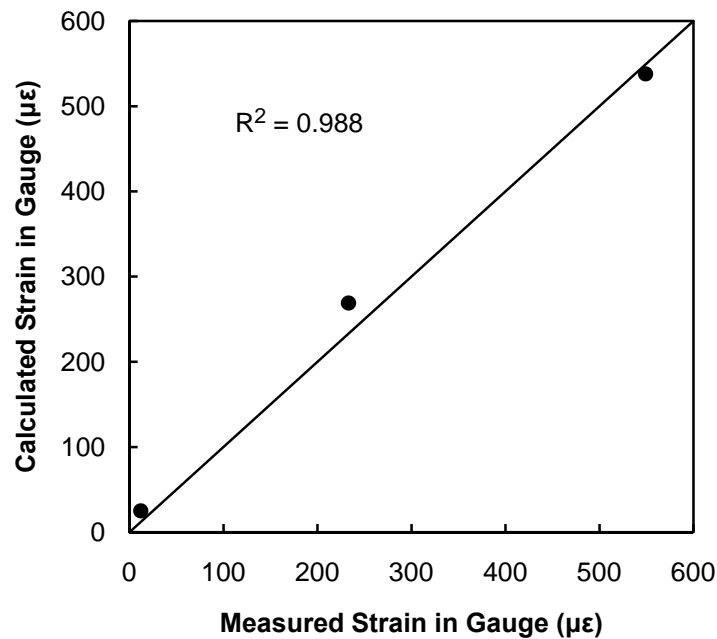


Figure 5-2: Beam Specimen FR-1 Measured versus Calculated Concrete Strains During Jacking Operation

To correlate with actual prestressed members, the effective prestress for the beam specimens must be kept at or above 60 percent of the guaranteed ultimate tensile strength of the strand, or as close as possible. In general, losses due to anchor seating, creep, shrinkage, friction, and steel relaxation within an actual prestressed member do not exceed 20 percent of the guaranteed ultimate tensile strength (*e.g.*, ACI 318 2008, ACI 215R 1997, Paulson 1983). Thus, with a maximum code allowable jacking stress of

$0.80f_{pu}$, the $0.60f_{pu}$ value represents a lower bound for an actual prestressed member. However, due to the relatively short beam specimen lengths (6'-0"), seating losses were very high, almost 22 percent of f_{pu} for the Fatigue Reference Series. Consequently, in order to partially compensate for these high seating losses, the author needed to increase the jacking stress for subsequent specimens, particularly those that would undergo durability testing and would thus experience higher long-term prestress losses than the Fatigue Reference Series specimens.

The author increased the jacking stress to $0.82f_{pu}$ for the next series of specimens, the Anchor Zone Grout Void Series. The decision to exceed the code allowable value was based on the following considerations:

1. The stressing operation would be temporary and of very short duration.
2. The stressing operation would not exceed the yield stress of the strand.
3. The anchorage hardware was designed for a seven-strand tendon, but only a six-strand tendon was used in the beam specimens. Therefore, even with the increased jacking stress, the total force was less than that for which the hardware was designed.
4. The calculated concrete stresses were still within code allowable values.
5. The mild reinforcement design for the local and general zones was based on a seven-strand tendon. Therefore, even with the increased jacking stress, the total force was less than that for which the mild steel was designed.

During the subsequent stressing operation, there were no signs of distress in the strand, anchorage, or concrete.

The results for the Anchor Zone Grout Void Series are shown in Table 5-2 and Figure 5-3. The same procedure as that used for the Fatigue Reference Series was used to determine the stress in the strand at transfer and due to long-term losses. However, the Anchor Zone Grout Void Series underwent fatigue testing within a month of stressing, thus the prestress losses due to creep and shrinkage were again minimal. As with the previous series, the response of the strain gauges during the jacking operation was essentially linear, similar to the response shown in Figure 5-1. Figure 5-3 is a comparison of the measured and calculated strains during the jacking operation for Beam Specimen AZ-1. Compared to a one-to-one relationship, which would indicate a perfect correlation, the strains have an R^2 value of 0.982. Therefore, the measured strains compared very well with the calculated strains and confirmed the accuracy of the measured results. The calculated and measured strain values are tabulated in Appendix E.

Table 5-2: Strand Stresses for Anchor Zone Grout Void Series

Specimen	Prestressing Strand Stress		
	Jacking	Transfer	Final
AZ-1	$0.82f_{pu}$	$0.61f_{pu}$	$0.61f_{pu}$
AZ-2	$0.82f_{pu}$	$0.61f_{pu}$	$0.61f_{pu}$
AZ-3	$0.55f_{pu}$	$0.33f_{pu}$	$0.33f_{pu}$

The author increased the jacking stress to $0.83f_{pu}$ for the last two series of specimens, the Anchor Zone Grout Void Corrosion Series and the Grout Void Corrosion Se-

ries. The further increase in jacking stress was an attempt to compensate for the long-term prestress losses of the durability series of specimens. These specimens underwent chloride exposure in the lab under full dead (sustained) and live load for six months, experiencing six months of creep and shrinkage losses. The decision to increase the jacking stress further was made because of the successful increase in jacking stress with the previous series. Although an increase above $0.83f_{pu}$ would have better helped to compensate for the long-term losses, this value was already above the proportional limit and was approaching the yield stress of the strand. During the subsequent stressing operations, there were no signs of distress in the strand, anchorage, or concrete.

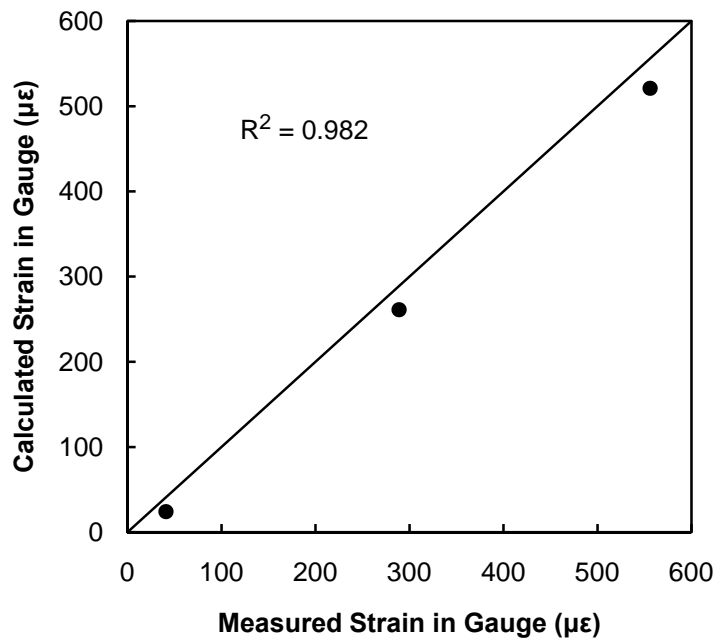


Figure 5-3: Beam Specimen AZ-1 Measured versus Calculated Concrete Strains During Jacking Operation

The results for the Anchor Zone Grout Void Corrosion Series are shown in Table 5-3 and Figure 5-4, and the results for the Crown Grout Void Corrosion Series are shown in Table 5-4 and Figure 5-5. The same procedure as that used for the previous two series was used to determine the stress in the strand at transfer and due to long-term losses. As with the previous series, the response of the strain gauges during the jacking operation was essentially linear, similar to the response shown in Figure 5-1. Figures 5-4 and 5-5 are comparisons of the measured and calculated strains during the jacking operation for Beam Specimen AZC-1 and Beam Specimen GVC-1, respectively. Compared to a one-to-one relationship, which would indicate a perfect correlation, the strains have an R^2 value of 0.987 for AZC-1 and 0.954 for GVC-1. Therefore, the measured strains compared very well with the calculated strains and confirmed the accuracy of the measured results. The calculated and measured strain values are tabulated in Appendix E.

Table 5-3: Strand Stresses for Anchor Zone Grout Void Corrosion Series

Specimen	Prestressing Strand Stress		
	Jacking	Transfer	Final
AZC-1	$0.83f_{pu}$	$0.62f_{pu}$	$0.60f_{pu}$
AZC-2	$0.83f_{pu}$	$0.62f_{pu}$	$0.60f_{pu}$
AZC-3	$0.55f_{pu}$	$0.33f_{pu}$	$0.31f_{pu}$

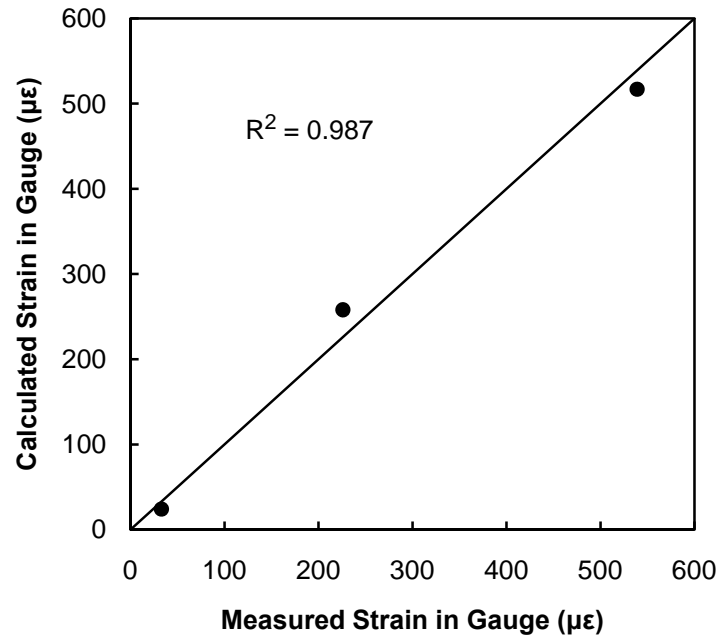


Figure 5-4: Beam Specimen AZC-1 Measured versus Calculated Concrete Strains During Jacking Operation

Table 5-4: Strand Stresses for Crown Grout Void Corrosion Series

Specimen	Prestressing Strand Stress		
	Jacking	Transfer	Final
GVC-1	$0.83f_{pu}$	$0.62f_{pu}$	$0.60f_{pu}$
GVC-2	$0.83f_{pu}$	$0.62f_{pu}$	$0.60f_{pu}$
GVC-3	$0.55f_{pu}$	$0.33f_{pu}$	$0.31f_{pu}$

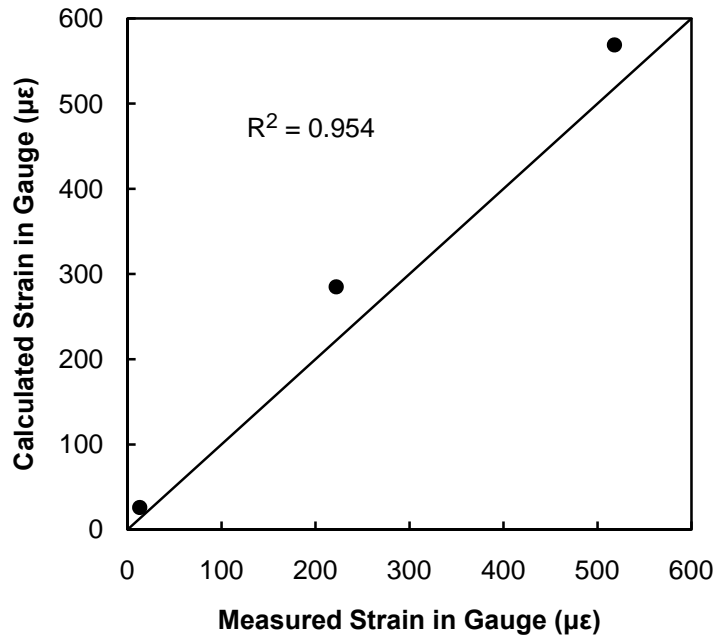


Figure 5-5: Beam Specimen GVC-1 Measured versus Calculated Concrete Strains During Jacking Operation

Only the fully prestressed specimens in each series were instrumented. The losses for the other two specimens in each series were estimated from the values determined for the fully prestressed beam. The previous results verified that this approach was acceptable for the following reasons:

1. Seating losses, which ranged from 57.1 to 58.8 ksi, represented the vast majority of the total losses, which ranged from 57.9 to 61.4 ksi.
2. Seating losses are only a function of the wedge, anchor head, and stressing jack hardware, which were identical for every specimen.
3. Seating losses were very consistent between specimens, ranging from 57.1 to 58.8 ksi, confirming Item 2 above.

4. Only the fully prestressed specimens remained uncracked under full service load. Long term prestress losses determined from concrete strains measured in cracked sections are often unreliable.

Based on the actual prestress losses listed in Tables 5-1 through 5-4, the author calculated a revised specimen loading. It was critically important to stress the concrete in tension during the fatigue loading to the same limits chosen in Chapter 4 for the original design, $3\sqrt{f'_c}$ (psi) for the fully prestressed specimens and $12\sqrt{f'_c}$ (psi) for the partially prestressed specimens. However, the original design assumed an effective prestress based on AASHTO (2008) and ACI (2008) recommendations, which was $0.6f_{pu}$. The actual effective prestress ranged from $0.58f_{pu}$ to $0.61f_{pu}$. These actual values were very close to the assumed value, but still necessitated a slight adjustment. The peak service load, and thus peak fatigue load, was determined from Eq. 5.1, with the key variables also shown in Figure 5-6, and the concrete stress in tension set equal to a value of $3\sqrt{f'_c}$ (psi) for the fully prestressed design. The partially prestressed design used the same service load as the fully prestressed design, as discussed in Chapter 4.

$$f_t = \frac{P}{A} \pm \frac{My}{I} = -\frac{(P_{load} + P_{eff})}{A} + \frac{(P_{load}e_t - P_{eff}e_p)y_t}{I} \quad 5.1$$

where f_t = concrete stress at the top of the section (positive for tension),

P = internal axial force,

A = cross sectional area,

M = internal bending moment,

y = distance to fiber from neutral axis,

I = moment of inertia,

P_{load} = applied loading,

P_{eff} = effective prestress force,

e_l = eccentricity of applied loading from neutral axis,

e_p = eccentricity of prestress force from neutral axis,

y_t = distance to top of section from neutral axis.

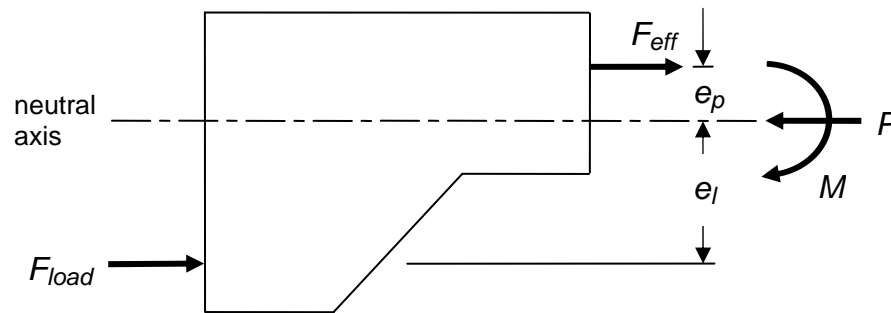


Figure 5-6: Beam Specimen Internal Forces During Load Application

In addition to the effective prestress, the dead (sustained)-to-live-load ratio affects the fatigue loading applied to the specimens. The lower the ratio, the higher the percentage of total load attributed to live load, which represents the cyclic portion of the total applied loading. As discussed in Section 4.3.5, the author chose a dead (sustained)-to-live-load ratio of 2.0. The revised peak service load and fatigue load (minimum and maximum load) for each series of specimens is shown in Table 5-5.

Table 5-5: Revised Specimen Loading Based on Actual Effective Prestress

Series	Effective Prestress	Service Load (kips)	Fatigue Load (kips)	
			Minimum	Maximum
Fatigue Reference	$0.58f_{pu}$	71.2	47.5	71.2
Anchor Zone Grout Void	$0.61f_{pu}$	74.4	49.6	74.4
Anchor Zone Grout Void with Corrosion	$0.60f_{pu}$	73.3	48.9	73.3
Crown Grout Void with Corrosion	$0.60f_{pu}$	73.3	48.9	73.3

5.1.2 During Fatigue Testing

During fatigue testing, the stresses in the strand were calculated through two independent analytical methods: a moment-curvature analysis and a finite element analysis.

The necessity for an analytical approach was due to the following constraints:

1. Flexural cracking of the partially prestressed specimens negated the ability to monitor the strand stress indirectly through the surface mounted strain gauges or even with internal concrete strain gauges.
2. Vibrating wire strain gauges are incapable of reading strains at the high rate of loading required during the cyclic testing (5Hz).

3. As discussed in Section 4.5, monitoring of the strand directly was extremely difficult due to the limited accessibility and very high strains experienced by the strand during stressing and thus during fatigue testing.

The necessity for two analytical methods was to develop both a sufficient level of certainty in the results and because the stress change due to loading is member-dependent since a portion of the strand was unbonded. In general, a moment-curvature analysis only applies to section-dependent behavior. The methodology and results from these two analytical approaches are discussed in the following sections.

5.1.2.1 Moment-Curvature Analysis

A well established method for both reinforced and prestressed concrete, a moment-curvature analysis relates the applied moment to the gradient of the strain profile (Lin and Burns 1981). Based on classical beam theory and strain compatibility between the steel and concrete, the moment-curvature relationship is uniquely defined according to the dimensions of the concrete section and the material properties of the steel and concrete. The iterative procedure involves assuming a strain profile, calculating the resulting stresses from the material stress-strain relationships, calculating internal forces, and determining a neutral axis depth to satisfy equilibrium. Once a solution is found, the strain profile is increased to evaluate the next step in the moment-curvature relationship.

One complicating factor for this study was that the beams possessed a portion of unbonded tendon, located within the “bathtub” region at the center of each specimen. For bonded tendons, the stress change in the strand due to loading is section-dependent be-

cause strain compatibility exists between the concrete and the strand. For unbonded tendons, the stress change in the strand due to loading is member-dependent because the stress relies on the overall deformations between anchorages. Strain compatibility does not exist for an unbonded tendon.

However, two characteristics of the beam specimens in this research study affected the response of the tendon and the subsequent change in stress during the fatigue loading. First, the method of loading the beams through an eccentric axial load resulted in a uniform moment throughout the specimen. Second, the end regions, where a very complex stress state existed due to the loading, were fully bonded. Consequently, the change in strain in the concrete due to loading was uniform throughout the center region of the specimen, which was the location of the unbonded tendon. It did not matter that the tendon was unbonded; it experienced the same change in strain that a fully bonded tendon would have experienced.

Based on this rationale, the author performed a moment-curvature analysis of the specimens assuming a fully bonded tendon. However, the author modified the standard moment-curvature analysis since the loading was applied through an eccentric axial load. The analysis used nonlinear material stress-strain relationships, including cracking of the concrete in tension. For the concrete, the analysis used the Hognestad stress-strain relationship recommended by Lin and Burns (1981) and reproduced as Eqs. 5.2a and 5.2b. For the strand, the analysis used a typical stress-strain diagram for Grade 270, low-relaxation strand, as shown in Figure 5-7 (*e.g.*, Lin and Burns 1981, Nilson 1987).

$$\text{for } 0 \leq \varepsilon \leq \varepsilon_o, \quad \frac{\sigma}{\sigma_{cu}} = 2 \frac{\varepsilon}{\varepsilon_o} \left(1 - \frac{\varepsilon}{2\varepsilon_o}\right) \quad 5.2a$$

$$\text{for } \varepsilon_o \leq \varepsilon \leq \varepsilon_{cu}, \quad \frac{\sigma}{\sigma_{cu}} = 1 - 0.15 \left(\frac{\varepsilon - \varepsilon_o}{\varepsilon_{cu} - \varepsilon_o} \right) \quad 5.2b$$

where ε = strain,

ε_o = strain at peak stress, taken as 0.002,

ε_{cu} = ultimate strain, taken as 0.003,

σ = stress,

σ_{cu} = maximum compressive strength, taken as 4,000 psi

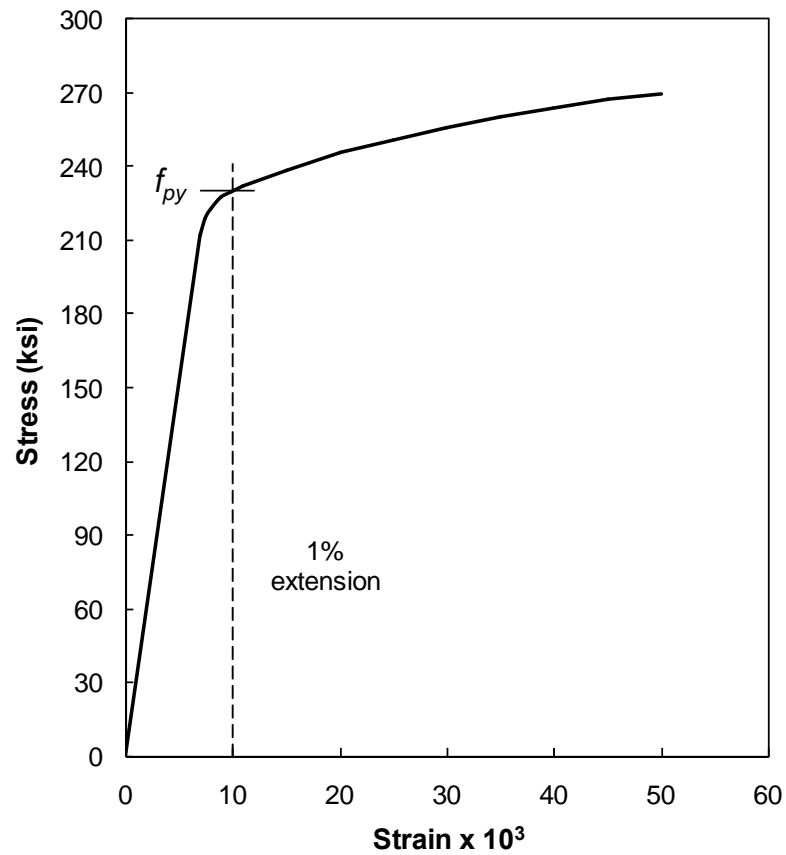


Figure 5-7: Stress-Strain Curve for Grade 270 Prestressing Strand

The results of the calculations indicated a change in strand stress of approximately 28.9 ksi, or $0.107f_{pu}$, for the partially prestressed specimens during the cyclic portion of the fatigue loading. The decompression load was slightly less than the dead load portion of the total load, which was based on a dead (sustained)-to-live-load ratio of 2.0 as discussed previously. Consequently, the strand experienced the largest change in stress during the application of the live load portion of the loading. The live load was the cyclic portion of the total fatigue loading.

In addition to the rationale discussed previously for assuming a fully bonded tendon, the behavior of the beam specimens during the fatigue loading also supported this approach. Partially prestressed beams with unbonded tendons tend to experience a small number of very wide cracks (Nilson 1987). All of the partially prestressed specimens developed relatively fine cracks (ACI 224.1R 2007) spaced at eight inches on center. Furthermore, Shahawi and Batchelor (1986) recommend the use of the FIP-CEB equation for predicting the maximum crack widths in partially prestressed beams subjected to fatigue. For a typical crack width of 0.009 inches (see Section 5.3), this translates into a change in steel stress from decompression of 33.2 ksi, which compares very favorably with the calculated value of 28.9 ksi.

5.1.2.2 Finite Element Analysis

The purpose of the finite element analysis was to independently verify, or disprove, the results of the moment-curvature analysis. Although promising, the results from the moment-curvature analysis were based on section-dependent behavior. The fi-

nite element analysis, on the other hand, included the member-dependent effects necessary with an unbounded tendon, where strain compatibility does not exist. The intent of the finite element analysis was not to predict crack locations *a priori*, predict crack propagation, predict fatigue crack formation, or serve as a starting point for a parametric investigation. The intent was only to calculate the change in strand stress for the partially prestressed specimens of this study during application of the fatigue loading.

The author chose the ANSYS[®] Academic Research Product, v. 11.0 (ANSYS), as the finite element package to perform the load stage analysis, which also included nonlinear material behavior. The load stage analysis followed the same sequence experienced by the partially prestressed specimens – prestressing, installation of the grout after prestressing, and flexural cracking of the concrete during loading. The same stress-strain relationships used in the moment-curvature analysis were used for the finite element analysis. For the concrete, the Hognestad stress-strain relationship, previously reproduced as Eqs. 5.2a and 5.2b. For the strand, a typical stress-strain diagram for Grade 270, low-relaxation strand, as shown in Figure 5-7.

The finite element model is shown in Figure 5-8. Due to symmetry, the author constructed only a quarter-model of the beam specimen. Along the two planes of symmetry, the boundary conditions allowed displacement parallel to the plane but restricted displacement perpendicular to the plane. To complete the boundary conditions, displacement was restricted in the y-direction along the bottom edge of the corbel. Loading was applied as a pressure over the same area as the test equipment actuator head, with the centroid located 6” above the edge of the corbel to match the specimen design as shown in Figure 4-3.

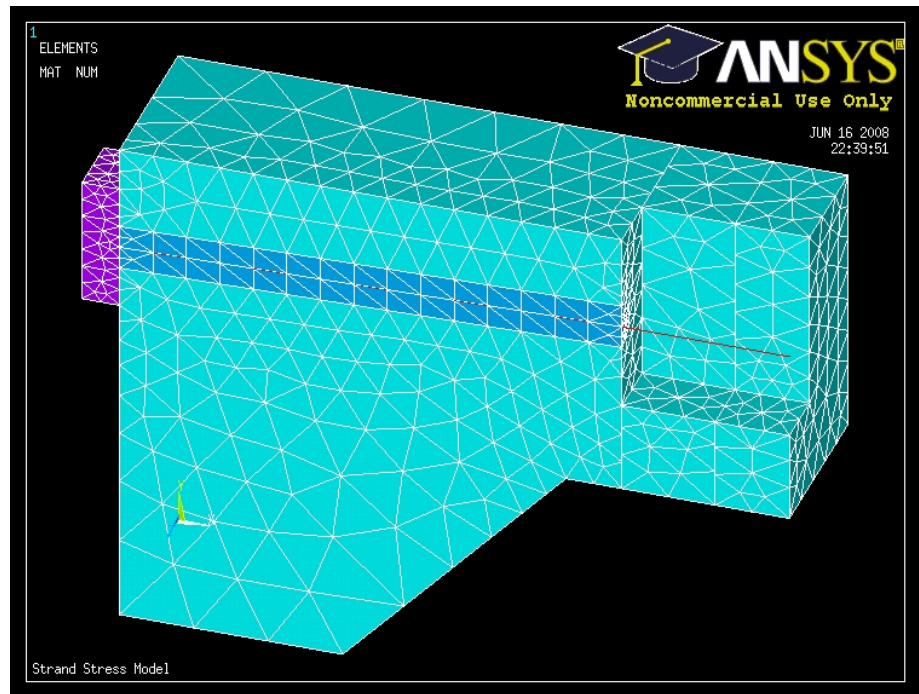


Figure 5-8: Finite Element Model for Determining Strand Stress During Fatigue Testing

The basic element used in the model was a higher-order, three-dimensional, 20-node, hexahedral, solid element that exhibits quadratic displacement behavior. This element, referred to as SOLID186 by the ANSYS program, is well suited to modeling irregular geometries (ANSYS 2007), such as those that occur with the beam specimens. As shown in Figure 5-8, an irregular mesh geometry resulted from the half-cylinder used to model the strand duct, particularly since the duct was sloped between the beam end and the “bathtub” region. Furthermore, SOLID186 degrades to a 10-node tetrahedral element during auto-meshing in order to maintain proper element geometry, further accommodating irregular geometries (ANSYS 2007). The author generated the initial mesh through a controlled auto-meshing process. After an initial analysis, a mesh refinement procedure was followed at locations of coarse stress distributions and/or high stress gradients.

The author modeled the tendon with a three-dimensional spar or truss element. Referred to as LINK8 by the ANSYS program, this element is a pin-jointed, uniaxial, tension-compression element with three degrees of freedom at each node (ANSYS 2007). This element allows input of an initial strain, which served to stress the tendon and prestress the finite element model of the beam specimens. The “prestressing” required an iterative approach to arrive at the same level of initial strain in the strand as that experienced by the actual specimens. Namely, a strain that corresponds to an effective prestress of $0.6f_{pu}$.

The author modeled installation of the grout after prestressing, as occurred in the actual specimens, by using the element birth command available in ANSYS. This feature is very beneficial for staged construction. In reality, the program assigns an extremely low stiffness to these elements prior to their “birth.” The grout stress-strain relationship was modeled with the Hognestad expression.

The author modeled flexural cracking with contact elements that resist compression but not tension. The cracking pattern was chosen to match the typical cracking that occurred in the test specimens (see Section 5.3). The contact zones extend completely through the cross section but, when under a compressive stress, remain unopened. In this way, the analysis opened and propagated the cracks as the stresses dictated.

Results of the finite element analysis confirmed the assumptions used in the moment-curvature analysis of the beam specimens, with a change in strand stress of 27.6 ksi during application of the live load portion of the fatigue load. This value compares very favorably with the calculated value of 28.9 ksi from the moment-curvature analysis.

5.2 Exposure Testing and Monitoring

The exposure testing, performed on six of the twelve specimens, involved exposing the specimens to saltwater for a period of six months while under full service load. Three of the specimens had a portion of the strand exposed immediately behind the anchor head due to a void in the grout. These specimens were referred to as the Anchor Zone Grout Void Corrosion Series (AZC) of test specimens. Three of the specimens had the center portion of the plastic duct removed so that the chlorides had direct access to the grouted tendon. These specimens were referred to as the Crown Grout Void Corrosion Series (GVC) of test specimens.

As was done during grouting of the tendons, the AZC specimens were placed vertically for exposure testing, as shown in Figure 5-9. With the specimens vertical, saltwater placed into the void behind the anchor head easily stayed in place. The saltwater would readily leak out through the strand tails if the specimens were left horizontal during the testing. The chloride exposure took the form of a five percent NaCl solution placed in the grout void immediately behind the anchor head.

Due to physical constraints, it was impossible to monitor the corrosion that occurred in the void behind the anchor head for the AZC specimens. Consequently, the author placed four-inch-long sections of strand into the empty holes of the anchor head. These small, unattached sections could be easily removed and periodically examined for signs of corrosion.



Figure 5-9: Anchor Zone Grout Void Corrosion Specimens Undergoing Exposure Testing

Unexpectedly, pitting corrosion occurred in the removable portions of strand placed into the empty holes of the anchor head. It was observed that over time the solution placed within the void became cloudy. Subsequent testing of the solution revealed a pH of between 12 and 13. The initial solution, composed of deionized water and five percent sodium chloride, had a pH of 7 prior to placement. It is speculated that hydroxides from the grout leached into the solution, causing it to become alkaline. This alkalini-

ty then caused the protective passive layer to form on the strand in the void and, consequently, resulted in pitting corrosion of the strand segments that were not encased in grout. This result was unexpected, as steel placed into a neutral solution should experience uniform corrosion, not pitting corrosion. Pitting corrosion is a much more detrimental form of corrosion for the prestressing strand.

Exposure testing of the GVC specimens involved removing the plastic duct in the center region of the beams and exposing the grouted strand to chlorides. The chloride exposure took the form of a five percent NaCl solution placed in a two-week-long, alternating wet-then-dry sequence. To remove the plastic duct without damaging the grout surrounding the tendon, a Dremel Variable-Speed MultiPro rotary tool with a 1-1/4-inch-diameter cutting wheel was used. The author very carefully cut the plastic duct longitudinally along each side. Then a circumferential cut was made at each end near the steel deviator. The plastic duct was then carefully removed, with the result as shown in Figure 5-10.

Immediately after removing the plastic duct, the author observed that the grout was cracked. Both longitudinal and circumferential cracks were observed in the grout for all three specimens. Whether the cracks occurred due to shrinkage of the grout or during the initial 10,000 cycle fatigue testing is unknown. Nonetheless, these cracks reduced the ability of the grout to protect the strand. Crack maps, including crack width measurements where sufficient access existed for the crack scope, are shown in Figures 5-11 through 5-13 for the exposed portion of the grouted tendons.



Figure 5-10: Exposed Grouted Tendon After Plastic Duct Removal

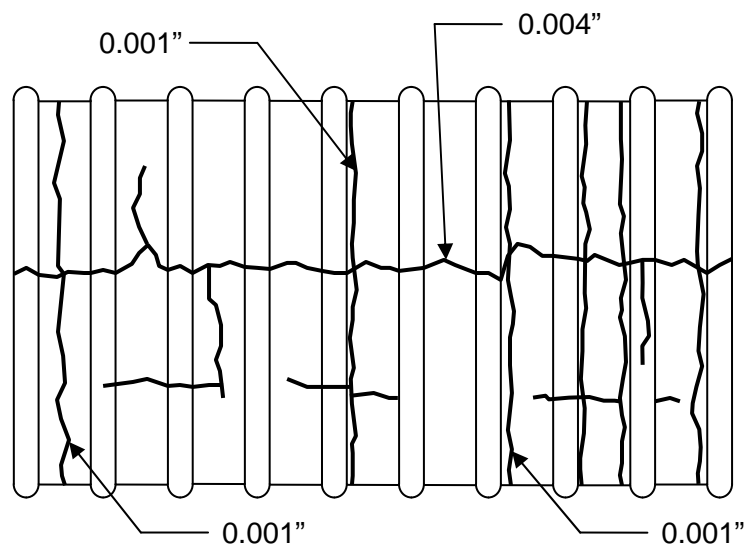


Figure 5-11: GVC-1 Grout Crack Map

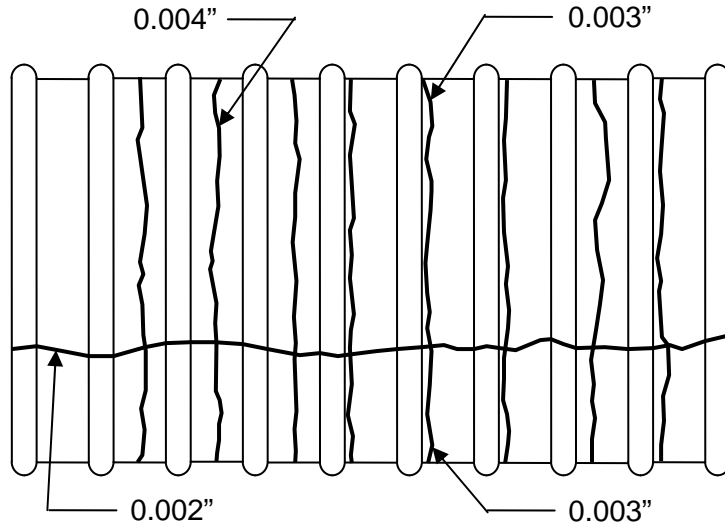


Figure 5-12: GVC-2 Grout Crack Map

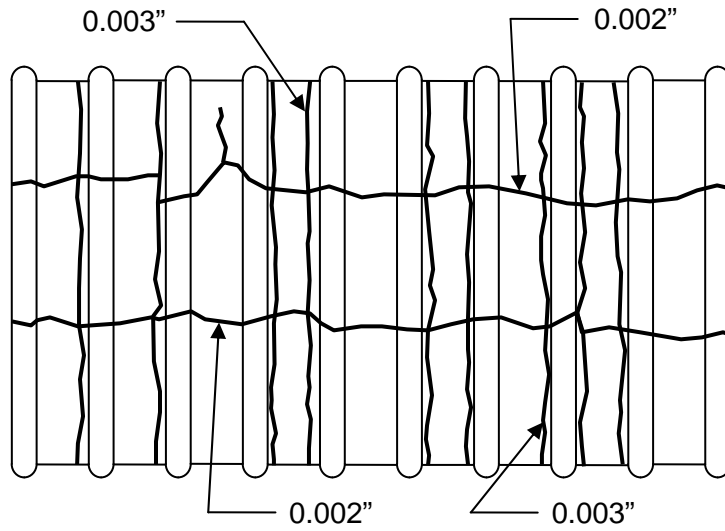


Figure 5-13: GVC-3 Grout Crack Map

All three GVC specimens showed signs of corrosion at some point during the six months of chloride exposure. However, the amount and locations of corrosion varied between each of the three specimens, with no apparent pattern revealing itself. Beam Specimen GVC-1 showed signs of corrosion after only one two-week cycle of saltwater exposure, as shown in Figure 5-14. The corrosion shown in Figure 5-14 occurred at the crack locations identified in Figure 5-11. This finding is very important, as it shows that the ability of the grout to protect the strand is independent of the level of prestress, which is also consistent with the fact that the grout is not precompressed because it is installed after the tensioning operation.



Figure 5-14: Exposed Grouted Tendon for GVC-1 Showing Signs of Corrosion

Figure 5-15 shows GVC-2, one of the partially prestressed specimens, just prior to fatigue testing. The most important aspect in the photograph is the extensive build-up of salt and calcium hydroxide on the outside surface of the specimen. The flexural cracks, which measured 0.006 to 0.009 inches in width, continued to leak saltwater throughout the six-month duration of the exposure testing. These crack widths are considered fine to very fine (ACI 224 2007), yet the saltwater continued to pass through the specimen, even after extensive build-up of salt and calcium hydroxide. This finding is very important in that it reaffirms that fine crack widths (those measuring less than 0.010 inches) can still act as transport mechanisms for chloride contamination. The same phenomenon occurred in Beam Specimen GVC-3, the other partially prestressed member.



Figure 5-15: Beam Specimen GVC-2 After Six-Month Duration of Exposure Testing

5.3 Fatigue Testing and Observations

To test the beam specimens in fatigue, they were placed vertically in a load frame containing a 110-kip, servo-hydraulic, fatigue-rated actuator manufactured by MTS Systems. A drawing of the test setup is shown in Figure 5-16, with photographs of the test setup shown in Figure 5-17. The beam specimens were positioned such that the actuator applied the necessary axial force at the same location as the prestressing bar. To account for the anchor head extending beyond the end of the beam at the bottom of the specimens, the beams were supported on steel plates along the bottom corbel. These plates also assured that the reacting force from the strong floor was applied directly opposite to the applied loading from the actuator.

All twelve beam specimens completed the full 2,000,000 cycles of fatigue testing without a catastrophic failure of either the concrete or tendon. In regions of compressive stress, the concrete did not show any signs of distress (cracking, splitting, or spalling), even though the fatigue loading placed a maximum stress of $0.50f'_c$ in these areas for all twelve specimens. However, the concrete did suffer cracking at various locations, some of which was expected and some of which was not. For instance, in general, the fully prestressed specimens remained uncracked in the precompressed tensile zone, which was to be expected. The partially prestressed specimens, on the other hand, cracked in the precompressed tensile zone, which was also to be expected.

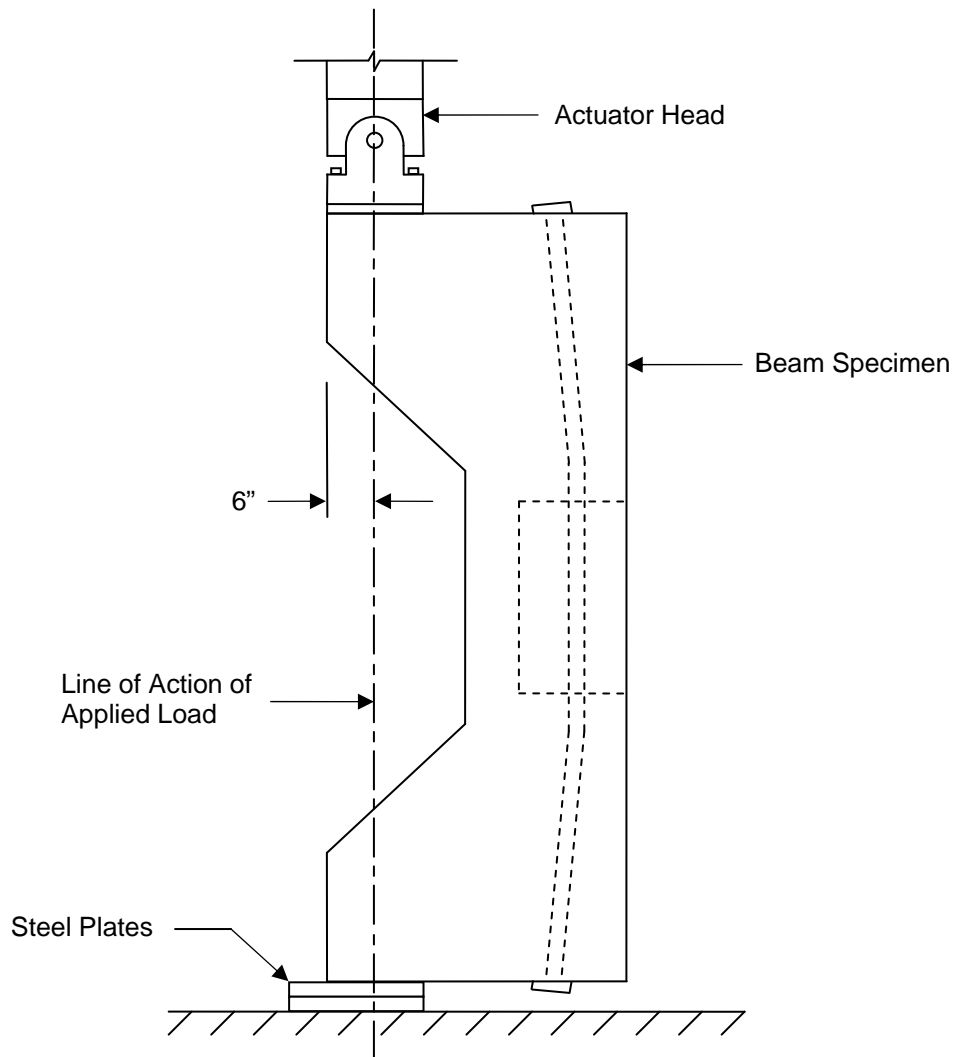


Figure 5-16: Beam Specimen Fatigue Test Setup

Unexpected cracking occurred in two situations. The first involved longitudinal cracking along the top of the specimens at the anchor head and at the opening in the center region of the beam, as shown in Figure 5-18. All of the fully prestressed specimens exhibited this type of cracking, while it occurred in only some of the partially prestressed specimens. It was speculated that the cause of the cracking near the anchor head was due to bursting stresses, and that the cause of the cracking near the “bathtub” region was due

to dispersion forces from the applied prestressing. This hypothesis was confirmed through a finite element analysis, the details of which are contained in Appendix F.



(a)

(b)

Figure 5-17: Beam Specimen Fatigue Test Setup

The second instance of unexpected cracking occurred in Beam Specimen GVC-1. This specimen was a fully prestressed design yet experienced flexural cracking in the precompressed tensile zone. Because this specimen underwent exposure to chlorides, it was possible that some of the prestressing wires failed during the fatigue testing, resulting in a corresponding increase in the tensile stress. Another alternative is that the specimen experienced an overload during the fatigue testing due to an equipment malfunction. The specimen autopsy results discuss these possibilities.

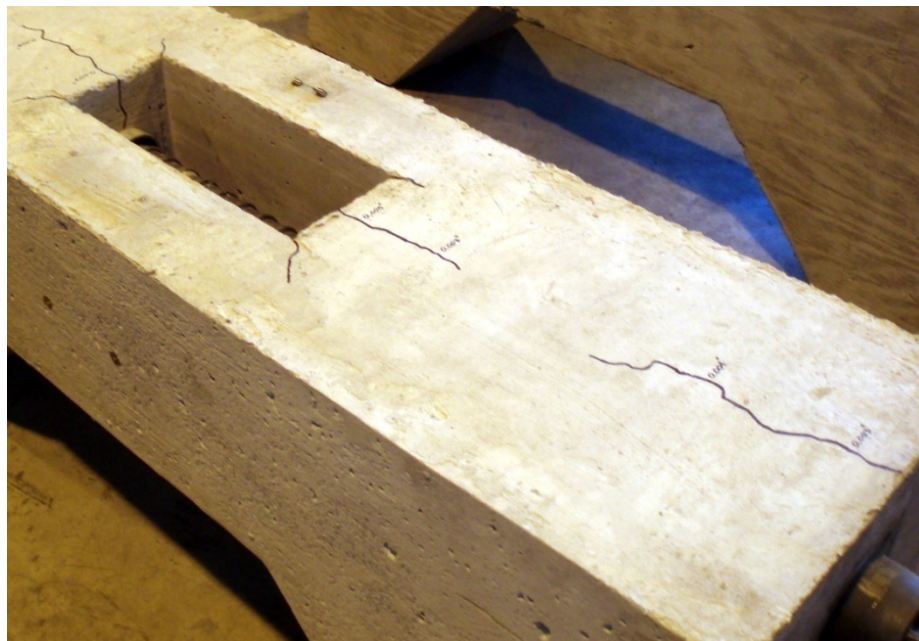


Figure 5-18: Longitudinal Cracking of Beam Specimens

All of the partially prestressed specimens experienced flexural cracking in the precompressed tensile zone. The cracking pattern was fairly consistent and amounted to four flexural cracks spaced approximately eight inches apart, as shown in Figure 5-19. The opening in the center region of the beam caused the cracks furthest away from the center to merge with shrinkage cracks occurring at the corners of the openings. This cracking pattern occurred in all but one of the partially prestressed specimens, Beam Specimen GVC-3, which had three flexural cracks instead of four.

Detailed crack maps for each specimen are contained in Appendix G. Crack width measurements were taken with a crack scope – a 60-magnification microscope with an inscribed scale on the lens. Initial crack width measurements were taken within the first 100,000 cycles, with final crack width measurements taken within the last 100,000 cycles. Crack width measurements were taken at two locations along each crack at the

top surface of the beam. Crack width measurements for the GVC Series were less precise, as it was difficult to remove all of the build-up in and around the cracks from the exposure testing. In general, the flexural crack widths increased during the fatigue loading. Some researchers have attributed this increase to creep, while others have attributed it to continued microcracking occurring over time (ACI 423.5R 1999).



Figure 5-19: Typical Crack Pattern for Partially Prestressed Specimens

With the possible exception of Beam Specimen GVC-1 (which exhibited flexural cracks in a fully prestressed design), the tendons did not show any signs of distress during the fatigue testing. Although the majority of the tendon is unexposed, distress in the tendon would normally be reflected by distress in the concrete, which did not occur. How-

ever, individual wire breaks or other minor fatigue damage to the tendons was possible. This condition is discussed in more detail in the autopsy results section.

It is informative to compare the calculated change in strand stress for the beam specimens with equations that predict the fatigue life of prestressing strand, and thus a prestressed beam. For a stress range of 28.9 ksi, Paulson's mean fatigue life equation (see Section 2.4) would predict slightly more than 3,000,000 cycles to failure. All of the unexposed specimens reached the full 2,000,000 cycles of fatigue loading.

For a stress range of 28.9 ksi, the equation proposed by the author that includes the effect of localized corrosion (see Section 3.5) would require an average pit depth of 0.013 inches in order to reduce the mean fatigue life to 2,000,000 cycles. The partially prestressed beam specimens for the Crown Grout Void Corrosion Series had an average pit depth of 0.007 inches (see Chapter 6), and all of these specimens reached the full 2,000,000 cycles of fatigue loading.

5.4 Summary

The following section contains a brief summary of the results from the beam specimen testing. Testing of the beam specimens included determination of the effective prestress prior to fatigue testing, calculation of the stress range during fatigue testing, exposure testing of the beam specimens, and fatigue testing of the beam specimens. From construction up to the point of fatigue testing, the strand stress was monitored indirectly through vibrating wire strain gauges installed on the surface of the concrete specimens. During fatigue testing, the stresses in the strand were calculated through two independent

analytical methods: a moment-curvature analysis and a finite element analysis. The exposure testing, performed on six of the twelve specimens, involved exposing the specimens to saltwater for a period of six months while under full service load. The fatigue testing, performed on all twelve specimens, involved loading the specimens for 2,000,000 cycles or until failure, whichever came first. Findings from the beam specimen testing are contained in Table 5-6.

Table 5-6: Summary of Findings from Beam Specimen Testing

Source	Finding
Strand Stress Determination	<p>The effective prestress ranged from $0.58f_{pu}$ to $0.61f_{pu}$, with values of $0.58f_{pu}$ for the Fatigue Reference Series (FR), $0.61f_{pu}$ for the Anchor Zone Grout Void Series (AZ), and $0.60f_{pu}$ for both the Anchor Zone Grout Void Corrosion Series (AZC) and the Crown Grout Void Corrosion Series (GVC).</p> <p>The results from the moment-curvature calculations indicated a change in strand stress of approximately 28.9 ksi, or $0.107f_{pu}$, for the partially prestressed specimens during the cyclic portion of the fatigue loading.</p> <p>The results from the finite element analysis indicated a change in strand stress of approximately 27.6 ksi, or $0.102f_{pu}$, for the partially prestressed specimens during the cyclic portion of the fatigue loading.</p>
Exposure Testing	<p>For the AZC Series, the pH of the saltwater solution placed into the void increased over time due to leaching of hydroxides from the grout. The higher pH caused a protective oxide film to form, resulting in pitting corrosion of the strand within the void.</p> <p>Both longitudinal and circumferential cracks were observed in the grout for all three beams from the GVC series. Whether the cracks occurred due to shrinkage of the grout or during the initial 10,000 cycles of fatigue testing is unknown.</p> <p>All three specimens from the GVC Series showed signs of corrosion at some point during the six months of exposure testing.</p> <p>The flexural cracks for the partially prestressed beams of the GVC Series continued to leak saltwater throughout the six-month duration of the exposure testing. The crack widths were relatively fine, measuring only 0.006 to 0.009 inches in width.</p>

Table 5-6: Summary of Findings from Beam Specimen Testing (cont'd)

Source	Finding
Fatigue Testing	<p>All twelve beam specimens successfully reached 2,000,000 cycles of fatigue testing.</p> <p>Typical flexural crack pattern for the partially prestressed specimens consisted of four cracks spaced at 8 inches on center.</p> <p>Typical flexural crack widths for the partially prestressed specimens ranged from 0.006 to 0.011 inches.</p> <p>Flexural crack widths increased from 15 to 30 percent during the course of the fatigue testing.</p> <p>One fully prestressed beam (Specimen GVC-1) experienced flexural cracking.</p> <p>With the possible exception of Beam Specimen GVC-1, the tendons did not show any signs of distress during the fatigue testing.</p> <p>All of the fully prestressed beams and six of the eight partially prestressed beams suffered longitudinal cracking along the top of the specimens at the anchor head and at the opening in the center region of the beam.</p>

Chapter 6

Beam Specimen Forensic Investigation

This chapter discusses the forensic investigation of the post-tensioned beam specimens. The main purpose of autopsying the specimens was to examine the condition of the tendon. This examination included all aspects of the tendon system: the duct, the grout, and the strand itself. Research has shown that the tendon is the single most critical component in predicting the fatigue life of a partially prestressed member (ACI 423.5 1999). Furthermore, since half of the specimens underwent exposure testing, what effect this had on the condition of the tendon needed to be investigated. The results are divided into two categories: general findings and specific findings. General findings refer to conditions that were found in all twelve beam specimens. Specific findings, on the other hand, refer to conditions that only occurred within an individual series or a member of that series. The detailed autopsy procedures are contained in Appendix H.

6.1 General Findings from Forensic Investigation

After removal of the tendons from the beam specimens, the author examined the condition and disposition of the plastic duct, the grout, and the strand. Some of the same tendon conditions occurred in all twelve beam specimens, while others were specific to an individual series or a member of that series. The findings discussed in this section applied to all beam specimens.

6.1.1 Grout Coverage

One aspect of this study, discussed in detail in Section 4.2, was to investigate the role that grouting defects may play in the durability and fatigue response of prestressing strand. Unplanned defects, not uncommon in actual post-tensioned structures, would have either negated or severely complicated this study, or would have required recasting of some of the beam specimens. Consequently, a thorough investigation of the condition of the grout was critical.

The investigation found that the grout completely filled the ducts and fully encapsulated the strands, with no signs of any voids, bleed pockets, or bleed lenses, except for the peaks of the ribs along the center region of the beams. The lack of grout at these locations was likely the result of small air pockets unable to escape during the grouting process. This portion of the duct was at a high point in the tendon profile, and it is most likely that air became trapped in the ribs. However, this result was anticipated, and it has little or no negative consequences. A photograph of the grouted tendon showing the amount of duct removed to perform the *in situ* portion of the inspection is shown in Figure 6-1. Inspection of the remaining portions occurred after removal of the tendon from the beam specimens. Figure 6-2 is a close-up of the grout showing the air pockets along the peaks of the ribs. These air pockets measured 3/8" in width and 1-1/2" in length.

The investigation also found that the grout completely filled the end anchorages and fully encapsulated the strands, with no signs of any voids or pockets. This result was very important as one of the planned grouting defects involved a purposeful void in the grout immediately behind the anchor head, referred to as the Anchor Head Grout Void

series of specimens. The behavior of the specimens without the void served as a reference point for comparison with those for which the void was purposefully planned. Furthermore, the coverage and tenacity of the grout was confirmed during removal, when the portion of the tendon within the end anchorages could only be removed after repeated blows from a 50-lb. jackhammer.



Figure 6-1: Exposed Grouted Tendon After Plastic Duct Removal for *In situ* Inspection

6.1.2 Grout Cracking

One assumption concerning the test matrix developed for this research study was that the grout would crack, likely due to shrinkage. This assumption, based on research at the University of Texas (Kotys 2003, Turco *et al.* 2007), was partially proven correct

when the author removed the plastic duct for the Crown Grout Void Corrosion Series (see Section 5.2). This assumption was further validated during the forensic investigation, which revealed cracking of the grout in all twelve beam specimens.



Figure 6-2: Close-Up of Air Pockets Along Peaks of Duct Ribs

The grout experienced both longitudinal and circumferential cracking, with crack widths measuring between 0.001 and 0.005 inches. Whether the cracks occurred due to shrinkage of the grout or during the fatigue testing is unknown. Nonetheless, these cracks reduced the ability of the grout to protect the strand. Furthermore, due to the specimen design, the author was able to examine the grout while it was still *in situ*. The University of Texas research, which was the first and only other research study to characterize this issue, found cracking of the grout but only after the autopsy (Kotys 2003, Turco *et al.* 2007), which may itself have caused some of the cracking.

6.1.3 Strand Location within Duct

Unless a straight tendon profile is used, there are locations where the strand will be pulled up tight to the duct wall during the stressing operation. At these locations, some of the tendons will have very little grout coverage adjacent to the duct. Furthermore, depending on the specific profile, these locations may extend over a significant length of the tendon. The beam specimens used in this study, for example, have a very typical two-point drape profile. This profile will result in the tendon being pulled up tight to the duct over the majority of its length, which was confirmed during the forensic investigation of the tendons.

All twelve beam specimens had some of their strands tight to the inside, bottom surface of the plastic duct. Either two or four strands touched the duct surface depending on whether the specimen had a four- or six-strand-tendon, respectively. The amount of contact and the corresponding amount of grout coverage at the strand/duct interface varied between specimens. In general, the specimen grout coverage varied between the extremes of Beam Specimen FR-1, pictured in Figures 6-3 and 6-4, and Beam Specimen AZ-3, pictured in Figures 6-5 and 6-6. The grout was so thin between the duct and strand in Beam Specimen FR-1 that it easily shattered during the autopsy procedure. The grout for Beam Specimen AZ-3, on the other hand, fared better during removal but was nonetheless extremely thin, measuring 1/16" in many places. In Figures 6-5 and 6-6, the little black dots running longitudinally along the grout are locations where the strand touched the duct surface.

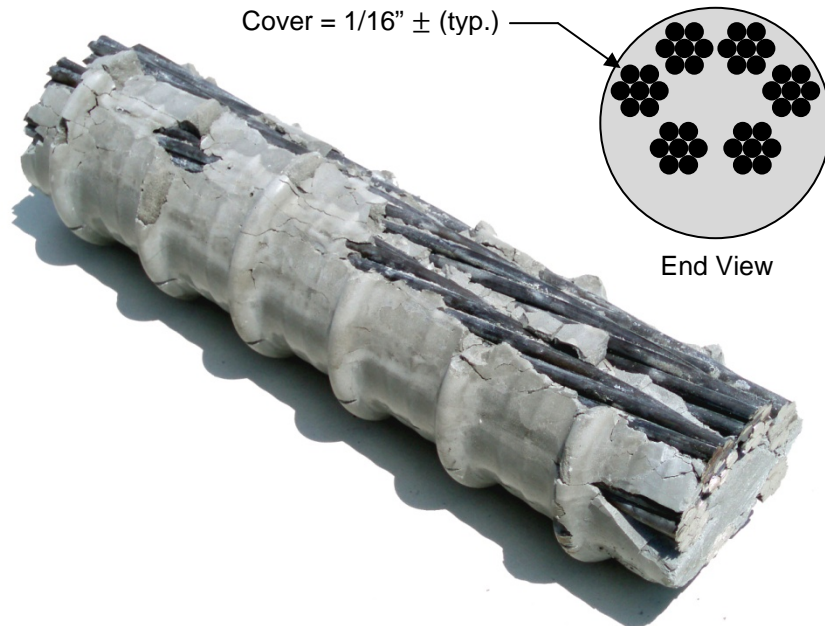


Figure 6-3: Beam Specimen FR-1 Grouted Tendon with Schematic End View

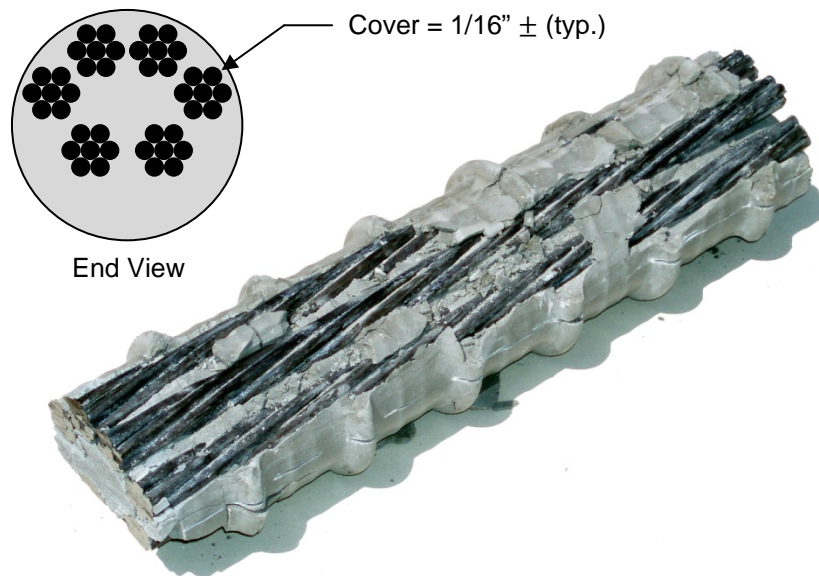


Figure 6-4: Beam Specimen FR-1 Grouted Tendon with Schematic End View

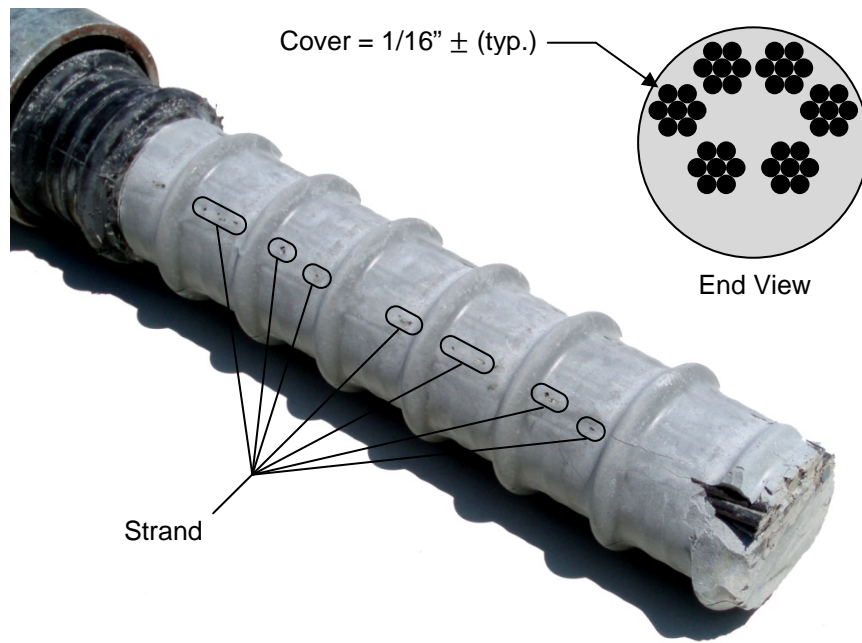


Figure 6-5: Beam Specimen AZ-3 Grouted Tendon with Schematic End View

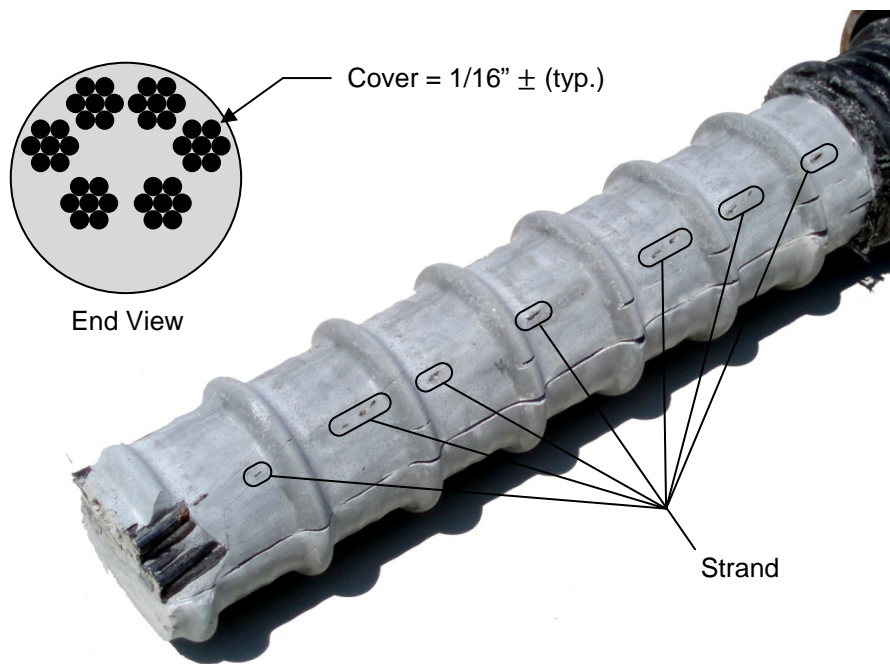


Figure 6-6: Beam Specimen AZ-3 Grouted Tendon with Schematic End View

Again, it is not that this condition was unexpected, but that these examples very vividly point out the problem that if chlorides breach the duct, the grout may be unable to protect the strand for an extended period of time even in a well-grouted post-tensioned beam. On the other hand, even with this situation, a well-grouted duct reduces the potential for corrosion by limiting areas for excess saltwater to reside and, even with minimal cover, still provides a passive environment for the strand.

6.1.4 Plastic Duct Performance at Deviators

Research at the University of Texas at Austin (Turco *et al.* 2007) indicated a potential problem with plastic duct at deviation or support points. During stressing, the ducts were squeezed between the steel strand and reinforcing bars used to support the duct during construction. The duct subsequently suffered severe abrasion and, in some locations, punctures. These puncture locations coincided with stirrups and subsequent flexural cracks in the partially prestressed members. As a result, during exposure testing, chlorides passed through the flexural cracks and came into direct contact with the strand without having to pass through either the concrete or grout. These chlorides also traveled along the strand through wicking action and resulted in widespread corrosion.

Consequently, the author investigated the condition of the tendons at the steel deviators. The plastic duct performed very well for all twelve specimens, only suffering a few minor scrapes or scratches – marks and indentations measuring less than 0.005 inches in depth compared to the 0.125-inch-thick duct. The only exception to this finding occurred for Beam Specimen FR-3, where the duct experienced small gouges at the

downhill edge of one of the steel deviators. These gouges, shown in Figure 6-7, measured a maximum of 0.027 inches in depth. This condition probably occurred due to a slight misalignment or movement of the deviator during concrete placement, causing the duct to bear more on the edge of the deviator than throughout its length. The important point to make, however, is that the damage to the duct was minor; measuring a maximum of 0.027 inches in depth compared to the 0.125-inch-thick duct, and did not adversely affect the performance of the plastic duct in any way.

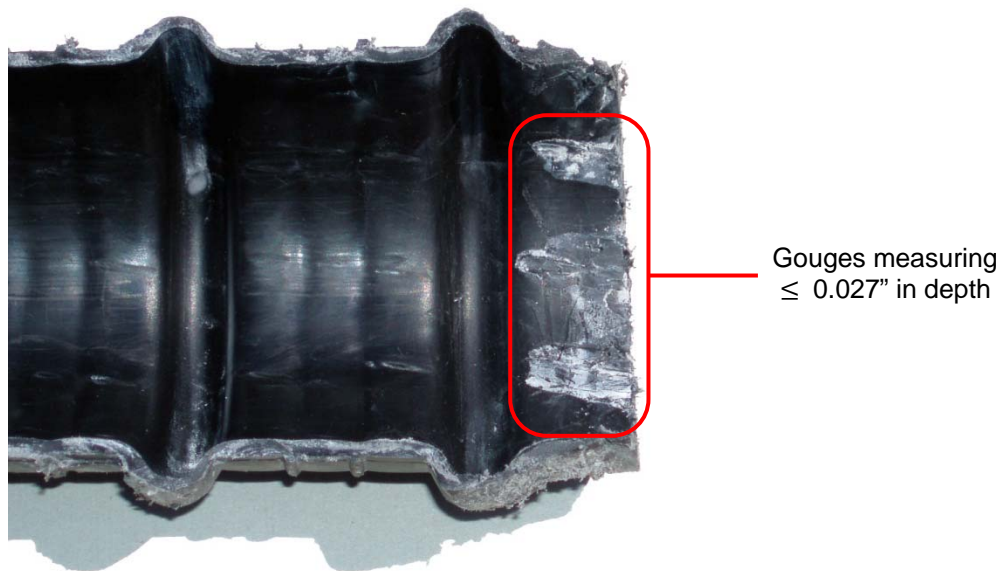


Figure 6-7: Gouges in Plastic Duct from Strand Stressing, Beam Specimen FR-3

The purpose of the steel deviators is to spread the load over a sufficient length to protect the duct during stressing of the strand and prevent any abrasion or gouging. The problem of plastic duct punctures at support points had been noted in the industry, and one proposed solution involved the use of metal cradles between bracing bars and the plastic duct (Turco *et al.* 2007). Based on the findings of this study with respect to the

steel deviators, it appears that the use of metal support cradles for plastic duct is a viable solution to this problem.

6.2 Specific Findings from Forensic Investigation

After removal of the tendons from the beam specimens, the author examined the condition and disposition of the plastic duct, the grout, and the strand. The findings discussed in this section are specific to each individual series or a member of that series. General findings, those that applied to all beam specimens, are discussed in Section 6.1.

6.2.1 Fatigue Reference Series

The Fatigue Reference Series specimens, as with all specimens, successfully reached the full 2,000,000 cycles of fatigue testing. However, the author examined the strand for any signs of fatigue cracking or individual wire breaks caused by the testing. To examine the strand in detail, it was first removed from the grout encasement, separated into individual wires, and thoroughly cleaned with a wire brush and steel wool pad. Subsequent examination of the strand did not reveal any wire breaks or fatigue cracks visible to the unaided eye.

Further examination involved visible dye penetrant inspection in accordance with ASTM E1417-05e1, Standard Practice for Liquid Penetrant Testing (ASTM E1417 2005). Dye penetrant inspection is a non-destructive test (NDT) method used to locate surface-breaking defects in non-porous materials. These defects include fatigue cracks,

which typically start on the surface of the metal. In general, this method is limited to detecting defects greater than 0.003 inches in width, although it varies between individuals (De Graaf and De Rijk 1981). Visible dye penetrant testing of the strand for the Fatigue Reference Series did not reveal any fatigue cracks. However, this finding does not preclude the formation of fatigue cracks too small to be detected through this method.

6.2.2 Anchor Zone Grout Void Series

The Anchor Zone Grout Void Series specimens also successfully reached the full 2,000,000 cycles of fatigue testing. However, the author examined the strand within and adjacent to the grout void for any signs of fatigue cracking or individual wire breaks caused by the testing. To examine the strand in detail, it was first removed from the grout encasement and anchor head, separated into individual wires, and thoroughly cleaned with a wire brush and steel wool pad. Subsequent examination of the strand did not reveal any wire breaks or fatigue cracks visible to the unaided eye.

Further examination involved visible dye penetrant inspection in accordance with ASTM E1417-05e1, Standard Practice for Liquid Penetrant Testing (ASTM E1417 2005). In general, this method is limited to detecting defects greater than 0.003 inches in width, although it varies between individuals (De Graaf and De Rijk 1981). Visible dye penetrant testing of the strand for the Anchor Zone Grout Void Series did not reveal any fatigue cracks. However, this finding does not preclude the formation of fatigue cracks too small to be detected through this method.

6.2.3 Anchor Zone Grout Void Corrosion Series

As discussed in Section 5.2, the saltwater solution placed into the void behind the anchor head experienced an increase in its pH from 7 to between 12 and 13. It is speculated that hydroxides from the grout leached into the solution, causing it to become alkaline. This alkalinity caused a protective passive layer to form on the strand in the void and, consequently, resulted in pitting corrosion of the strand segments that were not encased in grout. However, over time the pH of the solution returned to a value around 7, most likely due to a combination of carbonation and reduction of the hydroxide leaching, which caused the strand to also experience uniform corrosion. The result is shown in Figure 6-8 for Beam Specimen AZC-2.



Figure 6-8: Strand Corrosion within Void Behind Anchor Head

Unfortunately, the majority of the corrosion product was knocked off during the somewhat violent autopsy procedure. It was necessary to use a 50-lb. jackhammer to remove the anchor head and strand from the end anchorage due to corrosion product at the

interface of the metals. Nonetheless, signs of significant corrosion are still evident in the strand located within the void in the grout immediately behind the anchor head.

The localized corrosion of the strand took the same form as that found on the test specimens discussed in Chapter 3. Some of the localized corrosion formed within or very near the interstitial spaces between adjacent wires and took the form of elongated pitting. Typical hemispherical pitting formed at locations away from the interstitial spaces between adjacent wires. Pit depths ranged from a minimum of 0.002” to a maximum of 0.007”.

Another interesting phenomenon that occurred for one of these specimens was the strand acting as a conduit for the solution. This situation allowed corrosion to form within the strand away from the void in the grout, as shown in the center strand of Figure 6-9 for Beam Specimen AZC-3. Furthermore, for this specimen, the solution traveled to the far end of the strand, as shown in Figure 6-10. Although gravity helped this situation due to the vertical orientation of the specimen during exposure testing, this phenomenon also occurs in primarily horizontal strand (*e.g.*, Turco *et al.* 2007). The significance of this finding is that a single breach in the duct can allow corrosion to occur over a significant length of tendon beyond the breach, depending on the geometry and other characteristics of the tendon.

6.2.4 Crown Grout Void Corrosion Series

All three specimens experienced very similar corrosion of the strand in the area of the tendon that had the plastic duct removed prior to chloride exposure. The photograph

in Figure 6-11 exemplifies the type and extent of corrosion experienced by these tendons. The two top strands in the figure were located within the confines of the grout and had at least 3/8" of grout on all sides. The four bottom strands, on the other hand, were located tight to the bottom of the duct, with little or no grout between the strand and the plastic duct. Once the plastic duct was removed, the strand had limited protection and suffered significant corrosion throughout its length. This corrosion took the form of both uniform corrosion and pitting corrosion. The uniform corrosion likely took place where there was minimal or no grout coverage. The pitting corrosion likely took place where there was enough grout to form the protective oxide film but an insufficient amount to provide any long-term protection.



Figure 6-9: Strand Corrosion Within and Away from Grout Void



Figure 6-10: Strand Corrosion at Anchor Head Opposite to Grout Void



Figure 6-11: Strand Corrosion Experienced by GVC Beam Specimens

The localized corrosion of the strand took the same form as that found on the test specimens discussed in Chapter 3. Some of the localized corrosion formed within or very near the interstitial spaces between adjacent wires and took the form of elongated pitting. Typical hemispherical pitting formed at locations away from the interstitial spaces between adjacent wires. Pit depths ranged from a minimum of 0.003” to a maximum of 0.010”.

In addition, in a number of instances, the strand away from the bottom of the duct also suffered corrosion, although it was limited in its extent, as shown in Figure 6-12. This strand suffered corrosion at a location that coincided with a circumferential crack in the grout. This crack allowed fairly rapid passage of the chlorides, which circumvented the slower method of diffusion through the grout, resulting in significantly less time-to-corrosion at these locations.



Figure 6-12: Strand Corrosion of GVC Beam Specimen at Grout Crack

6.3 Summary

The following section contains a brief summary of the results from the beam specimen forensic investigation. The main purpose of autopsying the specimens was to ex-

amine the condition of the tendon. This forensic examination included all aspects of the tendon system: the duct, the grout, and the strand itself. The findings are as follows:

1. All twelve beam specimens were well grouted with only small air voids in the duct ribs at high points in the strand profile. The grout also completely filled the end anchorages and fully encapsulated the strands.
2. All twelve beam specimens experienced both longitudinal and circumferential cracking of the grout, with crack widths measuring between 0.001 and 0.005 inches.
3. All twelve beam specimens had some of their strands tight to the inside, bottom surface of the plastic duct due to the two-point drape profile. This condition resulted in minimal grout coverage between the strand and duct at these locations.
4. In general, the plastic duct performed very well for all twelve beam specimens, suffering only some minor scrapes or scratches.
5. The plastic duct suffered minor gouging at one location for one beam (Specimen FR-3). The gouging occurred due to a slight misalignment of the deviator, causing the duct to bear more on the edge of the deviator than throughout its length.
6. For all twelve beam specimens, the strand did not suffer any fatigue cracks detectable through dye penetrant inspection.
7. All three specimens from the AZC Series showed significant signs of corrosion for the portion of the tendons located within the grout void.

8. Specimen AZC-3 also showed signs of corrosion in the strand away from the grout void, indicating that the strand acted as a conduit for the saltwater.
9. All three specimens from the GVC Series showed significant signs of both uniform and pitting corrosion for the strands located tight to the plastic duct.
10. All three specimens from the GVC Series showed signs of corrosion on the strands located away from the plastic duct. This corrosion coincided with circumferential cracks in the grout.
11. The localized corrosion of the strand experienced by the AZC and GVC Series took the same form as that found on the test specimens discussed in Chapter 3. Pit depths ranged from a minimum of 0.002” to a maximum of 0.010”.

Chapter 7

Findings, Conclusions, and Recommendations

The overall objective of this study was to determine the viability of partially post-tensioned concrete members in an aggressive environment, including the impact of cyclic loading. This goal was accomplished by achieving the six specific objectives listed in Section 1.4. Toward that end, this chapter first includes the findings from the experimental testing and forensic evaluation of the full-scale, post-tensioned concrete beam specimens. Next, conclusions are presented based on those findings as well as the individual strand testing and analyses from Chapter 3. Finally, recommendations are presented based on the findings, conclusions, and opinions of the author.

7.1 Findings

Findings from the full-scale beam specimen testing and forensic evaluation are contained in Table 7-1. The findings are grouped according to the source of the data.

Table 7-1: Summary of Findings for Full-Scale Beam Specimens

Source	Finding
Strand Stress Determination	<p data-bbox="573 428 1414 621">The effective prestress ranged from $0.58f_{pu}$ to $0.61f_{pu}$, with values of $0.58f_{pu}$ for the Fatigue Reference Series (FR), $0.61f_{pu}$ for the Anchor Zone Grout Void Series (AZ), and $0.60f_{pu}$ for both the Anchor Zone Grout Void Corrosion Series (AZC) and the Crown Grout Void Corrosion Series (GVC).</p> <p data-bbox="573 661 1414 810">The results from the moment-curvature calculations indicated a change in strand stress of approximately 28.9 ksi, or $0.107f_{pu}$, for the partially prestressed specimens during the cyclic portion of the fatigue loading.</p> <p data-bbox="573 850 1414 999">The results from the finite element analysis indicated a change in strand stress of approximately 27.6 ksi, or $0.102f_{pu}$, for the partially prestressed specimens during the cyclic portion of the fatigue loading.</p>
Exposure Testing	<p data-bbox="573 1058 1414 1207">For the AZC Series, the pH of the saltwater solution placed into the void increased over time due to leaching of hydroxides from the grout. The higher pH caused a protective oxide film to form, resulting in pitting corrosion of the strand within the void.</p> <p data-bbox="573 1247 1414 1396">Both longitudinal and circumferential cracks were observed in the grout for all three beams from the GVC series. Whether the cracks occurred due to shrinkage of the grout or during the initial 10,000 cycles of fatigue testing is unknown.</p> <p data-bbox="573 1436 1414 1501">All three specimens from the GVC Series showed signs of corrosion at some point during the six months of exposure testing.</p> <p data-bbox="573 1541 1414 1690">The flexural cracks for the partially prestressed beams of the GVC Series continued to leak saltwater throughout the six-month duration of the exposure testing. The crack widths were relatively fine, measuring only 0.006 to 0.009 inches in width.</p>

Table 7-1: Summary of Findings for Full-Scale Beam Specimens (cont'd)

Source	Finding
Fatigue Testing	<p>All twelve beam specimens successfully reached 2,000,000 cycles of fatigue testing.</p> <p>Typical flexural crack pattern for the partially prestressed specimens consisted of four cracks spaced at 8 inches on center.</p> <p>Typical flexural crack widths for the partially prestressed specimens ranged from 0.006 to 0.011 inches.</p> <p>Flexural crack widths increased from 15 to 30 percent during the course of the fatigue testing.</p> <p>One fully prestressed beam (Specimen GVC-1) experienced flexural cracking.</p> <p>With the possible exception of Beam Specimen GVC-1, the tendons did not show any signs of distress during the fatigue testing.</p> <p>All of the fully prestressed beams and six of the eight partially prestressed beams suffered longitudinal cracking along the top of the specimens at the anchor head and at the opening in the center region of the beam.</p>
Forensic Investigation	<p>All twelve beam specimens were well grouted with only small air voids in the duct ribs at high points in the strand profile. The grout also completely filled the end anchorages and fully encapsulated the strands.</p> <p>All twelve beam specimens experienced both longitudinal and circumferential cracking of the grout, with crack widths measuring between 0.001 and 0.005 inches.</p> <p>All twelve beam specimens had some of their strands tight to the inside, bottom surface of the plastic duct due to the two-point drape profile. This condition resulted in minimal grout coverage between the strand and duct at these locations.</p>

Table 7-1: Summary of Findings for Full-Scale Beam Specimens (cont'd)

Source	Finding
Forensic Investigation	<p data-bbox="573 426 1414 495">In general, the plastic duct performed very well for all twelve beam specimens, suffering only some minor scrapes or scratches.</p> <p data-bbox="573 533 1414 678">The plastic duct suffered minor gouging at one location for one beam (Specimen FR-3). The gouging occurred due to a slight misalignment of the deviator, causing the duct to bear more on the edge of the deviator than throughout its length.</p> <p data-bbox="573 716 1414 821">For all twelve beam specimens, the strand did not suffer any fatigue cracks detectable through the dye penetrant inspection method.</p> <p data-bbox="573 858 1414 968">All three specimens from the AZC Series showed significant signs of corrosion for the portion of the tendons located within the grout void.</p> <p data-bbox="573 1005 1414 1115">Specimen AZC-3 also showed signs of corrosion in the strand away from the grout void, indicating that the strand acted as a conduit for the saltwater.</p> <p data-bbox="573 1152 1414 1262">All three specimens from the GVC Series showed significant signs of both uniform and pitting corrosion for the strands located tight to the plastic duct.</p> <p data-bbox="573 1299 1414 1409">All three specimens from the GVC Series showed signs of corrosion on the strands located away from the plastic duct. This corrosion coincided with circumferential cracks in the grout.</p> <p data-bbox="573 1446 1414 1591">The localized corrosion of the strand experienced by the AZC and GVC Series took the same form as that found on the test specimens discussed in Chapter 3. Pit depths ranged from a minimum of 0.002" to a maximum of 0.010".</p>

7.2 Conclusions

The following section presents conclusions based on the work performed during this research study. These conclusions, aimed at satisfying the six specific objectives listed in Section 1.4, are limited to the scope of this study (see Section 1.3). These conclusions also address the overall objective, namely that of determining the viability of partially post-tensioned concrete in an aggressive environment, including the impact of cyclic loading.

Conclusions for Specific Objective No. 1: With regard to developing a relationship between the amount of strand corrosion and the resultant fatigue capacity, the following conclusions are presented:

1. An empirical relationship was the most reliable method of predicting the response of corroded prestressing strand for the specific sequence of corrosion followed by fatigue to failure.
2. Average pit depth offered the best correlation between fatigue capacity and the amount of localized corrosion.
3. The fatigue capacity of corroded prestressing strand was well represented by an exponential decay function of the form shown by Eq. 7.1; where N_o is the mean fatigue life predicted from Paulson's equation (*i.e.*, with no corrosion present), S_r is the stress range in ksi, and d is the average pit depth for the strand in inches.

$$N = N_o e^{(-34d)} \quad 7.1a$$

$$\text{Log } N_o = 12.67 - 4.23 \text{ Log } S_r \quad 7.1b$$

Conclusions for Specific Objective No. 2: With regard to the potential of the strand fatigue-corrosion relationship to predict the response of full-scale, partially post-tensioned beam specimens, the following conclusions are presented:

1. Equation 7.1 successfully predicted that the beam specimens containing corroded prestressing strand would reach the full 2,000,000 cycles.
2. Although the result in Item 1 is promising, it is not possible to offer a definitive conclusion as the full-scale specimens were only tested to 2,000,000 cycles and not complete failure.

Conclusions for Specific Objective No. 3: With regard to performance of the tendon – duct, grout, and strand – within the full-scale, partially post-tensioned beam specimens, the following conclusions are presented:

1. The grout within post-tensioning ducts will contain both longitudinal and circumferential cracking. Furthermore, the potential for cracking is independent of the level of prestress.
2. Without full encapsulation of the strand by the grout, the tendon will act as a conduit for chloride transport.
3. Draped tendons in partially post-tensioned concrete members have a reduced resistance to chloride contamination due to their relative position within the grouted duct.
4. A robust plastic duct system will perform extremely well under the combination of fatigue and exposure to chlorides.
5. Steel saddles or pipes at tendon deviation points will eliminate the potential for puncturing plastic duct during the strand stressing operation. However,

accurate alignment is critical to prevent the duct from bearing on the edge of the steel embedment.

Conclusions for Specific Objective No. 4: With regard to quantifying the behavior of flexural cracks within the full-scale, partially post-tensioned beam specimens, the following conclusions are presented:

1. Concrete members designed for a nominal tensile stress in the precompressed tensile zone less than or equal to $12\sqrt{f'_c}$ will exhibit relatively fine flexural cracks (crack widths measuring less than or equal to 0.010 inches).
2. The relatively fine flexural crack widths mentioned in Item 1 will still act as transport mechanisms for chloride contamination.
3. Flexural crack widths will increase from 15 to 30 percent due to cyclic loading during the life of the concrete member.

Conclusions for Specific Objective No. 5: With regard to the role of grouting defects on the durability and fatigue performance of prestressing strand for full-scale, partially post-tensioned beam specimens, the following conclusions are presented:

1. Grouting defects, such as voids and fine cracks, do adversely affect corrosion protection of the strand, allowing chlorides access to the strand.
2. Grouting defects, such as voids and fine cracks, do not adversely affect fatigue performance of the strand.

Discussion relative to Specific Objective No. 6 is contained in the recommendation section. This specific objective dealt with developing a set of best practices for the

durability of partially post-tensioned concrete members in an aggressive environment, including cyclic loading.

With regard to the study's overall objective, partially post-tensioned concrete is a viable construction method in an aggressive environment, even with cyclic loading, but it relies on a robust plastic duct system as the primary protection method for the tendon.

7.2 Recommendations

With regard to developing a set of best practices for the durability of partially post-tensioned concrete members in an aggressive environment, including cyclic loading, the following recommendations are presented:

1. A robust plastic duct system is required as it serves as the primary protection method for the tendon and also performs very well under cyclic loading.
2. Install steel or plastic saddles at all deviation points to protect the duct during the stressing operation.
3. Design for a maximum nominal tensile stress in the precompressed tensile zone of $12\sqrt{f'_c}$. This limit will result in well distributed and relatively fine flexural cracking of the concrete (crack widths measuring less than or equal to 0.010 inches). Furthermore, this limit will assure a minimum of 2,000,000 cycles for the strand under the imposed live load without the need for detailed fatigue calculations.
4. Design for a maximum compressive stress of $0.50f'_c$ under full service load. This limit will prevent damage to the concrete in the form of spalling and

cracking within the compression zone during cyclic loading. It will also limit the effect of creep on increasing deflections and the growth of flexural cracks due to cyclic loading.

5. Post-tensioned concrete will crack in the anchorage zones due to bursting and dispersion tensile stresses. This cracking can adversely affect the durability of a post-tensioned member and must be repaired.

In addition to the recommendations for a set of best practices discussed previously, the following recommendations are also presented:

1. Use Eq. 7.1 to predict the fatigue response of prestressing strand that exhibits localized corrosion.
2. Complete further studies to evaluate the potential of Eq. 7.1 to predict the fatigue response of full-size, partially post-tensioned concrete beams containing corroded prestressing strand.
3. When inspecting failed tendons due to corrosion, consider fatigue as a potential cause due to similar fracture surfaces as that caused by hydrogen embrittlement or stress corrosion cracking.

Bibliography

- AASHTO Bridge Committee, Technical Committee T-5 Loads, Agenda Item: 22, Subject: LRFD Bridge Design Specification, Section 3, Article 3.6.1.3.1, 2007.
- AASHTO LRFD Bridge Design Specifications, 4th edition (Including 2008 Interim Revisions), American Association of State and Highway Transportation Officials, Washington, D.C., 2008.
- Abeles, P. W., Barton, F. W., and Brown, E. I., "Fatigue Behavior of Prestressed Concrete Bridge Beams," *First International Symposium on Concrete Bridge Design*, SP-23, American Concrete Institute, Farmington Hills, MI, 1969, pp. 579-599.
- ACI Committee 215, "Considerations for Design of Concrete Structure Subjected to Fatigue Loading (ACI 215R-74 [Reapproved 1997])," American Concrete Institute, Farmington Hills, MI, 1997, 24 pp.
- ACI Committee 222, "Corrosion of Prestressing Steels (ACI 222.2R-01)," American Concrete Institute, Farmington Hills, MI, 2001, 43 pp.
- ACI Committee 224, "Causes, Evaluation, and Repair of Cracks in Concrete Structures (ACI 224.1R-07)," American Concrete Institute, Farmington Hills, MI, 2007, 22 pp.
- ACI Committee 315, "Details and Detailing of Concrete Reinforcement (ACI 315-99)," American Concrete Institute, Farmington Hills, MI, 1999, 44 pp.
- ACI Committee 318, "Building Code Requirements for Structural Concrete (ACI 318-08) and Commentary (ACI 318R-08)," American Concrete Institute, Farmington Hills, MI, 2008, 467 pp.
- ACI-ASCE Committee 423, "State-of-the-Art Report on Partially Prestressed Concrete (ACI 423.5R-99)," American Concrete Institute, Farmington Hills, MI, 1999, 37 pp.
- ACI-ASCE Committee 423, "Specification for Unbonded Single-Strand Tendon Materials and Commentary (ACI 423.7-07)," American Concrete Institute, Farmington Hills, MI, 2007, 21 pp.

- Ahern, Michael, E., "Design and Fabrication of a Compact Specimen for Evaluation of Corrosion Resistance of New Post-Tensioning Systems," M.S. Thesis, The University of Texas at Austin, Austin, TX, May 2005.
- AISC, "Specification for Structural Steel Buildings (ANSI/AISC 360-05)," American Institute of Steel Construction, Inc., Chicago, IL, 2005, 460 pp.
- Anderson, T. L., "Fracture Mechanics: Fundamentals and Applications," 2nd Edition, CRC Press, Inc. Publisher, 1995, 680 pp.
- ANSYS Academic Research, Release 11.0, Documentation for ANSYS, ANSYS, Inc., Canonsburg, PA, 2007.
- ASTM A36-05, "Standard Specification for Carbon Structural Steel," ASTM International, West Conshohocken, PA, 2005.
- ASTM A53-07, "Standard Specification for Pipe, Steel, Black and Hot Dipped Zinc-Coated, Welded and Seamless," ASTM International, West Conshohocken, PA, 2007.
- ASTM A722-07, "Standard Specification for Uncoated High-Strength Steel Bars for Prestressing Concrete," ASTM International, West Conshohocken, PA, 2007.
- ASTM A370-05, "Standard Test Methods and Definitions for Mechanical Testing of Steel Products," ASTM International, West Conshohocken, PA, 2005.
- ASTM A416-05, "Standard Specification for Steel Strand, Uncoated Seven-Wire for Prestressed Concrete," ASTM International, West Conshohocken, PA, 2005.
- ASTM C39-05, "Standard Test Method for Compressive Strength of Cylindrical Concrete Specimens," ASTM International, West Conshohocken, PA, 2005.
- ASTM C109-07, "Standard Test Method for Compressive Strength of Hydraulic Cement Mortars (Using 2-in. Cube Specimens)," ASTM International, West Conshohocken, PA, 2007.
- ASTM C143-08, "Standard Test Method for Slump of Hydraulic-Cement Concrete," ASTM International, West Conshohocken, PA, 2008.
- ASTM C469-02, "Standard Test Method for Static Modulus of Elasticity and Poisson's Ratio of Concrete in Compression," ASTM International, West Conshohocken, PA, 2002.
- ASTM E1417-05e1, "Standard Practice for Liquid Penetrant Testing," ASTM International, West Conshohocken, PA, 2005.

- Balaguru, P. N., "Analysis of Prestressed Concrete Beams for Fatigue Loading," *PCI Journal*, V. 26, No. 3, May-July 1981, pp. 70-94.
- Balaguru, P. N., and Shah, S. P., "Method of Predicting Crack Widths and Deflections for Fatigue Loading," *Fatigue of Concrete Structures*, SP-75, S.P. Shah, ed., American Concrete Institute, Farmington Hills, MI, 1982, pp. 153-175.
- Bannantine, Julie A., Comer, Jess J., and Handrock, James L., "Fundamentals of Metal Fatigue Analysis," 1st Edition, Prentice Hall Publisher, Englewood Cliffs, NJ, 1990, 273 pp.
- Baran, E., Shield, C. K., and French, C. E., "A Comparison of Methods for Experimentally Determining Prestress Losses in Pretensioned Prestressed Concrete Girders," SP231-10, American Concrete Institute, Farmington Hills, MI, 2005, pp. 161-180.
- Barr, P. J., Stanton, J. F., and Eberhard, M. O., "Effects of Temperature Variations on Precast, Prestressed Concrete Bridge Girders," *ASCE Journal of Bridge Engineering*, Vol. 10, No. 2, March-April 2005, pp. 186-194.
- Bennett, E. W., "Some Problems of Partial Prestressing," *Partial Prestressing, from Theory to Practice*, Volume 1: Survey Reports, M.Z. Cohn, Ed., 1986, pp. 135-149.
- Bentur, A., Diamond, S., and Berke, N. S., "Steel Corrosion in Concrete," 1st Edition, E & FN Spon, Chapman & Hall Publisher, London, UK, 1997, 201 pp.
- Beretta, S. and Matteazzi, S., "Short Crack Propagation in Eutectoid Steel Wires," *International Journal of Fatigue*, Vol. 18, No. 7, 1996, pp. 451-456.
- Beretta, S. and Boniardi, M. "Fatigue Strength and Surface Quality of Eutectoid Steel Wires," *International Journal of Fatigue*, Vol. 21, No. 4, 1999, pp. 329-335.
- Billington, David. P., "Historical Perspective on Prestressed Concrete," *PCI Journal*, V. 49, No. 1, Jan.-Feb. 2004, pp. 14-30.
- Böhni, Hans, "Localized Corrosion of Passive Metals," pp. 173-190, *Uhlig's Corrosion Handbook*, R. Winston Revie, ed., 2nd Edition, John Wiley & Sons Publisher, NY, 2000, 1302 pp.
- Broomfield, J. P., "Corrosion of Steel in Concrete: Understanding, Investigation, and Repair," 1st Edition, E & FN Spon, Chapman & Hall Publisher, London, UK, 1997, 240 pp.

- Box, George E. P., Hunter, William G., and Hunter, J. Stuart, "Statistics for Experimenters – An Introduction to Design, Data Analysis, and Model Building," 1st Edition, John Wiley & Sons Publisher, 1978, 655 pp.
- Burns, N. H., Gross, S. P., and Byle, K. A. "Instrumentation and Measurements – Behavior of Long-Span Prestressed High Performance Concrete Bridges." Proceedings, PCI/FHWA International Symposium on High Performance Concrete, Ottawa, pp. 566–577.
- Chen, Liao, Wan, Gao, and Wei, "Pitting Corrosion and Fatigue Crack Nucleation," Effects of the Environment on the Initiation of Crack Growth, ASTM STP 1298, W. A. Van Der Sluys ed., ASTM International, West Conshohocken, PA, 1997.
- Cho, K. and Pickering, H. W., "The Role of Chloride Ions in the $IR > IR^*$ Criterion for Crevice Corrosion in Iron," Journal of The Electrochemical Society, V. 138, No. 10, October 1991, pp. L56-L58.
- Christensen, Bruce J., Mason, Thomas O., and Jennings, Hamlin M., "Influence of Silica Fume on the Early Hydration of Portland Cement Pastes Using Impedance Spectroscopy," Journal of the American Ceramic Society, V. 75, No. 4, April 1992, pp. 935-939.
- Ciolko, A. T. and Tabatabai, H., "Nondestructive Methods for Condition Evaluation of Prestressing Steel Strands in Concrete Bridges. Final Report Phase I: Technology Review," NCHRP Project 10-53, Transportation Research Board, National Academy Press, Washington, D. C., March 1999, 81 pp.
- Cleveland, W. S., "The Elements of Graphing Data," 2nd Edition, Hobart Press, Summit, New Jersey, 1994, 323 pp.
- Cohn, M. Z., "Some Problems of Partial Prestressing," *Partial Prestressing, from Theory to Practice, Volume 1: Survey Reports*, M.Z. Cohn, Ed., 1986, pp. 15-63.
- Comité Euro-Internationale du Bèton, "CEB-FIP Model Code 1990," Bulletin d'Information, No. 213/214, Lausanne, Switzerland, 1993, 437 pp.
- Corven, J. A., "Mid-Bay Bridge Post-Tensioning Evaluation," Florida Department of Transportation Report, Corven Engineering, Inc., Tallahassee, FL, 2001.
- D'Arcy, Thomas J., Nasser, George D., and Ghosh, S. K., "Building Code Provisions for Precast/Prestressed Concrete: A Brief History," PCI Journal, V. 48, No. 6, Nov.-Dec. 2003, pp. 116-124.

- De Graaf, E. and De Rijk, P., "Comparison Between Reliability, Sensitivity, and Accuracy of Nondestructive Inspection Methods," 13th Symposium on Nondestructive Evaluation Proceedings, San Antonio, TX, published by NTIAC, Southwest Research Institute, San Antonio, TX, April 1981, pp. 311-322.
- Edwards, A. D. and Picard, A., "Fatigue Characteristics of Prestressing Strand," Proceedings, Institution of Civil Engineers, 53 (Part 2), September 1972, pp. 325-336.
- Fett, T. and Munz, D., "Stress Intensity Factors and Weight Functions," Computational Mechanics Publications, Billerica, Massachusetts, 1997, 385 pp.
- Florida Department of Transportation, "Mid-Bay Bridge Post-Tensioning Evaluation, Final Report," Florida Department of Transportation District 3, October 10, 2001.
- Foo, M. H. and Warner, R. F., "Fatigue Tests on Partially Prestressed Concrete Beams," *Partial Prestressing, from Theory to Practice, Volume 2: Prepared Discussion*, M.Z. Cohn, Ed., 1986, pp.177-186.
- Freyermuth, C. L., "Practice of Partial Prestressing for Continuous Post-Tensioned Structures," *Partial Prestressing, from Theory to Practice, Volume 1: Survey Reports*, M.Z. Cohn, Ed., 1986, pp. 303-327.
- Hale, W. M. and Russell, B. W., "Effect of Allowable Compressive Stress at Release on Prestress Losses and on the Performance of Precast, Prestressed Concrete Bridge Girders," *PCI Journal*, V. 51, No. 2, Mar.-Apr. 2006, pp. 14-25.
- Hamilton, H. R., III, "Investigation of Corrosion Protection Systems for Bridge Stay Cables," Ph.D. Dissertation, The University of Texas at Austin, Austin, TX, September 1995.
- Hill, Aaron T., Jr., "Material Properties of the Grade 300 and Grade 270 Prestressing Strands and Their Impact on the Design of Bridges," M.S. Thesis, Virginia Polytechnic Institute and State University, Blacksburg, VA, 2006.
- Ivering, J. W. and Trost, H., "The Merit of Partial Prestressing in the Design of Precast I-Girders," *Developments in Short and Medium Span Bridge Engineering '90*, Vol. 1, B. Bakht, R.A. Dorton, and L.G. Jaeger, Eds., 1990, pp. 27-35.
- Jones, Denny A., "Principles and Prevention of Corrosion," 2nd Edition, Prentice Hall Publisher, New Jersey, 1996, 572 pp.
- Klein, T. W., "Wire Rope and Strand Assemblies in Bridge Applications," pp. 239-246, *Advances in Cable-Supported Bridges*, K. M. Mahmoud, ed., Taylor & Francis Group, London, 2006, 265 pp.

- Koch, G. H., Brongers, M. P. H., Thompson, N. G., Virmani, Y. P., and Payer, J. H., "Corrosion Cost and Preventive Strategies in the United States," FHWA Research Report FHWA-RD-01-156, September 30, 2001.
- Kotys, Andrea L., "Durability Examination of Bonded Tendons in Concrete Beams Under an Aggressive Corrosive Environment," M.S. Thesis, The University of Texas at Austin, Austin, TX, May 2003.
- Krom, A. H. M., Koers, R. W. J., and Bakker, A., "Hydrogen Transport Near a Blunting Crack Tip," *Journal of the Mechanics and Physics of Solids*, V. 47, No. 4, February 1999, pp. 971-992.
- Lin, T. Y. and Burns, Ned H., "Design of Prestressed Concrete Structures," 3rd Edition, John Wiley & Sons Publisher, New York, NY, 1981, 646 pp.
- Llorca, J. and Sanchez-Galvez, V., "Fatigue Threshold Determination in High Strength Cold Drawn Eutectoid Steel Wires," *Engineering Fracture Mechanics*, Vol. 26, No. 6, 1987, pp. 869-892.
- Llorca, J. and Sanchez-Galvez, V., "Fatigue Limit and Fatigue Life Prediction in High Strength Cold Drawn Eutectoid Steel Wires," *Fatigue and Fracture of Engineering Materials and Structures*, Vol. 12, No. 1, 1989, pp. 31-45.
- Lopes, S. M. R. and Simoes, L. M. L. P., "Influence of Corrosion on Prestress Strands," *Canadian Journal of Civil Engineering*, V. 26, No. 6, Dec. 1999, pp. 782-788.
- MacDougall, C. and Bartlett, F. M., "Tests of Corroded Unbonded Seven-Wire Tendons with Broken Wires," *ACI Structural Journal*, V. 99, No. 6, Nov.-Dec. 2002, pp. 803-810.
- Moses, F., "Calibration of Load Factors for LRFR Bridge Evaluation," NCHRP Report 454, Transportation Research Board, National Academy Press, Washington, D.C., 2001.
- Murakami, Y. (ed.), "Stress Intensity Factors Handbook," Vols. 1 and 2, Pergamon Press Publisher, Oxford, England, U.K., 1987, 1456 pp.
- Naaman, A. E., "Fatigue in Partially Prestressed Beams," *Fatigue of Concrete Structures*, SP-75, S.P. Shah, ed., American Concrete Institute, Farmington Hills, MI, 1982, pp. 25-46.
- Naaman, A. E., "Partially Prestressed Concrete Members Under Static Loading: American Perspective," *Partial Prestressing, from Theory to Practice, Volume 1: Survey Reports*, M.Z. Cohn, Ed., 1986, pp. 79-134.

- Neville, A. M., "Properties of Concrete," 4th Edition, Pearson Education Limited, Prentice Hall Publisher, Harlow, England, UK, 1995, 844 pp.
- Nilson, Arthur H., "Design of Prestressed Concrete," 2nd Edition, John Wiley & Sons Publisher, NY, 1987, 586 pp.
- Novokshchenov, V., "Brittle Fractures of Prestressed Bridge Steel Exposed to Chloride-Bearing Environments Caused by Corrosion-Generated Hydrogen," Corrosion, NACE International, V. 50, No. 6, 1994.
- Nowak, A. S., "Calibration of LRFD Bridge Design Code," NCHRP Report 368, Transportation Research Board, National Academy Press, Washington, D.C., 1999.
- Nürnbergger, U., "Corrosion Induced Failure Mechanisms of Prestressing Steel," Materials and Corrosion, Wiley-VCH, V. 53, No. 8, 2002, pp. 591-601.
- Oesterle, Ralph G. and Volz, Jeffery S., "Evaluation of the Bunting Avenue Bridge," Construction Technology Laboratories, Inc., Report No. 940103, Skokie, IL, March 1994.
- Oesterle, R. G., Tabatabai, H., Lawson, T. J., Refai, T. M., Volz, J. S., and Scanlon, A., "Jointless and Integral Abutment Bridges, Summary Report," U.S. Department of Transportation, Federal Highway Administration, Washington, D.C., Publication No. FHWA- , April 2007.
- Overman, T. R., Breen, J. E., and Frank, K. H., "Fatigue Behavior of Pretensioned Concrete Girders," Research Report 300-2F, Center for Transportation Research, Bureau of Engineering Research, The University of Texas at Austin, November 1984.
- Paikowsky, S. G., "Load and Resistance Factor Design (LRFD) for Deep Foundations," NCHRP Report 507, Transportation Research Board, National Academy Press, Washington, D.C., 2004.
- Paulson, C., Frank, K. H., and Breen, J. E., "A Fatigue Study of Prestressing Strand," Research Report 300-1, Center for Transportation Research, Bureau of Engineering Research, The University of Texas at Austin, April 1983.
- Perenchio, W. F., Fraczek, J. and Pfeifer, D. W., "Corrosion Protection of Prestressing Systems in Concrete Bridges," NCHRP Report 313, Transportation Research Board, Washington, D.C., February 1989.
- Pickering, Howard W., "Important Early Developments and Current Understanding of the *IR* Mechanism of Localized Corrosion," Journal of The Electrochemical Society, V. 150, No. 5, March 2003, pp. K1-K13.

- Podolney, W. Jr., "Understanding the Steel in Prestressing," *PCI Journal*, V. 37, No. 3, May-Jun. 1967, pp. 54-64.
- Post-Tensioning Institute, "Guide Specification for Grouting of Post-Tensioned Structures," *PTI Committee on Grouting Specifications*, 2nd edition, Post-Tensioning Institute, 2003.
- Pook, L. P., "Linear Elastic Fracture Mechanics for Engineers," 1st Edition, WIT Press Publisher, Southampton, U.K., 2000, 154 pp.
- Preston, H. K., "Testing 7-Wire Strand for Prestressed Concrete—State of the Art," *PCI Journal*, V. 30, No. 3, May-Jun. 1985, pp. 134-155.
- Preston, H. K., "Handling Prestressed Concrete Strand," *PCI Journal*, V. 35, No. 6, Nov.-Dec. 1990, pp. 68-71.
- Rabbat, B. G., Karr, P. H., Russel, H. G., and Bruce, N. G., Jr., "Fatigue Tests of Full Size Prestressed Girders," Research Report 113, Portland Cement Association, June 1978.
- Rigon, C. and Thurlimann, B., "Fatigue Tests on Post-Tensioned Concrete Beams," Rport 8101-1, Institut fur Baustatik und Konstruktion, ETH Zurich (Swiss Federal Institute of Technology), May 1985.
- Ryals, K. K., Breen, J. E., and Kreger, M. E., "Fretting Fatigue in External Post-Tensioned Tendons," Research Report 1211-1F, Center for Transportation Research, Bureau of Engineering Research, The University of Texas at Austin, December 1992.
- Schokker, A. J., Koester, B. D., Breen, J. E., and Kreger, M. E., "Development of High Performance Grouts for Bonded Post-Tensioned Structures," Research Report 1405-2, Center for Transportation Research, Bureau of Engineering Research, The University of Texas at Austin, October 1999a.
- Schokker, A. J., West, J. S., Breen, J. E., and Kreger, M. E., "Interim Conclusions, Recommendations and Design Guidelines for Durability of Post-Tensioned Bridge Substructures," Research Report 1405-5, Center for Transportation Research, October 1999b.
- Schokker, A. J., Breen, J. E., and Kreger, M. E., "Grouts for Bonded Post-Tensioning in Corrosive Environments," *ACI Materials Journal*, Vol. 98 No. 4, July-August 2001, pp. 296-305.

- Schokker, A. J., Breen, J. E., and Kreger, M. E., "Simulated Field Testing of High Performance Grouts for Post-Tensioning," *ASCE Journal of Bridge Engineering*, Vol. 7, No. 2, March-April 2002a, pp. 127-133.
- Schokker, A. J., Hamilton, H. R., and Schupack, M., "Estimating Post-Tensioning Grout Bleed Resistance Using a Pressure-Filter Test," *PCI Journal*, Vol. 47, No. 1, March-April 2002b, pp. 32-39.
- Schupack, M., "Grouting Tests on Large Post-Tensioning Tendons for Secondary Nuclear Containment Structures," *Journal of the Prestressed Concrete Institute*, March-April 1971, pp. 85-97.
- Schupack, M., "Admixture for Controlling Bleed in Cement Grout Used in Post-Tensioning," *Journal of the Prestressed Concrete Institute*, November-December 1974.
- Schupack, M. and O'Neil, F., "Observations on the Results of a 33 Year Test of the Durability of 20 Post-Tensioned Beams Exposed at the Corps of Engineers Severe Weather Exposure Station at Treat Island, Maine," *U.S. Army Engineer Waterway Experiment Station Report*, Volumes I & II, 1997.
- Seber, George A. F. and Wild, Christopher J., "Nonlinear Regression," *Wiley Series in Probability and Statistics*, John Wiley & Sons Publisher, 2003, 792 pp.
- Shahawi, M., and Batchelor, B., "Fatigue of Partially Prestressed Concrete," *Journal of Structural Engineering*, ASCE, V. 112, No. 3, March 1986, pp. 524-537.
- Shipilov, S. A., "Corrosion Fatigue," pp. 329-389, *Advances in Fatigue, Fracture and Damage Assessment of Materials*, A. Varvani-Farahani, ed., WIT Press, Billerica, MA, 2005, 502 pp.
- Siegwart, M., "Influence of Electrochemical Chloride Extraction on the Performance of Prestressed Concrete Under Dynamic Loading Conditions," *ASCE Journal of Materials in Civil Engineering*, Nov.-Dec. 2006, pp. 800-812.
- Sumiden Wire Products Corporation, "Production Process for ASTM A416 Low-Relaxation PC Strand," Sumiden Wire Products Corporation, Stockton, CA, 2006.
- Tide, R. H. R. and VanHorn, D. A., "A Statistical Study of the Static and Fatigue Properties of High Strength Prestressing Strand," Report 309.2, Fritz Engineering Laboratory, Lehigh University, June 1966.

- Turco, G. P., Salas, R. M., Schokker, A. J., West, J. S., Kreger, M. E., and Breen, J. E., "Durability Evaluation of Post-Tensioned Concrete Beam Specimens After Long-Term Aggressive Exposure Testing," Research Report 4562-2, Center for Transportation Research, Bureau of Engineering Research, The University of Texas at Austin, November 2007.
- VSL, "Detailing for Post-Tensioning," VSL Report Series 3, VSL International Ltd., Bern, Switzerland, April 1991, 52 pp.
- Wang, Y. Z., "Corrosion Fatigue," pp. 221-232, Uhlig's Corrosion Handbook, R. Winston Revie, ed., 2nd Edition, John Wiley & Sons Publisher, NY, 2000, 1302 pp.
- Warner, R. F. and Hulsbos, C. L., "Probable Fatigue Life of Prestressed Concrete Beams," PCI Journal, V. 11, No. 2, April 1966, pp. 16-39.
- West, J. S., Vignos, R. P., Breen, J. E., and Kreger, M. E., "Corrosion Protection for Bonded Internal Tendons in Precast Segmental Construction," Research Report 1405-4, Center for Transportation Research, Bureau of Engineering Research, The University of Texas at Austin, October 1999.
- Withiam, J., Votyku, E., Barker, R., Duncan, J. M., Kelly, B., Musser, S., and Elias, V., "Load and Resistance Factor Design (LRFD) for Highway Bridge Substructures," U.S. Department of Transportation, Federal Highway Administration, Washington, D.C., Publication No. FHWA HI-98-032, 1998.
- Wollmann, G. P., Yates D. L., Breen, J. E., and Kreger, M. E., "Fretting Fatigue in Post-Tensioned Concrete," Research Report 465-2F, Center for Transportation Research, Bureau of Engineering Research, The University of Texas at Austin, November 1988.

Appendix A

Accelerated Strand Corrosion Process

The most important consideration with respect to corroding the individual strand samples is to mimic the exact conditions encountered in the field. Steel located in a high pH environment, such as concrete or grout, is protected from corrosion by the formation of an oxide film (Böhni 2000). However, if chloride ions in sufficient concentration come in contact with this film, the passivating layer will break down, resulting in pitting corrosion (Böhni 2000).

To mimic this mechanism, strand samples were placed in a simulated concrete pore water solution containing five percent by mass of NaCl salts. The pore water solution consisted of deionized water mixed with the following concentrations of hydroxides (Christensen *et al.* 1992):

0.32 mol/L of KOH,

0.17 mol/L of NaOH,

0.07 mol/L of Ca(OH)₂

To accelerate the degradation process, the author subjected the strand samples within the above solution to an electrode potential of +200mV_{sce}, as shown in Figure A-1. This step artificially reduces the time required to corrode, and ultimately test, numerous strand samples. However, initial fatigue testing of these samples indicated very unexpected results. All three strand samples failed at essentially the same number of cycles, approximately 310,000, even though the samples contained drastically different

amounts of corrosion. (Without corrosion, the strand samples should have failed at approximately 740,000 cycles.) Initially, the author considered the onset of severe hydrogen embrittlement as a potential cause. However, hydrogen will not form at the applied electrode potential of $+200\text{mV}_{\text{sce}}$, although some type of gas formed on the counter electrode during the process.

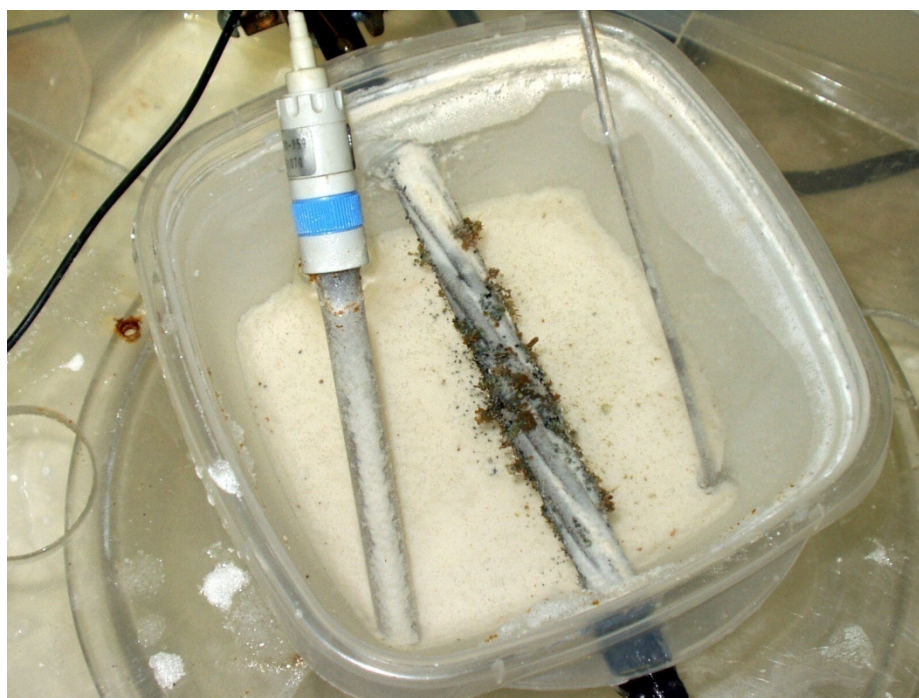


Figure A-1: Accelerated Corrosion Setup

Furthermore, the potentiostatic anodic polarization of the strand resulted in an unusually dense pit distribution, as shown in Figure A-2. Very closely spaced pitting occurs because the cathodic reaction is removed to the counter electrode, preventing the naturally occurring cathodic protection state of the strand immediately adjacent to a pit (Jones 1996). The author subsequently abandoned this approach, as it would vary considerably from the conditions encountered within an actual structure.



Figure A-2: Artificially Dense Pitting Structure

Appendix B

Strand Protection for Individual Strand Testing

One of the most critical aspects of strand testing, either static or fatigue, involves protecting the strand within the end grip region. Almost all gripping mechanisms employ serrated teeth to secure the tension specimen in place. However, whether a wedging action or hydraulic grip is used, the teeth will notch the specimen, resulting in significant stress concentrations. These stress concentrations are substantial enough to cause the strand specimens to fail prematurely within the end grip region during nearly every test (*e.g.*, Hill 2006, Paulson *et al.* 1983). Unfortunately, it is impossible to use a dog-bone or upset end strand specimen due to the manufacturing process required to fabricate prestressing strand.

Researchers have employed a variety of measures to protect the strand during testing, with various levels of success. ASTM A416 (2005) recommends installing a material between the strand and grips to cushion the interface. Aluminum foil, carborundum cloth, and bra shims are given as potential materials. Paulson's method (1983) involved a variation to the ASTM recommendations. He used small ductile wires, aluminum foil, and a reusable chuck. The process involved placing the wires within the interstitial spaces of the strand, wrapping the strand and wires with aluminum foil, and then placing the strand into the reusable chuck. This method worked well and resulted in a significant number of fatigue failures within the gage length of the strand sample. However, he later

refined the method by double chucking the ends to reduce slippage that occurred during some of the tests.

Hill (2006) investigated a variety of methods employed by previous researchers, including Paulson's method and several methods proposed by Preston (1985). Preston's recommendations included the use of the PLP Grip (no longer manufactured by Florida Wire and Cable Company), the Sand Grip, the Tinius Olsen Grip, and aluminum angle inserts. The most successful method employed by Hill used aluminum tubing, 80 grit aluminum oxide, water, epoxy, and standard V-Grips. The process involved splitting the aluminum tubing in half; creating a mixture of aluminum oxide, water, and epoxy; coating the inside of the tubing with the mixture; then placing the tubing around the strand ends and clamping it in place to cure. Once cured, the specimen ends were placed in the V-Grip and installed in the testing machine.

The author initially used the method proposed by Paulson, with limited success, and later switched to a variation of Hill's method. This method used 1/2" diameter aluminum tubing, 30 grit aluminum oxide, high strength/high modulus two-part epoxy (Sikadur 31 High Mod 2 Component Epoxy), and reusable chucks. The process began by cutting the aluminum pipe into six inch long segments with a band saw. Then the segments were split longitudinally into sections slightly less than half the original diameter. These sections were then wrapped around a dummy piece of strand and shaped closer to the actual strand diameter (approximately 0.464" across interstices and 0.508" across outer wire edges) with a vice grip. The next step involved mixing the two-part epoxy and then adding approximately ten percent by volume of aluminum oxide grit. At this time, the insides of two sections of the aluminum tubing were coated with the epoxy grit mix-

ture, placed around the end region of a strand specimen, and clamped in place to cure. The result is shown in Figure B-1. The same process was then repeated at the other end of the strand. When the epoxy reached full strength, the strand sample was ready for fatigue testing.



Figure B-1: Strand End Treatment for Fatigue Testing

Appendix C

Beam Specimen Construction Details

In general, fabrication of the beam specimens followed typical construction practices for construction of the formwork; fabrication of the reinforcing cages; placement and curing of the concrete; installation and stressing of the post-tensioning tendons; and grouting of the tendons. This appendix discusses the details of each facet involved in fabricating the specimens. Results of the material property testing are also contained within this appendix.

C.1 Formwork

The formwork design was based on casting three specimens at one time. These specimens coincided with each test series shown in the beam specimen test matrix (see Table 4-1). A series of three specimens also allowed for economy of formwork and the ability to have the concrete mixed and delivered by a ready-mix supplier.

Construction of the formwork followed traditional construction methods. Materials for the majority of the formwork consisted of 1/2-inch-thick plywood and 2x4's. However, for the complex trapezoidal shape along the center of the specimen and the NaCl reservoirs, the author used 1/2-inch-thick wood boards and both 1x2's and 2x4's. A photo of the basic formwork is shown in Figure C-1.



Figure C-1: Basic Formwork for Casting Specimens

The most challenging part of the formwork design involved removing the specimens without damaging the formwork so that it could be reused for all twelve specimens. The critical areas involved the post-tensioning bar, steel deviator, and tendon duct.

To solve the problem with the post-tensioning bar, the author installed 2-inch-diameter PVC tubing through 2-inch-diameter holes cut in the formwork endwalls. The PVC tubing did not extend completely through the formwork but terminated at the trapezoidal form. During fabrication of the specimens, the PVC tubing was placed through the endwall holes and threaded through the previously installed reinforcing cage. However, to maintain alignment, the author cut 1-1/2-inch-diameter holes in the trapezoidal forms and installed the post-tensioning bar inside of the PVC tubing. Thus, the post-tensioning bar extended completely through the formwork and maintained alignment and support for

the PVC tubing, yet was unbonded to the specimen. During stripping of the formwork, the post-tensioning bar was removed, allowing removal of the beam specimen and reuse of the trapezoidal forms for subsequent specimens.

The problem with the deviators and tendon duct was more problematic. The plastic tendon duct had to pass through the formwork for the NaCl reservoir. This formwork also had to provide support for the steel deviators. For the first series of specimens, the author designed the NaCl reservoir formwork to be removed intact. However, in practice, this proved very difficult due to the confining work space and clamping effect from shrinkage of the concrete. As a result, the formwork needed to be cut out of the reservoir and refabricated for each specimen.

To condition the wood forms for reuse and provide form release during removal, the author coated the formwork with Duogard N.E., manufactured by W.R. Meadows. In addition to acting as a form release agent, the Duogard N.E. sealed the wood and provided protection against warping from moisture. Except for some minor repairs, all twelve specimens were able to be cast from the original formwork.

C.2 Reinforcing Cage

All reinforcement for the beam specimens was detailed in the laboratory from straight bars. The decision to bend the bars in-house was primarily due to two factors: (1) the complex shapes and tight tolerances required for the specimens; and (2) the lack of local expertise in reinforcing bar detailing. The author used a Hitachi VB16Y Rebar Cutter/Bender to fabricate the required shapes for the specimens. All reinforcement was

detailed in accordance with ACI 315, *Details and Detailing of Concrete Reinforcement* (1999).

Construction of the cages required considerable planning due to the complex design of the beam specimens. The cage layout had to allow for subsequent placement of the NaCl reservoir formwork, prestressing bar PVC inserts, lifting inserts, and prestressing strand deviators and plastic duct. A completed cage is shown in Figure C-2 prior to placement into the formwork.



Figure C-2: Completed Reinforcing Cage

C.3 Post-Tensioning Anchorage, Duct, and Deviator Hardware and Installation

The author chose the VSL Type EC stressing anchorage for the post-tensioning tendon. The benefits of the Type EC include: (1) use as both a live- and dead-end anchorage; (2) double flange design; and (3) compact size. Based on the tendon design discussed previously, the author used galvanized 5-7 Type EC stressing anchorages. The choice of galvanized was based on needing to eliminate the potential for corrosion of the anchorage, which was not a variable under study. The 5-7 designation stands for 1/2-inch-diameter strand in a maximum seven-strand tendon. Figure C-3 is a photograph of the two-part wedges, anchor head, and anchorage used in the construction of the specimens.



Figure C-3: VSL Type EC Stressing Anchorage

The author chose the VSL PT-PLUS System for the tendon duct. The benefits of a plastic duct include: (1) enhanced corrosion protection; (2) improved tendon fatigue resistance; and (3) reduced tendon friction. In addition, when a tendon is external, as it

was for a portion of the test specimens, the industry standard is the use of a plastic duct. Plastic duct also eliminates the phenomenon of strand-to-duct fretting fatigue, which reduced the number of test variables to consider.

Due to the complexity of the beam specimens, the anchorages, deviators, and ducts required a very precise installation sequence. First, the anchorages needed to be placed within the reinforcing cage while the cage was being tied. This requirement was due to the corbel reinforcement along the end of the beam combined with the double flange of the Type EC anchorage. Next, the completed reinforcing cage was lowered into the formwork, without the endwalls present. Following that, the reservoir formwork was installed. Then, the steel pipe deviators were installed into openings within the reservoir formwork. Finally, the precut plastic duct was threaded through the reinforcing spiral at one end of the reinforcing cage, through the deviators and reservoir formwork, through the reinforcing spiral at the far end, and into the far anchorage.

The final step involved securing all the elements. The deviators were tightly wedged into the openings in the reservoir formwork, usually without the need for any shims. Then the plastic duct was attached to the anchorages with duct tape. The next step was to install the formwork endwalls and bolt the anchorages at pre-drilled locations in the endwalls. At this point, small wood wedges were inserted into the deviator to align the duct with the bottom of the pipe. The plastic duct was secured to the deviators at the ends away from the reservoir formwork with duct tape and electrical tape, which also served to seal the annular space between the deviator and duct. Figure C-4 shows the completed formwork, reinforcing cage, deviators, prestressing anchorages, and plastic duct ready for concrete placement.



Figure C-4: Completed Specimen Setup Ready for Concrete Placement

C.4 Concrete Mix Design, Placement, and Curing

Normally, a structural engineer specifies a minimum 28-day compressive strength for different concrete elements within a structure. The concrete supplier, usually based on previous mix designs and experience, will supply concrete with a target strength of 200 to 400 psi above the minimum specified compressive strength. In many instances, the concrete will be even more than 400 psi above the minimum specified strength. It is beneficial to the concrete supplier to always exceed the specified value, whereas falling below the specified value can result in significant financial penalties.

However, for this study, the author had a target 28-day compressive strength and wanted to stay as close to this value as possible. The author would rather have some batched concrete strengths fall slightly below the target than to ever have them substantially over the target. The target 28-day compressive strength was 4,000 psi, the value used to design the beam specimens.

The largest sample set of mix designs available were based on specifications from the Pennsylvania Department of Transportation (PennDOT). PennDOT's categories of structural concrete mixes are referred to as Class A, Class AA, and Class AAA. Class A has a 28-day structural design compressive strength of 3,000 psi, and a minimum 28-day mix design compressive strength of 3,300 psi. Furthermore, based on discussions with the local testing agency, the Class A mix provided by Centre Concrete Company regularly tests very near 4,000 psi. Consequently, the author chose the PennDOT Class A mix provided by Centre Concrete. The only change from the standard PennDOT Class A mix was to specify PennDOT 1B stone, which has a maximum 3/4" aggregate. The standard mix uses a maximum 1-1/2" aggregate (2B), but the tight clearances within the beam specimens necessitated a smaller maximum aggregate size. Table C-1 contains the mix design proportions for the PennDOT Class A provided by Centre Concrete. The pozzolan used in the mix was GranCem, a ground granulated blast-furnace slag manufactured by Holcim.

Table C-1: PennDOT Class A Mix Design Proportions Per Cubic Yard

Type I Cement	367 lb.
Pozzolan (GranCem)	197 lb.
1B Stone (max. 3/4")	1760 lb.
Sand (Type A)	1336 lb.
Water	252 lb.
Air-Entraining Admixture (BASF MBVR)	8 fl. oz.
Water-Reducing Admixture (BASF Glenium 3030)	18 fl. oz.

In addition to the quality control and volume available, the use of a ready-mix supplier also helped in placement of the concrete. The front-end discharge trucks used by Centre Concrete were able to enter the lab and pull up adjacent to the forms. Consequently, placement of the concrete was directly from the truck's chute into the formwork. During placement, the crew used hand-held vibrators to compact the concrete and remove any voids. Even with the complex and congested formwork, there were no voids or honeycombing observed in the finished specimens. The final placement step involved screeding the concrete to the level of the top of the forms. The concrete was bullfloated and then, after evaporation of the bleed-water, trowel finished.

All specimens were moist cured for seven days. The curing consisted of leaving the specimens in the formwork, covering the top surface with wet burlap, and encasing everything in sheets of plastic. The burlap was periodically re-wetted to maintain the moisture lost due to evaporation. The concrete surface temperature reached a maximum of 105° Fahrenheit for concrete placed during the summer. In the winter, the lowest surface temperature recorded was 60° Fahrenheit. The room containing the specimen formwork was not heated or air-conditioned.

C.5 Prestressing Strand Stressing Operation

VSL provided a multi-strand stressing jack for prestressing the beam specimen tendons. The jack included an electric pump and calibrated pressure gauges to monitor the overall force in the tendon. The procedure for stressing the tendon consisted of the following:

1. Thread the required number of strands through one of the anchor heads and install the two-part wedges. This anchorage served as the dead end.
2. Wrap the far end of the tendon in duct tape to facilitate threading through the prestressing duct.
3. Thread the tendon through the prestressing duct.
4. Remove the duct tape and thread the individual strands through one of the anchor heads, carefully lining up corresponding strands at the far end.
5. Place the two-part wedges on the strands and snug fit the tendon and anchor head assemblies.

6. Install a retainer plate over the tendon at the live end. The retainer plate allowed the wedges to pull out slightly during stressing.
7. Using a gantry crane, place the jack over the tendons.
8. Record the strains in the vibrating wire gauges attached to the beam specimens.
9. Begin the stressing operation by placing a small amount of force on the tendon to tightly seat the wedges at the dead end.
10. Stress the tendons to the full jacking force and record the value.
11. Record the strains in the vibrating wire gauges attached to the beam specimens.
12. Remove the jacking force and allow the live end wedges to seat in the anchor head.
13. Record the strains in the vibrating wire gauges attached to the beam specimens.
14. Remove the jack, and if everything looks sound, cut the strand tails with an abrasive grinder in preparation for grouting.

The setup for the tendon stressing operation is shown in Figure C-5. All beam specimens were tensioned at 28 days after casting.

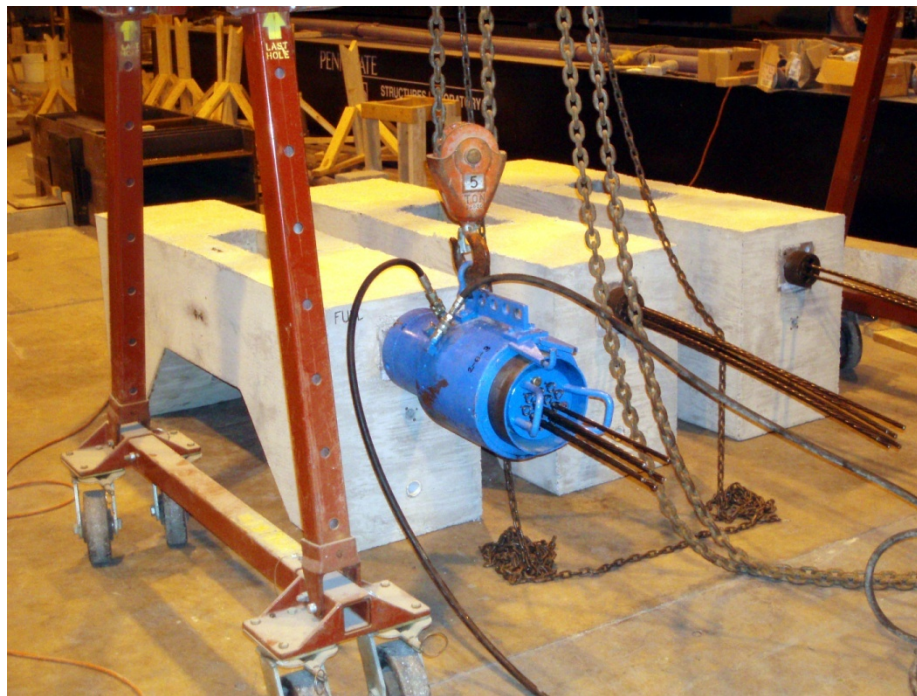


Figure C-5: Prestressing Tendon Stressing Operation

C.6 Tendon Grouting

Grouting of the tendons was performed in accordance with the Post-Tensioning Institute's Guide Specification for Grouting of Post-Tensioned Structures (2003). All grouting was completed within 24 hours of the stressing operation. The author chose SikaGrout 300 PT, manufactured by Sika Corporation, to grout the tendons. SikaGrout 300 PT is a high-performance, sand-free, prepackaged, cementitious grout for post-tensioning applications. The author chose a high-performance prepackaged grout to reduce the potential for any unplanned grouting defects such as bleed lenses. Due to the relatively small rise in the duct at the crown, intermediate grout vents were not required, and grout-

ing was performed using grout tubes at both ends of the duct. VSL supplied the temporary anchor head grout caps, plastic grout tubing, and mechanical shutoffs. A photograph of the tendon grouting setup is shown in Figure C-6.



Figure C-6: Tendon Grouting Setup

After installation of the grouting attachments, the procedure for grouting the tendon consisted of the following:

1. Measure the recommended amount of water for the prepackaged grout.
2. Open both shutoffs attached to the grout tubes at each end of the tendon.
3. Using an electric drill and paddle mixer, mix two 50-lb bags of SikaGrout 300 PT in two five gallon buckets according to the manufacturer's recommendations.
4. Place the grout in the holding chamber of the hand-operated, positive-displacement pump.
5. Begin pumping grout into the duct.

6. Plug the vent holes in the temporary anchor head grout caps once consistent flow appears.
7. Close mechanical shutoff in far end grout tube once consistent flow appears.
8. Close mechanical shutoff in near end grout tube.

Subsequent removal of the ducts and tendons during the testing and autopsy revealed excellent coverage of the grout within the tendons.

The only variation from the grouting procedure discussed above involved the two series that had anchor zone grout void imperfections. These specimens were placed vertically and grouted from the bottom up. This procedure allowed the author to stop the grout approximately 1” short of the anchor head, thus leaving the desired grout imperfection. A photograph of this setup is shown in Figure C-7.

C.7 Prestressing Bar Stressing Operation

The prestressing bar extended between the corbels located at each end of the beam. When the bar was tensioned, it provided a uniform moment to the beam cross-section. This force was calculated to provide the full dead and live load moment to the beam specimens as part of the durability study.

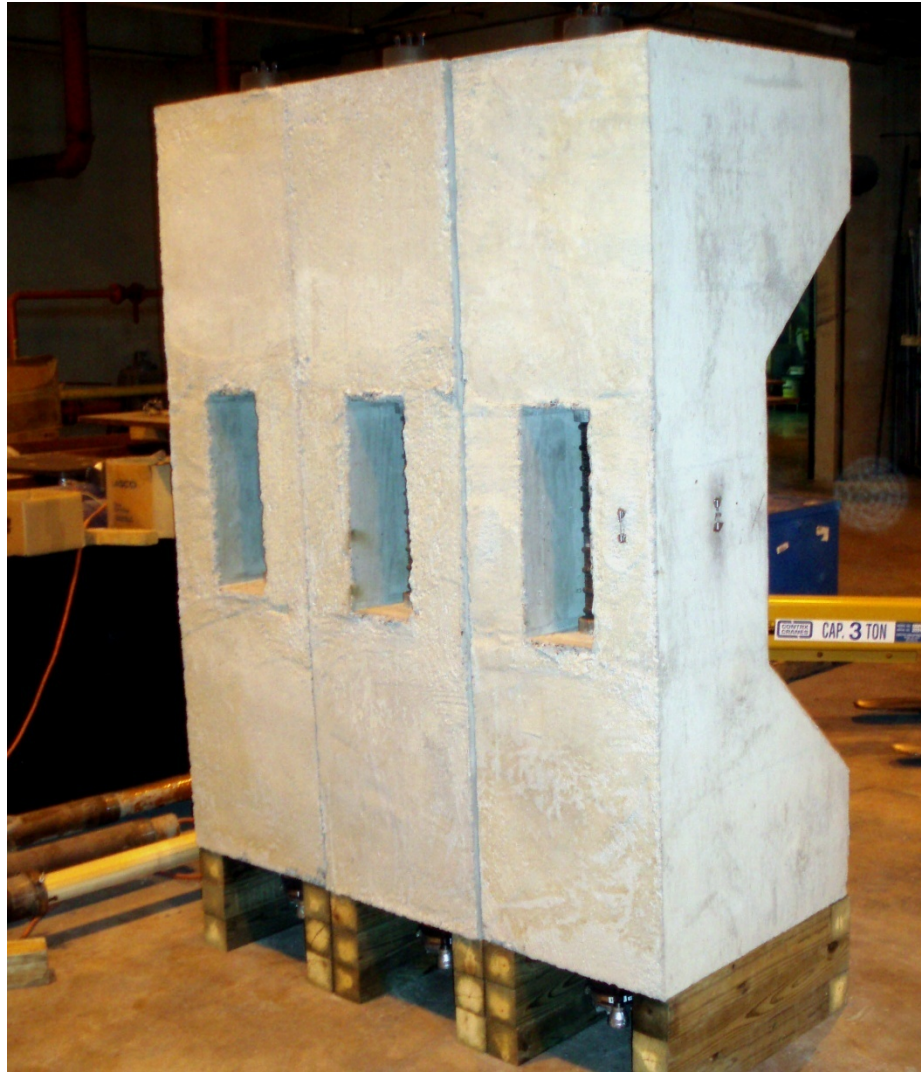


Figure C-7: Grouting Setup for Anchor Zone Grout Void

Stressing of the prestressing bar was accomplished with a 60-ton, through-hole, hydraulic ram. The procedure for stressing the bar consisted of the following:

1. Place the two halves of the prestressing bar through the 2-inch-diameter PVC tubing inserts in the beam specimens.
2. Install an instrumented coupler between the two halves of the prestressing bar.

3. Install the bearing plates and spherical hex nuts at each end of the prestressing bar.
4. Record the strain in the vibrating wire gauge attached to the coupler.
5. Install a temporary coupler and 3' section of prestressing bar at the live end of the prestressing bar.
6. Install bearing plates, two concrete blocks, and a 2-inch-thick support plate at the live end.
7. Install the hydraulic ram, bearing plate, and spherical nut.
8. Tension the prestressing bar with the hydraulic ram at increments of 10 kips, and record the corresponding strains in the vibrating wire gauge attached to the coupler.
9. After reaching the desired prestressing bar force, tighten the spherical hex nut at the live end.
10. Remove the jacking force.
11. Record the strain in the vibrating wire gauge attached to the coupler.
12. If required, retension the prestressing bar to adjust for any seating losses.

Based on subsequent tensioning operations, it was found that there was very little seating loss due to the spherical hex nut configuration used to anchor the prestressing bar. A photograph of the prestressing bar stressing setup is shown in Figure C-8. A photograph of three finished specimens is shown in Figure C-9.



Figure C-8: Prestressing Bar Stressing Setup



Figure C-9: Set of Three Specimens After Stressing of Post-Tensioning Bar

C.8 Beam Specimen Material Property Testing

Both the concrete and grout were tested to verify the material properties of these constituents. The results of the testing are contained in the following section.

C.8.1 Concrete Testing

The author tested the concrete for slump, compressive strength, and modulus of elasticity for each of the four batches used during the construction of the beam specimens. Each of the four batches measured 2-1/2 cubic yards. Slump of the concrete was determined in accordance with ASTM C143-08, Standard Test Method for Slump of Hydraulic-Cement Concrete (ASTM C143 2008). Compressive strength of the concrete was determined in accordance with ASTM C39-05, Standard Test Method for Compressive Strength of Cylindrical Concrete Specimens (ASTM C39 2005). Modulus of elasticity of the concrete was determined in accordance with ASTM C469-02, Standard Test Method for Static Modulus of Elasticity and Poisson's Ratio of Concrete in Compression (ASTM C469 2002). Results of the testing are shown in Table C-2. Note that the actual compressive strengths came very close to the target compressive strength of 4,000 psi. In addition to the tested value for modulus of elasticity, the table contains the calculated value based on the ACI-recommended equation and the average value from the compressive strength tests.

Table C-2: Concrete Material Properties

Series	Slump (in.)	28-Day Compressive Strength (psi)		Modulus of Elasticity (psi)	
		Test Value	Average	Test Value	$57000\sqrt{f'_c}$
Fatigue Reference	3-1/2	3760 3965 4228	3984	3,514,000	3,598,000
Anchor Zone Grout Void	4	4270 3850 4133	4084	3,727,000	3,643,000
Anchor Zone Grout Void with Corrosion	4	4413 4030 4441	4295	3,805,000	3,736,000
Crown Grout Void with Corrosion	3-1/2	3948 3908 3870	3909	3,453,000	3,564,000

C.8.2 Grout Testing

The critical properties for post-tensioning grout are flowability, bleed resistance, reduced shrinkage, and ability to protect the strand through a high-pH environment by completely filling the duct (PTI Guide Specification 2003). Compressive strength is usually not a critical property provided the strength meets or exceeds the surrounding concrete strength, which it usually does. In this study, testing of the compressive strength of the grout was a quality control measure. As such, the grout was tested for compressive

strength at seven days. Compressive strength of the grout was determined in accordance with ASTM C109-07, Standard Test Method for Compressive Strength of Hydraulic Cement Mortars (Using 2-in. Cube Specimens) (ASTM C109 2007). Results of the testing are shown in Table C-3.

Table C-3: Post-Tensioning Grout 7-Day Compressive Strengths

Series	7-Day Compressive Strength (psi)	
	Test Value	Average
Fatigue Reference	6010 5765 5593	5789
Anchor Zone Grout Void	6332 6770 6147	6416
Anchor Zone Grout Void with Corrosion	5373 5034 4990	5132
Crown Grout Void with Corrosion	4749 4058 4110	4306

These results are consistent with the strength gains reported by the manufacturer and indicate that the material was mixed to the proper proportions. Visual observations

of the grout placement and subsequent forensic analyses indicated that the grout performed in accordance with the manufacturer's specifications.

Appendix D

Vibrating Wire Strain Gauges

This appendix discusses the particular vibrating wire strain gauges chosen, verification of their acceptability, and “calibration” data for the prestressing bar couplers that act as “load cells.”

The choice of vibrating wire strain gauges was based on many factors. First, vibrating wire strain gauges have a history of long-term reliability (*e.g.*, Barr *et al.* 2005, Burns *et al.* 1997). Due to the length of time required for the durability portion of the study, the gauges must remain stable for a period of six to nine months. Second, vibrating wire strain gauges have a history of successful use with reinforced and prestressed concrete (Burns *et al.* 1997). Third, due to the particular specimen design, only axial strains occurred within the concrete beam. Thus, a strain rosette was not required as these were the principal strains experienced by the specimens. Lastly, vibrating wire strain gauges offer simplicity of use and thus a decreased potential for error. The author chose Geokon Model 4150 vibrating wire strain gauges for the strain measurements.

The author verified the acceptability of the Geokon Model 4150 vibrating wire strain gauges by comparing measured versus calculated strains on standard 6”x12” cylinders of the same mix design used for the full-scale beam specimens. The calculated strains were based on the calculated stresses imposed by the cylinder test machine converted to strains through the modulus of elasticity measured for the particular concrete placement (see Section C.8.1). Figures D-1 and D-2 are plots of measured strains versus

calculated strains for the test cylinders. Compared to a one-to-one relationship, which would indicate a perfect correlation, the strains have R^2 values of 0.989 and 0.983 for Figures D-1 and D-2, respectively. Therefore, the measured strains compared very well with the calculated strains and confirmed the accuracy of the strain gauges chosen.

The load versus strain data for the coupler “load cells” are shown in Figures D-3 through D-6.

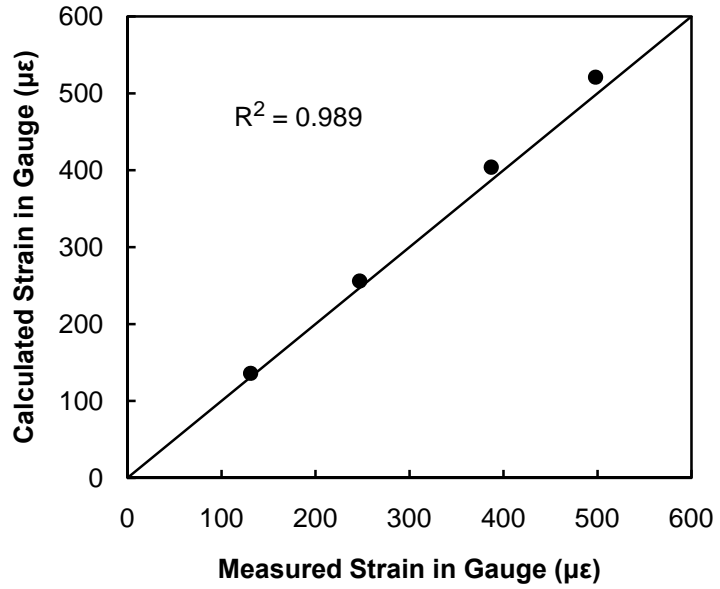


Figure D-1: Measured versus Calculated Concrete Strains for a Standard 6''x12'' Cylinder

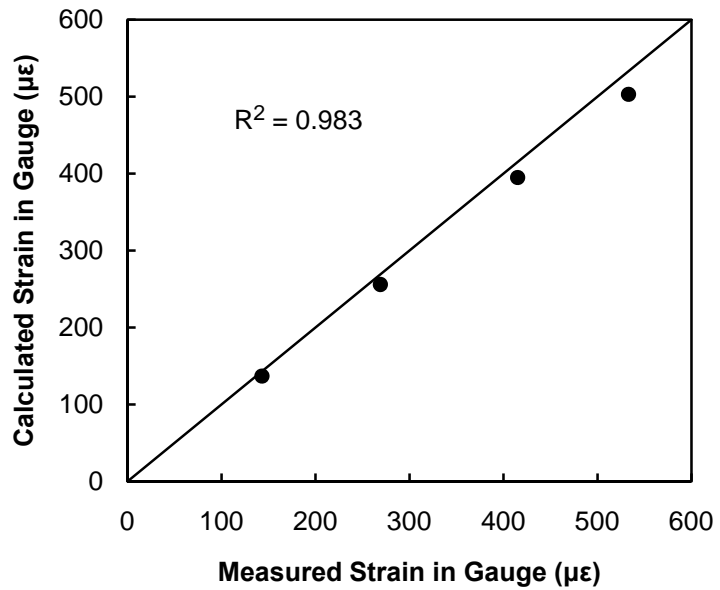


Figure D-2: Measured versus Calculated Concrete Strains for a Standard 6''x12'' Cylinder

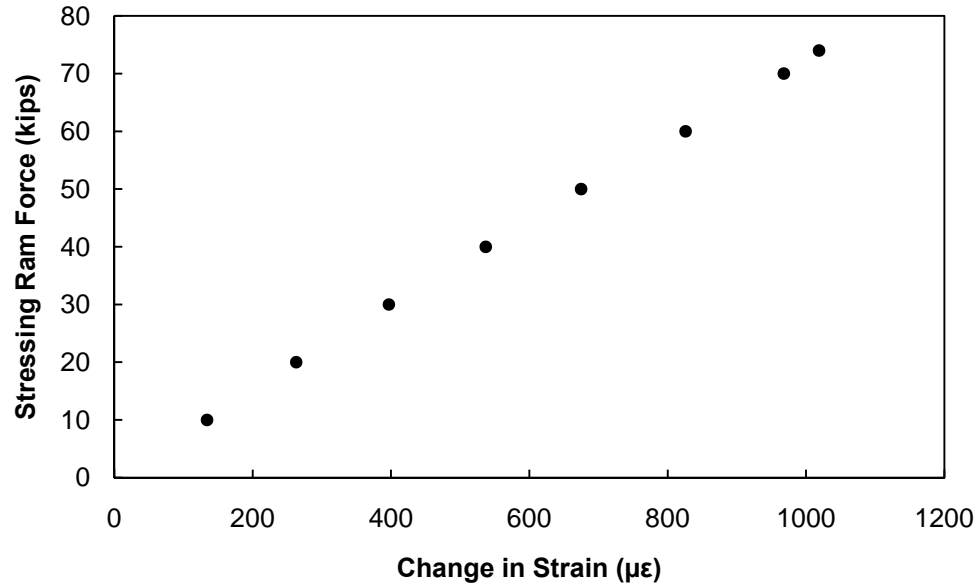


Figure D-3: Coupler Load-Strain Data for Fatigue Reference Series

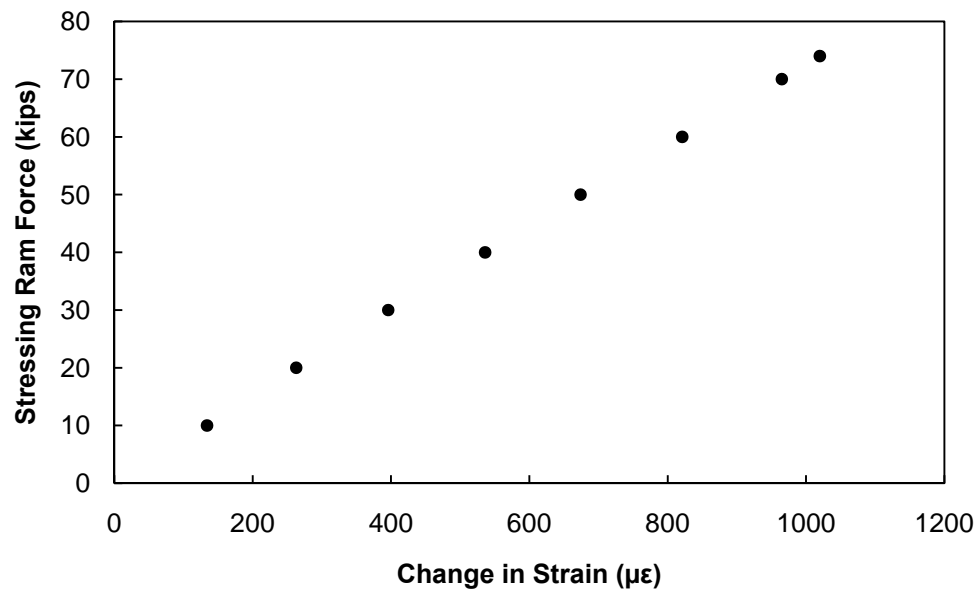


Figure D-4: Coupler Load-Strain Data for Anchor Zone Grout Void Series

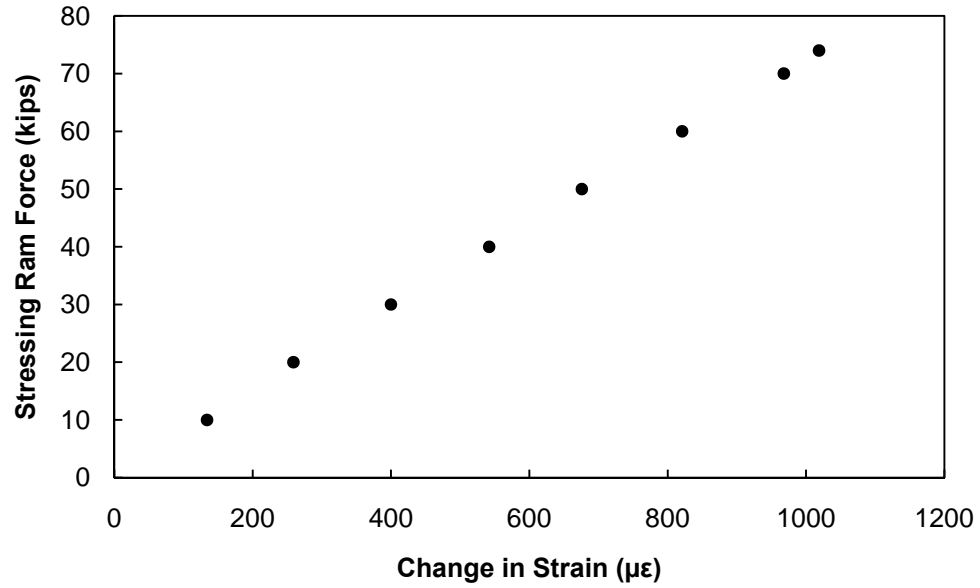


Figure D-5: Coupler Load-Strain Data for Anchor Zone Grout Void Corrosion Series

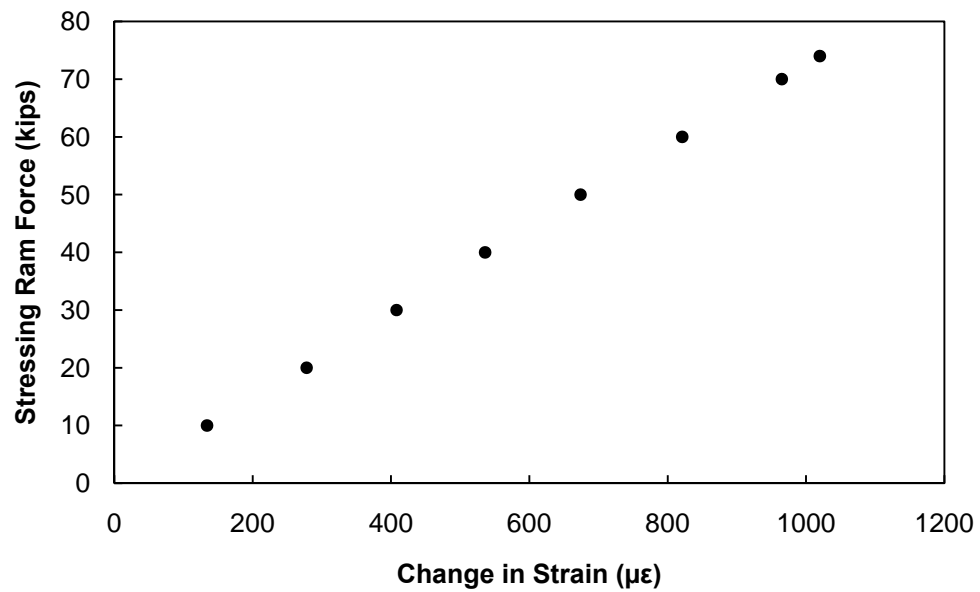


Figure D-6: Coupler Load-Strain Data for Crown Grout Void Corrosion Series

Appendix E

Calculated and Measured Concrete Strains

This appendix contains the calculated and measured concrete strains during the beam specimen jacking operation. The calculated strains were based on the calculated stresses imposed by the jacking force converted to strains through the modulus of elasticity measured for the particular concrete placement (see Section C.8.1). The strain gauge locations are shown in Figure 4-9. Only the fully prestressed specimens in each series were instrumented, as discussed in Chapter 5.

Table E-1: Calculated and Measured Concrete Strains for Beam Specimen FR-1

Gauge No.	Strain ($\mu\epsilon$)	
	Calculated	Measured
1	538	549
2	269	233
3	25	12

Table E-2: Calculated and Measured Concrete Strains for Beam Specimen AZ-1

Gauge No.	Strain ($\mu\epsilon$)	
	Calculated	Measured
1	521	556
2	261	289
3	24	41

Table E-3: Calculated and Measured Concrete Strains for Beam Specimen AZC-1

Gauge No.	Strain ($\mu\epsilon$)	
	Calculated	Measured
1	517	539
2	258	226
3	24	33

Table E-4: Calculated and Measured Concrete Strains for Beam Specimen GVC-1

Gauge No.	Strain ($\mu\epsilon$)	
	Calculated	Measured
1	569	518
2	285	222
3	26	13

Appendix F

Longitudinal Cracking Finite Element Analysis

All of the fully prestressed beams and six of the eight partially prestressed beams suffered longitudinal cracking along the top of the specimens near the anchor head and at the opening in the center region of the beam. The author initially noticed this cracking during an examination of the Fatigue Reference Series following fatigue testing. However, subsequent inspections of the remaining specimens revealed that the cracking occurred after post-tensioning but before the fatigue testing. Consequently, it was speculated that the cause of the cracking must be related to the strand stressing operation and be due to bursting stresses near the anchor head and dispersion forces near the “bathtub” region. To investigate the cause further, the author performed a finite element analysis of the beam specimens under the loading caused by the jacking force. Due to the use of a multi-strand stressing jack, the beams experience the full jacking force at the location of each end anchorage during the stressing operation.

The purpose of the finite element model was to evaluate the elastic stresses caused by the jacking force prior to cracking in the concrete. Consequently, the author modeled the concrete with a linear stress-strain relationship and ignored the affect of the mild steel within the beams. The duct and deviator were modeled as cylindrical- and torus-shaped voids in the concrete, respectively, and followed the same profile as the actual specimens. The author chose the ANSYS[®] Academic Research Product, v. 11.0 (ANSYS), as the finite element package to perform the numerical simulation.

The finite element model is shown in Figure F-1. Due to symmetry, the author constructed only a quarter-model of the beam specimen. Along the two planes of symmetry, the boundary conditions allowed displacement parallel to the plane but restricted displacement perpendicular to the plane. To complete the boundary conditions, displacement was restricted in the y-direction along the bottom edge of the corbel. Loading was applied as a pressure over the same area as the stressing jack, with the centroid located to coincide with the actual anchor head location.

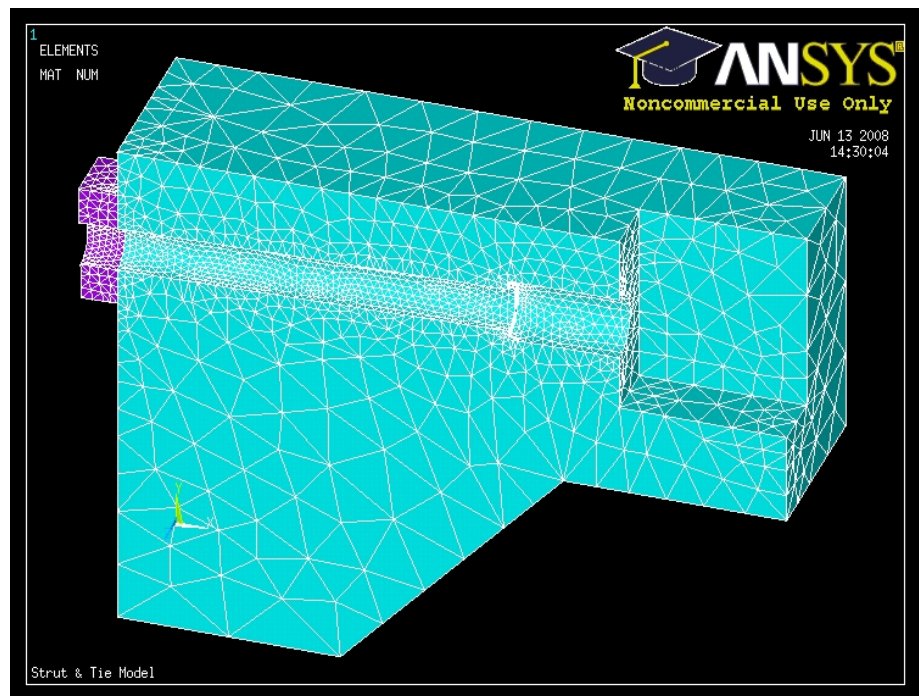


Figure F-1: Finite Element Model for Longitudinal Cracking

The basic element used in the model was a higher-order, three-dimensional, 20-node, hexahedral, solid element that exhibits quadratic displacement behavior. This element, referred to as SOLID186 by the ANSYS program, is well suited to modeling irregular geometries (ANSYS 2007), such as those that occur with the beam specimens. As

shown in Figure F-1, an irregular mesh geometry resulted from the cylindrical- and torus-shaped voids in the concrete used to model the strand duct and deviator, particularly since the duct was sloped between the beam end and the “bathtub” region. Furthermore, SOLID186 degrades to a 10-node tetrahedral element during auto-meshing in order to maintain proper element geometry, further accommodating irregular geometries (ANSYS 2007). The author generated the initial mesh through a controlled auto-meshing process. After an initial analysis, a mesh refinement procedure was followed at locations of coarse stress distributions and/or high stress gradients.

Results of the analysis of the model for the jacking force are shown in Figure F-2, and a corresponding photograph of the longitudinal cracking for one of the beam specimen is shown in Figure F-3. Figure F-2 is a plot of stresses perpendicular to the longitudinal plane of the beam, with the red areas indicating tensile stresses ranging from 300 to 1000 psi. The uniaxial tensile strength of concrete is approximately equal to $5\sqrt{f'_c}$ (Neville 1995), which translates into a tensile strength of 316 psi for concrete with a compressive strength of 4000 psi. (As shown in Appendix B, the compressive strengths for the beam specimens ranged from 3984 to 4295 psi.) Consequently, the areas in red would be expected to crack during application of the jacking force while stressing the strands, particularly for the fully prestressed designs, and these areas coincide directly where the cracking actually occurred.

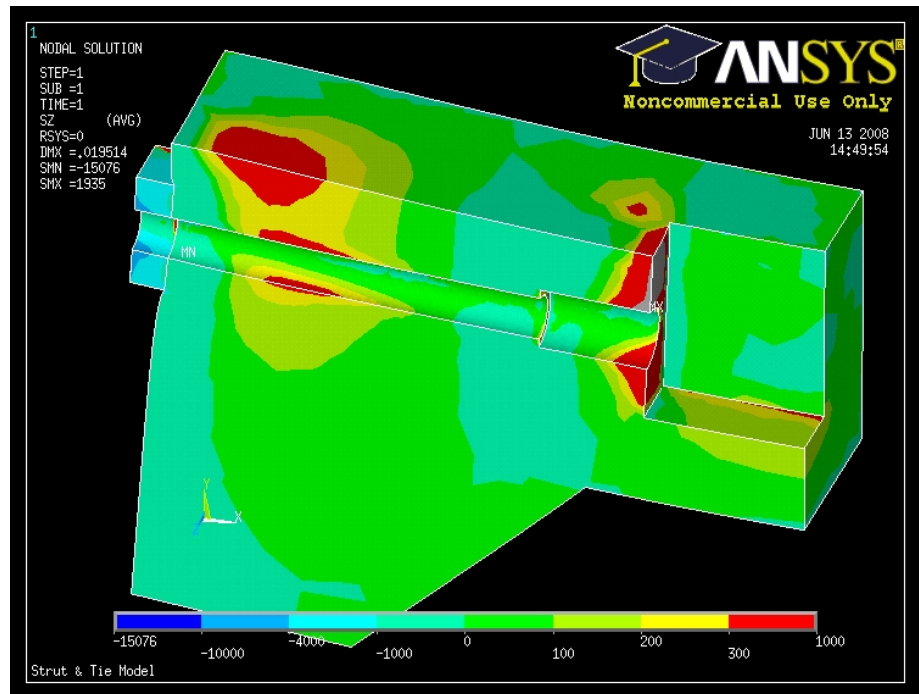


Figure F-2: Stresses Perpendicular to Longitudinal Plane During Jacking



Figure F-3: Typical Longitudinal Cracking of Beam Specimens

The finite element analysis confirmed the hypothesis as to the likely cause of the longitudinal cracking. The high tensile stresses near the end anchorage are bursting stresses caused by the high compressive force from the stressing jack. The reinforcing spiral installed at this location was meant to carry these forces, provide confinement, and prevent failure of the local zone. The end anchorage location was pushed to the edge distance limits imposed by the manufacturer, which increased the bursting stresses well above the tension capacity of the concrete.

The high tensile stresses near the opening in the center region are caused by dispersion of the high compressive force from the stressing jack. The researchers designed the general zone as a strut-and-tie to resist these forces (see Section 4.3.2). Following recommended guidelines for the slope of the compressive strut, the tie forces should have been located approximately 14 inches from the end of the beam, which is about halfway between the end of the beam and the opening. However, the opening disturbed the flow of forces, resulting in a shift of the elastic stresses. Usually, a discontinuity is critical because it can shorten the dispersion zone, causing a corresponding increase in the tie forces (AASHTO 2008). However, in this case, the opening elongated the dispersion zone, shifting the high tensile elastic stresses and causing the beams to crack near the openings. The benefit of reinforced concrete is that the forces find their way to the reinforcing through redistribution after the concrete cracks.

It is nonetheless important to point out two issues with regard to the cracking. First, all of the fully prestressed beams and six of the eight partially prestressed beams suffered longitudinal cracking, at least cracking visible to the unaided eye. This result is consistent with the fact that the jacking force for the partially prestressed beams was only

two-thirds of the force for the fully prestressed beams, so the tensile stresses for the partially prestressed beams are two-thirds of those shown in Figure F-2. Second, cracking will often occur in the anchorage zone of post-tensioned concrete members, even fully post-tensioned concrete members. Both bursting forces and dispersion forces occur due to the method of applying the prestressing force through an end anchorage, and there is no prestressing force in the direction of these resulting tensile stresses. This cracking can impair the durability of a post-tensioned concrete member.

Appendix G

Beam Specimen Crack Maps and Crack Width Measurements

This appendix contains detailed crack maps and crack width measurements for each beam specimen. The crack maps are shown in Figures G-1 through G-12, with the corresponding crack widths shown in Tables G-1 through G-4. Crack width measurements were taken with a crack scope – a 60-magnification microscope with an inscribed scale on the lens. Initial crack width measurements were taken within the first 100,000 cycles, with final crack width measurements taken within the last 100,000 cycles. Crack width measurements were taken at two locations along each crack at the top surface of the beam. Crack width measurements for the GVC Series were less precise, as it was difficult to remove all of the build-up in and around the cracks from the exposure testing. In general, the flexural crack widths increased during the fatigue loading. Some researchers have attributed this increase to creep, while others have attributed it to continued micro-cracking occurring over time (ACI 423.5R 1999).

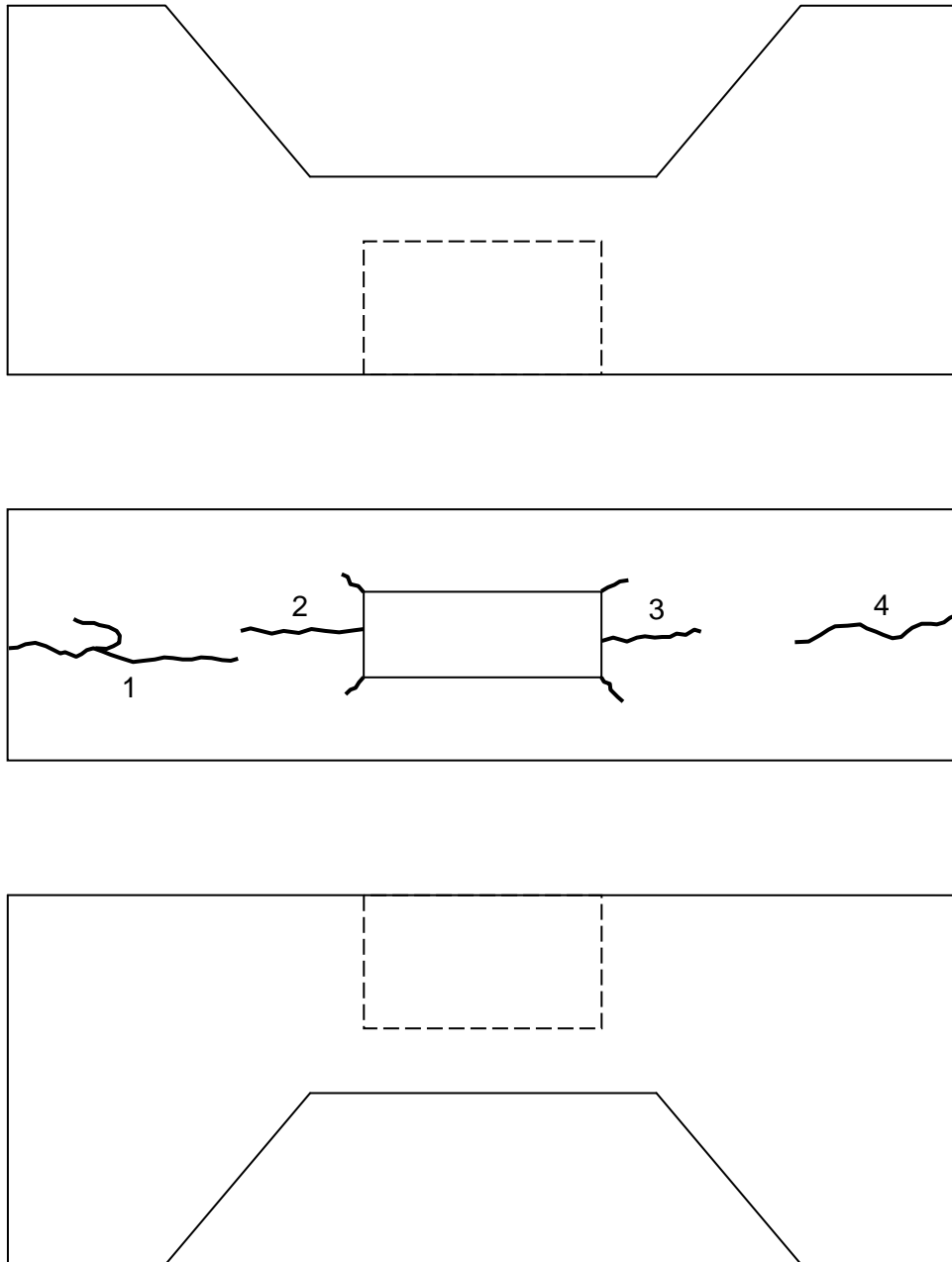


Figure G-1: Beam Specimen FR-1 Crack Map

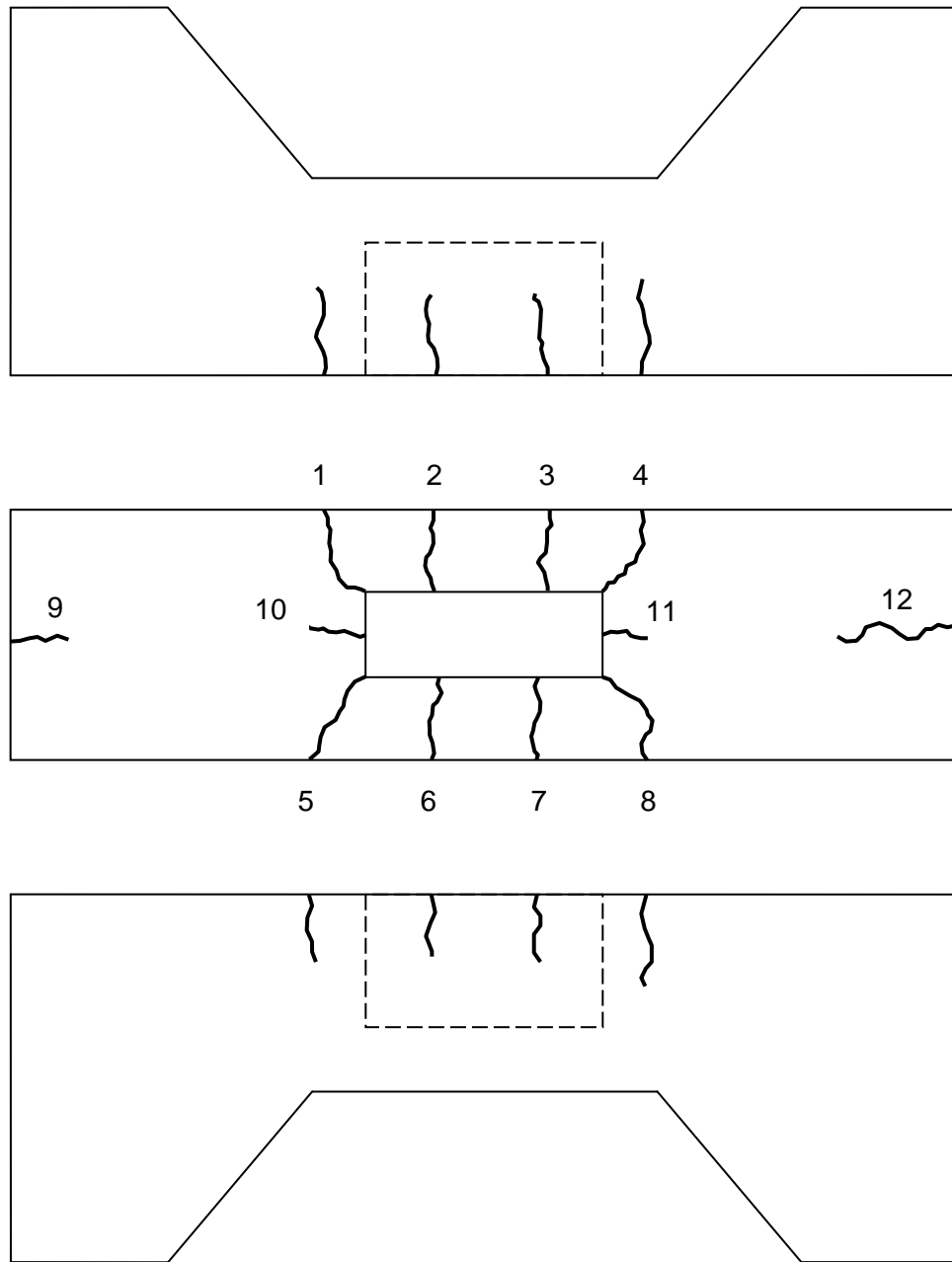


Figure G-2: Beam Specimen FR-2 Crack Map

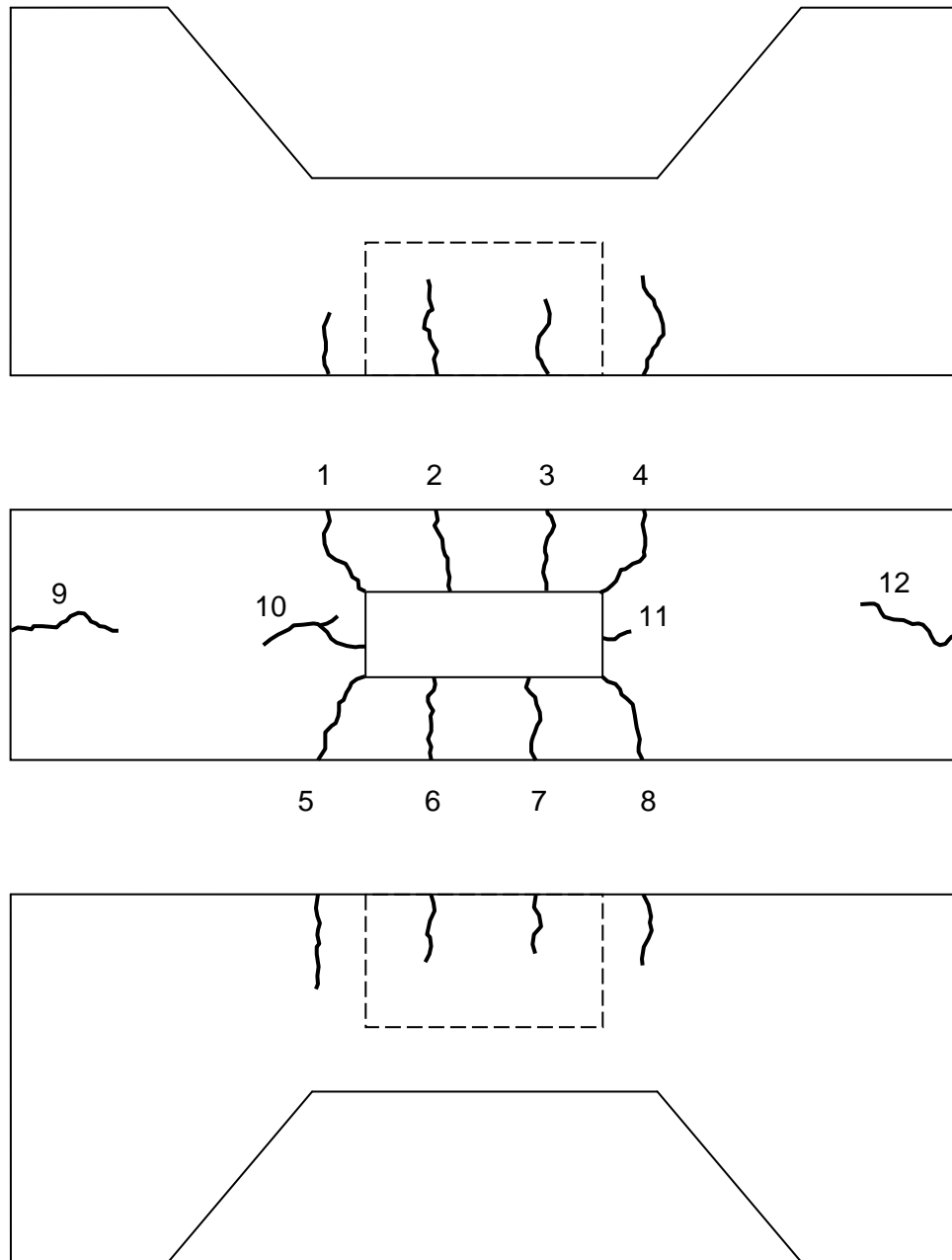


Figure G-3: Beam Specimen FR-3 Crack Map

Table G-1: Crack Widths for Fatigue Reference Series

Specimen	Crack Number	Initial Crack Width (in.)		Final Crack Width (in.)	
FR-1	1	0.004	0.004	0.004	0.004
	2	0.003	0.007	0.003	0.007
	3	0.005	0.003	0.005	0.003
	4	0.004	0.003	0.004	0.003
FR-2	1	0.006	0.006	0.007	0.008
	2	0.007	0.008	0.008	0.008
	3	0.008	0.008	0.010	0.009
	4	0.008	0.008	0.009	0.009
	5	0.006	0.006	0.006	0.007
	6	0.008	0.007	0.010	0.009
	7	0.009	0.008	0.011	0.010
	8	0.009	0.008	0.010	0.010
	9	0.002	0.002	0.002	0.002
	10	0.001	0.001	0.001	0.001
	11	0.001	0.001	0.001	0.001
	12	0.002	0.001	0.002	0.001
FR-3	1	0.007	0.007	0.008	0.009
	2	0.008	0.008	0.010	0.011
	3	0.007	0.007	0.009	0.009
	4	0.007	0.009	0.009	0.010
	5	0.007	0.007	0.009	0.008
	6	0.007	0.007	0.009	0.009
	7	0.008	0.007	0.010	0.009
	8	0.007	0.007	0.009	0.009
	9	0.002	0.002	0.002	0.002
	10	0.001	0.003	0.001	0.003
	11	0.001	0.001	0.001	0.001
	12	0.002	0.001	0.002	0.001

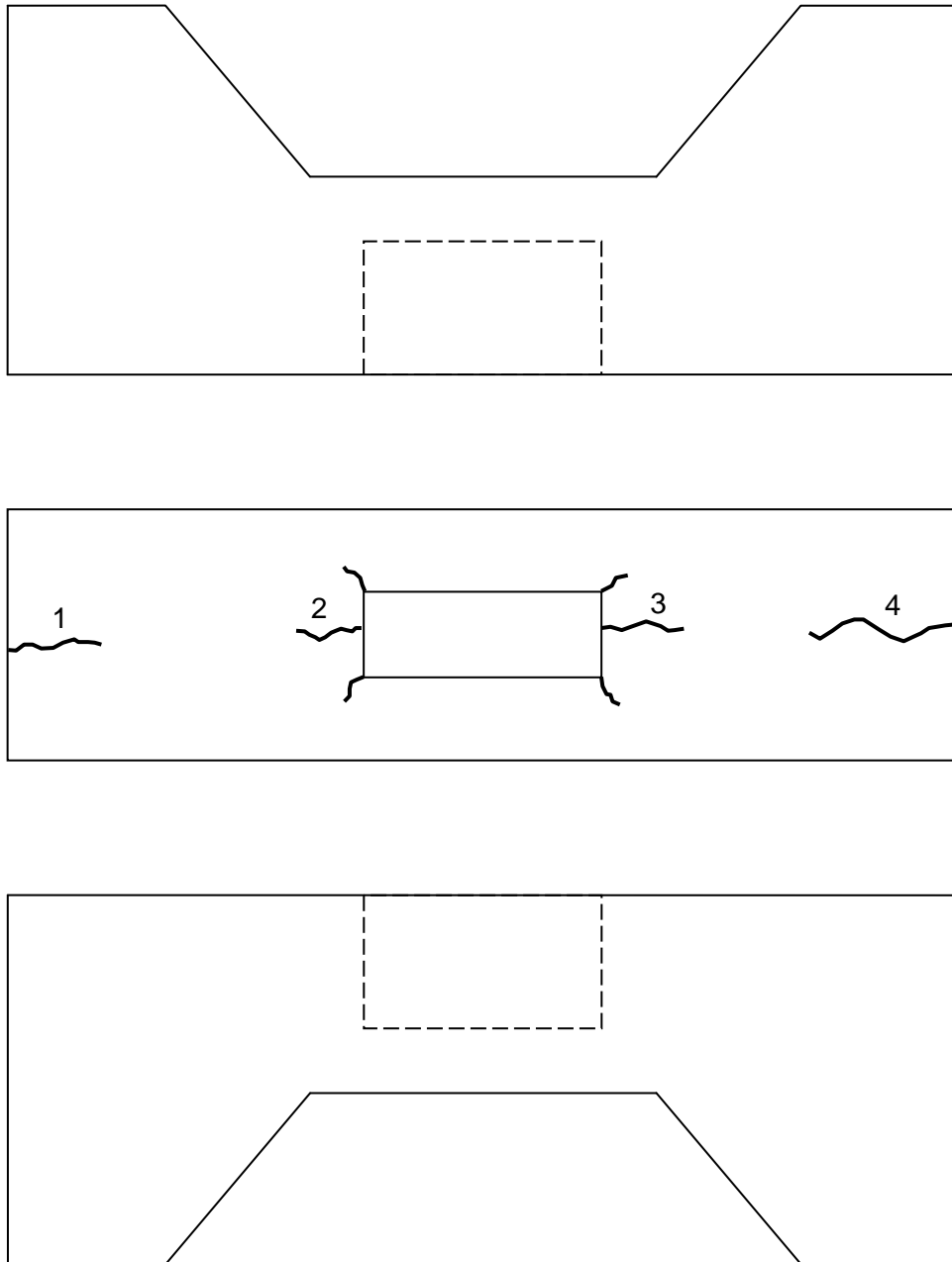


Figure G-4: Beam Specimen AZ-1 Crack Map

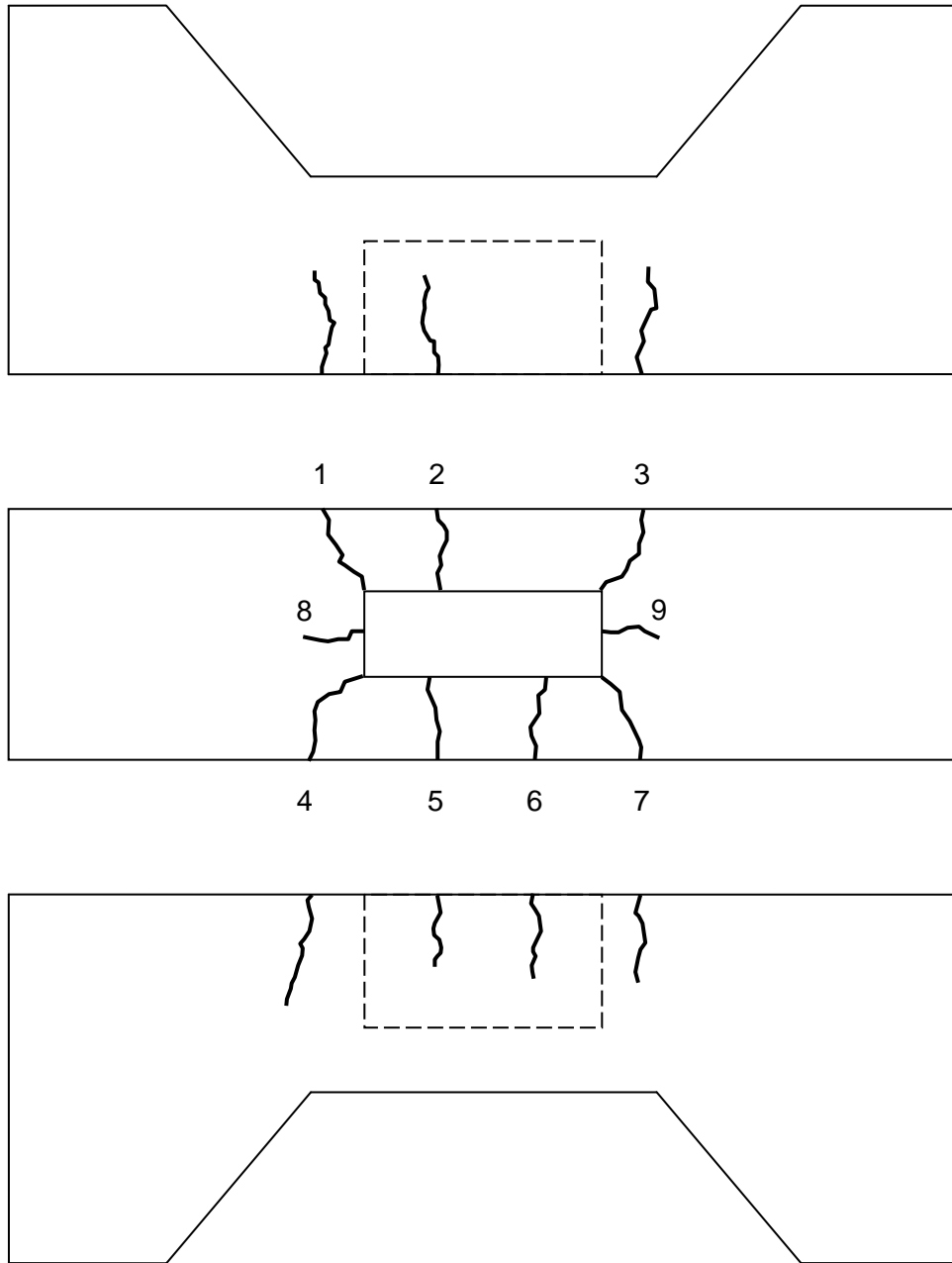


Figure G-5: Beam Specimen AZ-2 Crack Map

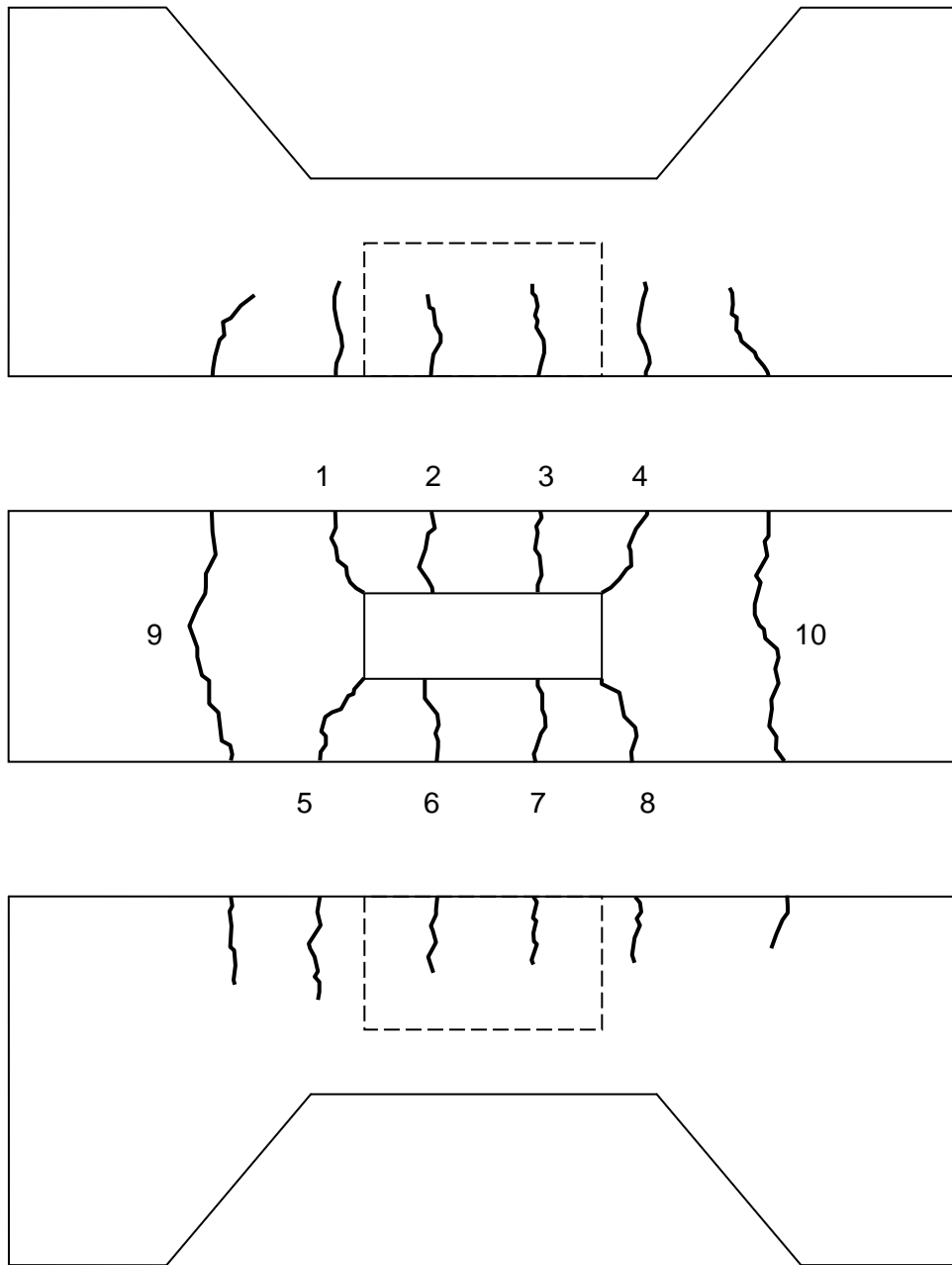


Figure G-6: Beam Specimen AZ-3 Crack Map

Table G-2: Crack Widths for Anchor Zone Grout Void Series

Specimen	Crack Number	Initial Crack Width (in.)		Final Crack Width (in.)	
AZ-1	1	0.004	0.004	0.004	0.004
	2	0.003	0.005	0.003	0.005
	3	0.006	0.005	0.006	0.005
	4	0.002	0.005	0.002	0.005
AZ-2	1	0.008	0.007	0.010	0.009
	2	0.011	0.009	0.014	0.012
	3	0.009	0.009	0.011	0.010
	4	0.005	0.005	0.006	0.007
	5	0.006	0.007	0.008	0.009
	6	0.006	0.007	0.007	0.007
	7	0.005	0.007	0.007	0.009
	8	0.001	0.002	0.001	0.002
	9	0.003	0.002	0.003	0.002
AZ-3	1	0.007	0.008	0.008	0.008
	2	0.009	0.010	0.010	0.011
	3	0.010	0.012	0.011	0.012
	4	0.010	0.011	0.012	0.013
	5	0.006	0.007	0.007	0.007
	6	0.011	0.009	0.013	0.012
	7	0.010	0.009	0.011	0.011
	8	0.010	0.010	0.011	0.012
	9	0.007	0.008	0.009	0.009
	10	0.008	0.008	0.009	0.010

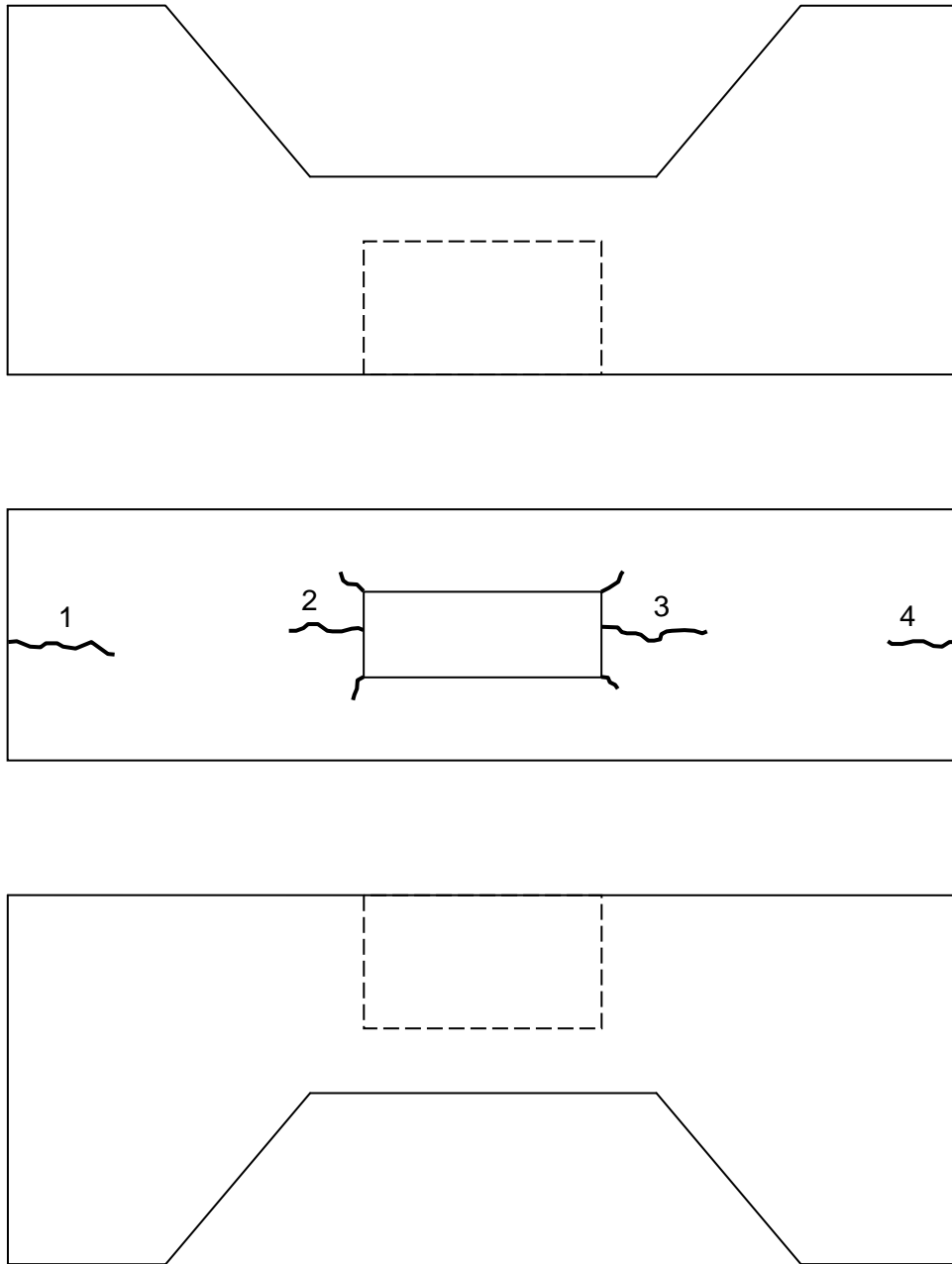


Figure G-7: Beam Specimen AZC-1 Crack Map

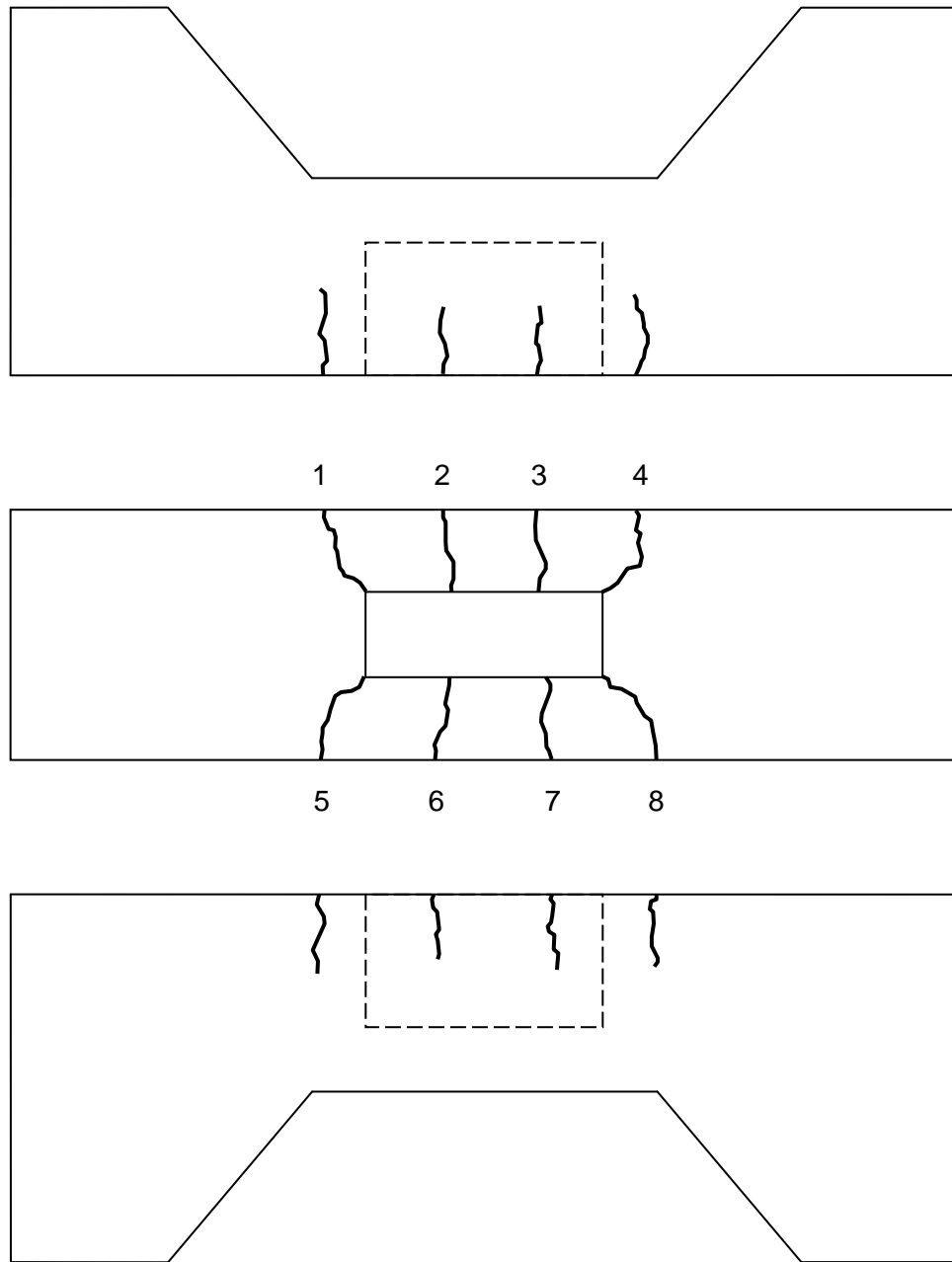


Figure G-8: Beam Specimen AZC-2 Crack Map

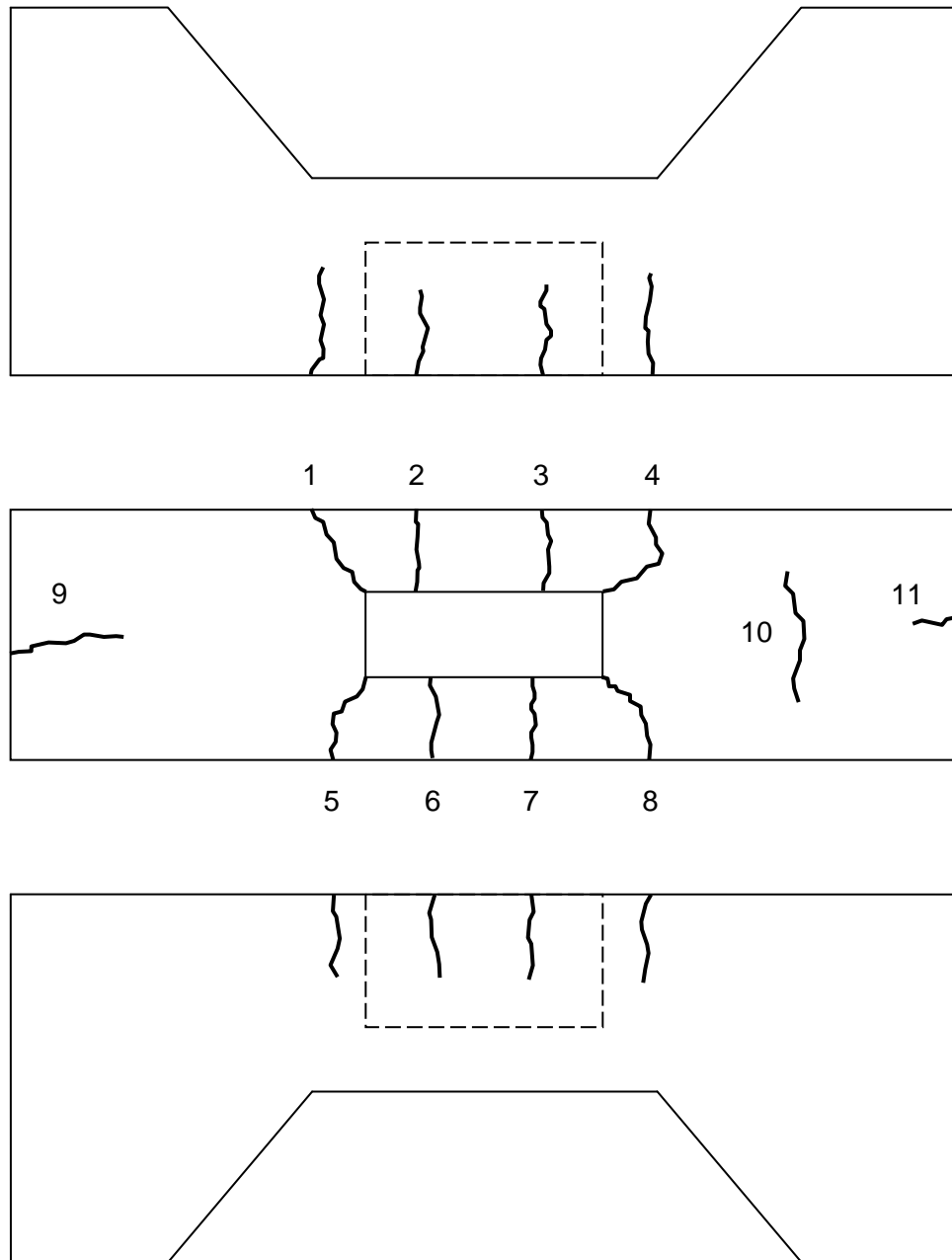


Figure G-9: Beam Specimen AZC-3 Crack Map

Table G-3: Crack Widths for Anchor Zone Grout Void Corrosion Series

Specimen	Crack Number	Initial Crack Width (in.)		Final Crack Width (in.)	
AZC-1	1	0.005	0.004	0.005	0.004
	2	0.006	0.007	0.006	0.007
	3	0.005	0.003	0.005	0.003
	4	0.003	0.003	0.003	0.003
AZC-2	1	0.008	0.007	0.010	0.009
	2	0.009	0.010	0.010	0.011
	3	0.009	0.008	0.012	0.011
	4	0.008	0.008	0.010	0.010
	5	0.008	0.006	0.010	0.008
	6	0.010	0.009	0.011	0.011
	7	0.009	0.008	0.010	0.011
	8	0.008	0.008	0.010	0.011
AZC-3	1	0.006	0.007	0.007	0.008
	2	0.008	0.008	0.009	0.009
	3	0.007	0.008	0.009	0.009
	4	0.007	0.009	0.009	0.010
	5	0.007	0.007	0.008	0.009
	6	0.007	0.006	0.009	0.007
	7	0.006	0.006	0.007	0.008
	8	0.007	0.007	0.009	0.009
	9	0.003	0.002	0.003	0.002
	10	0.006	0.006	0.006	0.006
	11	0.001	0.002	0.001	0.002

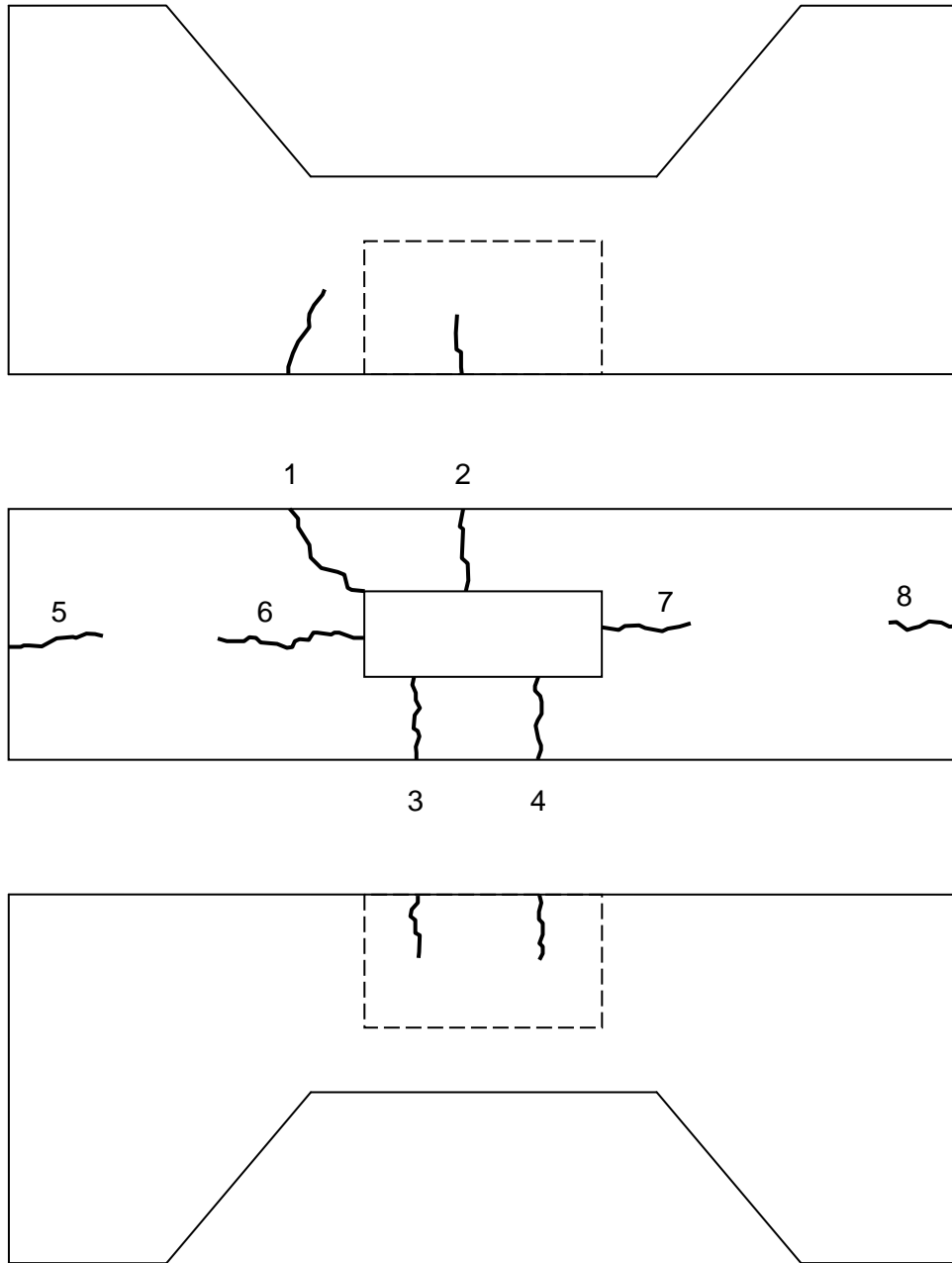


Figure G-10: Beam Specimen GVC-1 Crack Map

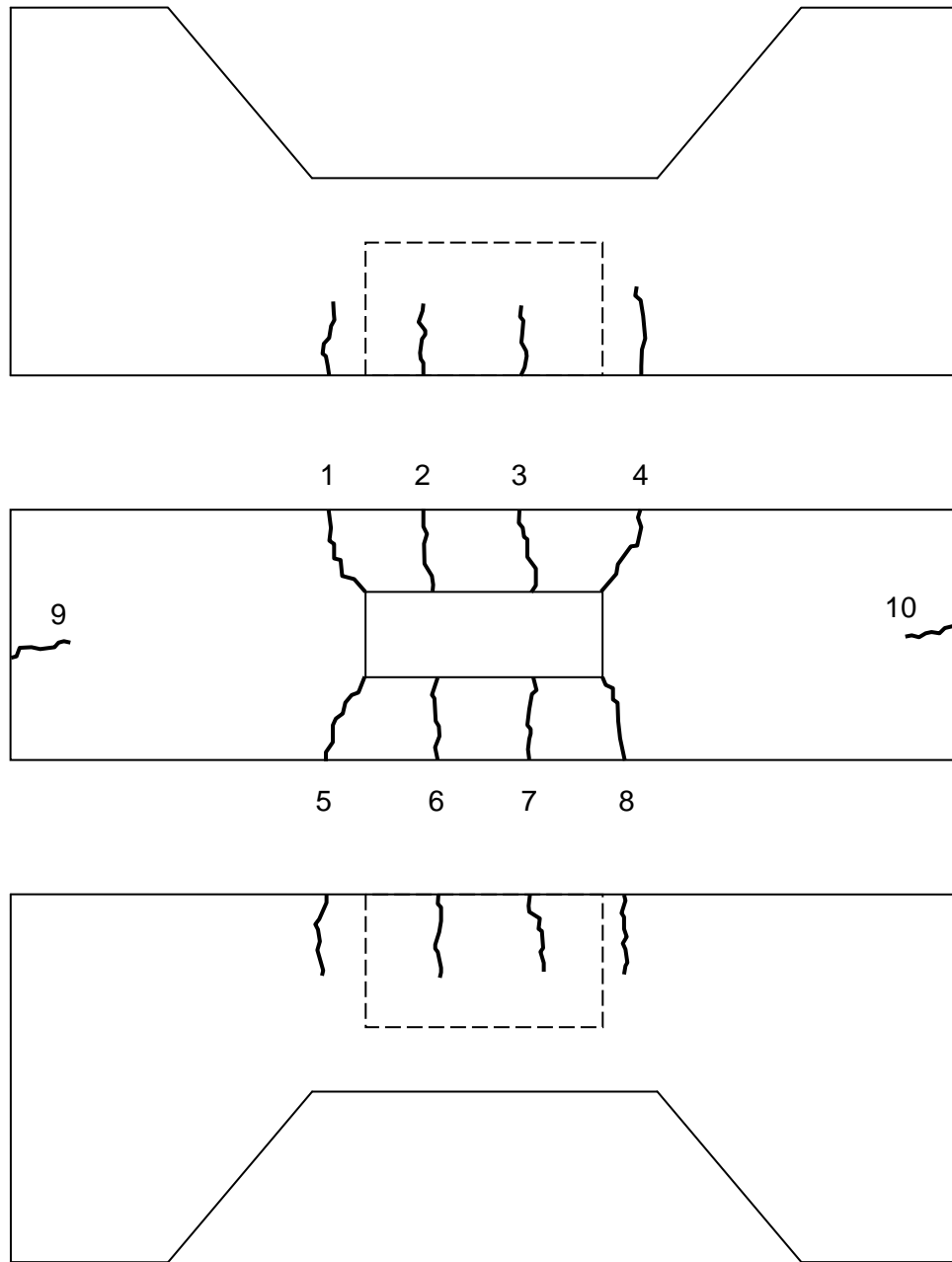


Figure G-11: Beam Specimen GVC-2 Crack Map

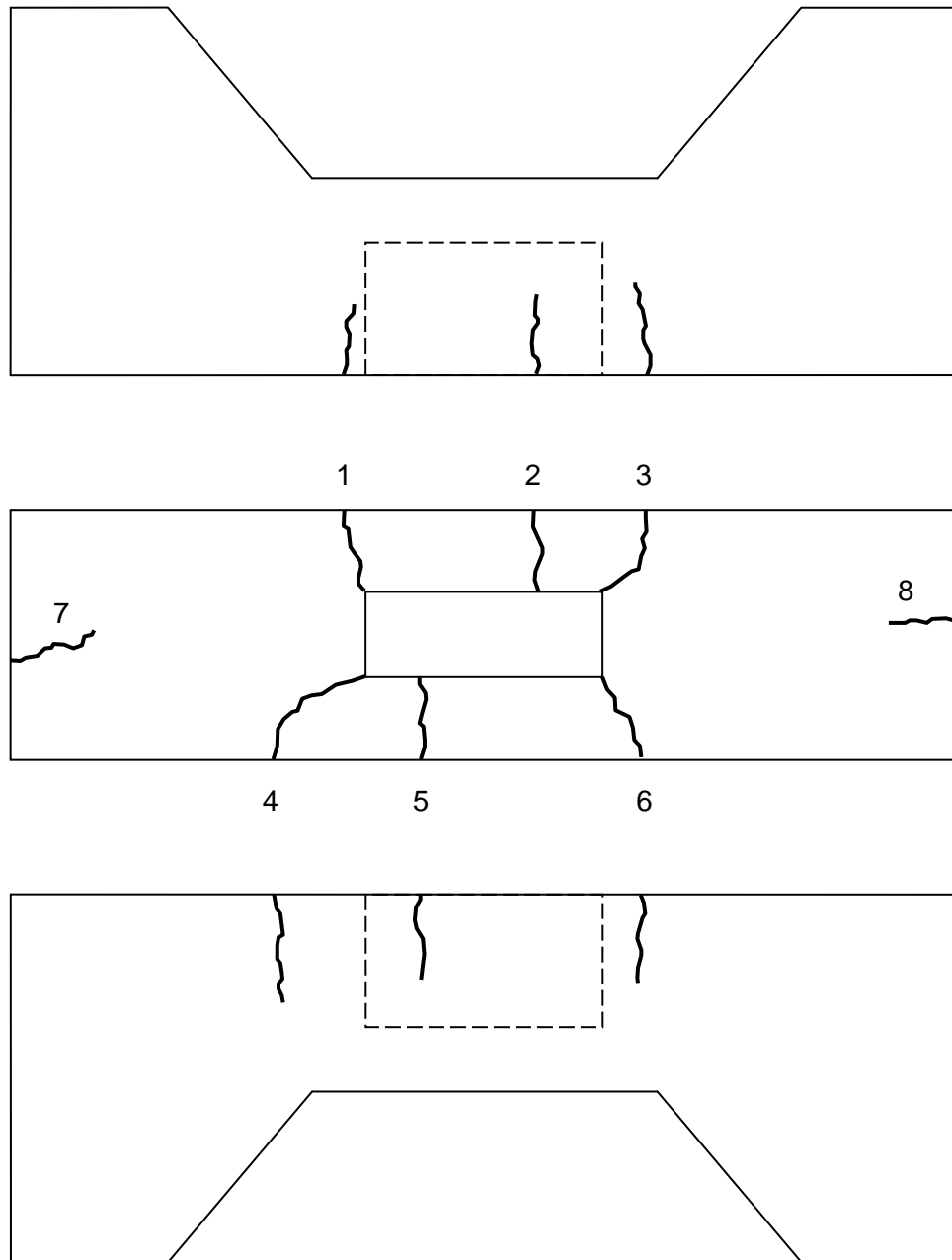


Figure G-12: Beam Specimen GVC-3 Crack Map

Table G-4: Crack Widths for Crown Grout Void Corrosion Series

Specimen	Crack Number	Initial Crack Width (in.)		Final Crack Width (in.)	
GVC-1	1	0.002	0.002	0.003	0.002
	2	0.003	0.004	0.004	0.004
	3	0.002	0.001	0.002	0.002
	4	0.002	0.002	0.002	0.003
	5	0.004	0.004	0.004	0.004
	6	0.004	0.007	0.004	0.007
	7	0.005	0.003	0.005	0.003
	8	0.003	0.004	0.003	0.004
GVC-2	1	0.009	0.007	0.010	0.009
	2	0.008	0.006	0.010	0.008
	3	0.007	0.008	0.009	0.010
	4	0.006	0.006	0.008	0.007
	5	0.007	0.007	0.008	0.009
	6	0.008	0.008	0.010	0.010
	7	0.008	0.009	0.010	0.011
	8	0.008	0.008	0.009	0.009
	9	0.002	0.002	0.002	0.002
	10	0.001	0.002	0.001	0.002
GVC-3	1	0.009	0.010	0.010	0.011
	2	0.009	0.009	0.011	0.011
	3	0.008	0.009	0.010	0.011
	4	0.008	0.008	0.010	0.010
	5	0.010	0.010	0.012	0.011
	6	0.011	0.010	0.012	0.011
	7	0.002	0.002	0.002	0.002
	8	0.002	0.002	0.002	0.002

Appendix H

Beam Specimen Autopsy Procedure

This appendix contains the detailed autopsy procedure followed for each beam specimen. Autopsying prestressed concrete members requires safety precautions due to the very high forces in each strand. Autopsying post-tensioned concrete members can be particularly problematic since the strand is contained within a duct where it may or may not be completely bonded to the concrete section and has the potential to recoil during the autopsy procedure. As such, the researchers consulted with members of the Florida Department of Transportation and the University of Texas at Austin concerning their experiences in autopsying post-tensioned concrete members. With their help, the researchers developed a plan to minimize safety risks and maximize results while autopsying the beam specimens.

The plan specifics varied depending on which specimens were undergoing autopsy. For the Fatigue Reference Series and the Crown Grout Void Corrosion Series, the critical area of the strand to examine was the center region (including the portions within the deviators), for a total tendon length of approximately 3'-0" centered on the beam. For these two series, this section of the tendon was critical for three reasons. First, the center region represents the typical beam cross-section of the specimen, with the Fatigue Reference Series serving as the baseline condition. Second, for the Crown Grout Void Corrosion Series, the center region was the location with the exposed grouted duct. Third, the deviators were purposely selected to maximize local bending stresses in the tendon,

which may manifest itself through wire breakage or signs of fatigue cracking at these locations.

The autopsy procedure developed for removing this portion of the tendon consisted of the following:

1. Remove the exposed portion of the plastic duct in the center of the beam with a Dremel rotary tool as was done for the Crown Grout Void Corrosion Series. This step was necessary in order to inspect the tendon for signs of cracking in the grout prior to the actual autopsy.
2. Cut through the tendon adjacent to each deviator with a 7-1/4-inch-diameter diamond concrete blade attached to a Bosch Angle Grinder. Once the tendon is cut at both ends, remove this portion from the beam specimen. The result is shown in Figure H-1. This step removed a considerable portion of the prestressing force, with wires frequently pinging during the cutting operation.
3. Saw cut the concrete above the tendon on each side of the “bathtub” for a distance of approximately 12” along the beam. This step was accomplished with a 14-inch-diameter diamond concrete blade attached to a gas-powered saw, as shown in Figure H-2.
4. Remove the concrete to expose the tendon on each side of the “bathtub” for a distance of approximately 12” along the beam. This step was accomplished with a 50-lb jackhammer, and the result is shown in Figure H-3 after the steel deviator was removed.



Figure H-1: Removed Center Portion of Tendon



Figure H-2: Saw Cutting of Concrete Above Tendon



Figure H-3: Concrete Removed to Expose Tendon

5. Cut through the now-exposed portions of the tendon with the 7-1/4-inch-diameter diamond concrete blade attached to the Bosch Angle Grinder. Once the tendons are cut, remove these portions from the beam specimen.

For the Anchor Zone Grout Void Series and the Anchor Zone Grout Void Corrosion Series, the critical area of the strand to examine was the portion at the anchor head that contained the void. As previously mentioned, this imperfection allows chlorides access to the tendon and, in the case of cyclic loading, may allow localized bending stresses due to the lack of tendon support. The autopsy procedure developed for removing this portion of the tendon consisted of the following:

1. Remove the exposed portion of the plastic duct in the center of the beam with a Dremel rotary tool as was done for the Crown Grout Void Corrosion Series.

This first step was necessary in order to inspect the tendon for signs of cracking in the grout prior to the actual autopsy.

2. Cut through the tendon adjacent to each deviator with the 7-1/4-inch-diameter diamond concrete blade attached to the Bosch Angle Grinder. Once the tendon is cut at both ends, remove this portion from the beam specimen. The result is shown in Figure H-1. This step removed a considerable portion of the prestressing force, with wires frequently pinging during the cutting operation.
3. Saw cut the concrete above the tendon and end anchorage for a distance of approximately 18" from the end of the beam. This step was accomplished with the 14-inch-diameter diamond concrete blade attached to the gas-powered saw, as shown in Figure H-4.
4. Remove the concrete at the beam end to expose the tendon and the top of the anchorage. This step was accomplished with the 50-lb jackhammer.
5. Cut through the now-exposed portion of the tendon immediately behind the anchorage with the 7-1/4-inch-diameter diamond concrete blade attached to the Bosch Angle Grinder.
6. Remove the concrete to expose the remaining portion of the anchorage, and then remove the anchorage from the beam specimen. The result is shown in Figure H-5.
7. Jackhammer the anchor head and strand out of the anchorage. The result is shown in Figure H-6.



Figure H-4: Saw Cutting of Concrete Above Tendon and Anchorage



Figure H-5: Beam Specimen After Anchorage Removal



Figure H-6: Anchor Head and Strand After Removal from Anchorage

Vita
Jeffery S. Volz

Education

Doctor of Philosophy in Civil and Environmental Engineering, The Pennsylvania State University, University Park, PA, December 2008

Master of Science in Architectural Engineering, The Pennsylvania State University, University Park, PA, August 1987

Bachelor of Architectural Engineering, The Pennsylvania State University, University Park, PA, May 1985

Work Experience

Instructor & Undergraduate Academic Officer, Department of Civil and Environmental Engineering, The Pennsylvania State University, University Park, PA, 2002-2008

Associate & Project Structural Engineer, Holabird & Root LLC, Chicago, IL, 1999-2002

Lead Structural Engineer, Harza Engineering Company, Chicago, IL, 1989-1999

Principal Structural Engineer, CTL, Inc., Skokie, IL, 1990-1998

Structural Design Engineer, Skidmore, Owings & Merrill, Chicago, IL 1986-1990

Selected Publications

Volz, J.S. and Schokker, A.J., "Fatigue Durability of Partially Post-Tensioned Concrete Members," *Proceedings*, SEI/ASCE Structures Congress, SEI Committee on Concrete and Masonry Structures, April-May 2009 (Accepted).

Volz, J.S., Schokker, A.J., and Pacheco, A.R., "Linear Polarization Resistance for Acceptance Testing of Post-tensioning Grouts," *Proceedings*, Concrete Bridge Conference, St. Louis, Missouri, May 2008.

Oesterle, R.G. and Volz, J.S., "Effective Temperature and Longitudinal Movement in Integral Abutment Bridges," *Proceedings*, FHWA Conference on Integral Abutment and Jointless Bridges, Baltimore, Maryland, March 16-18, 2005.